National Library of Canada
Bibliothèque nationale du Canada

Canadian Theses Service
Services des thèses canadiennes

Ottawa, Canada
K1A 0N4

CANADIAN THESES

THÈSES CANADIENNES

NOTICE

The quality of this microfiche is heavily dependent upon the quality of the original thesis submitted for microfilming. Every effort has been made to ensure the highest quality of reproduction possible.

If pages are missing, contact the university which granted the degree.

Some pages may have indistinct print especially if the original pages were typed with a poor typewriter ribbon or if the university sent us an inferior photocopy.

Previously copyrighted materials (journal articles, published tests, etc.) are not filmed.

Reproduction in full or in part of this film is governed by the Canadian Copyright Act, R.S.C. 1970, c. C-30. Please read the authorization forms which accompany this thesis.

AVIS

La qualité de cette microfiche dépend grandement de la qualité de la thèse soumise au microfilmage. Nous avons tout fait pour assurer une qualité supérieure de reproduction.

S'il manque des pages, veuillez communiquer avec l'université qui a conféré le grade.

La qualité d'impression de certaines pages peut laisser à désirer, surtout si les pages originales ont été dactylographiées à l'aide d'un ruban usé ou si l'université nous a fait parvenir une photocopie de qualité inférieure.

Les documents qui font déjà l'objet d'un droit d'auteur (articles de revue, examens publiés, etc.) ne sont pas microfilmés.

La reproduction, même partielle, de ce microfilm est soumise à la Loi canadienne sur le droit d'auteur, SRC 1970, c. C-30. Veuillez prendre connaissance des formules d'autorisation qui accompagnent cette thèse.

THIS DISSERTATION
HAS BEEN MICROFILMED
EXACTLY AS RECEIVED

LA THÈSE A ÉTÉ
MICROFILMÉE TELLE QUE
NOUS L'AVONS REÇUE

NL 339 (r. 86/01)

Canada

197

National Library of Canada | Bibliothèque nationale du Canada

Canadian Theses Division | Division des thèses canadiennes

Ottawa, Canada
K1A 0N4

0-315-26929-4

PERMISSION TO MICROFILM — AUTORISATION DE MICROFILMER

• Please print or type — Écrire en lettres moulées ou dactylographier

Full Name of Author — Nom complet de l'auteur

THOMAS MICHAEL CURRAN

Date of Birth — Date de naissance

APRIL 1, 1955

Country of Birth — Lieu de naissance

CANADA

Permanent Address — Résidence fixe

#1407 11135 - 83 AVENUE,
EDMONTON, ALBERTA

T6G 2C6

Title of Thesis — Titre de la thèse

R.F. HYPERTHERMIA APPLICATOR USING ORBITING ELECTRODES

University — Université

UNIVERSITY OF ALBERTA

Degree for which thesis was presented — Grade pour lequel cette thèse fut présentée

MASTER OF SCIENCE

Year this degree conferred — Année d'obtention de ce grade

1983

Name of Supervisor — Nom du directeur de thèse

DR. W.A.G. VOSS

Permission is hereby granted to the NATIONAL LIBRARY OF CANADA to microfilm this thesis and to lend or sell copies of the film.

The author reserves other publication rights, and neither the thesis nor extensive extracts from it may be printed or otherwise reproduced without the author's written permission.

L'autorisation est, par la présente, accordée à la BIBLIOTHÈQUE NATIONALE DU CANADA de microfilmer cette thèse et de prêter ou de vendre des exemplaires du film.

L'auteur se réserve les autres droits de publication; ni la thèse ni de longs extraits de celle-ci ne doivent être imprimés ou autrement reproduits sans l'autorisation écrite de l'auteur.

Date

OCT. 4, 1983

Signature

T. Curran

NL-91 (4/77)

R.F. HYPERTHERMIA APPLICATOR USING ORBITING ELECTRODES

by

(C) THOMAS M. CURRAN

A THESIS

SUBMITTED TO THE FACULTY OF GRADUATE STUDIES AND RESEARCH

IN PARTIAL FULFILMENT OF THE REQUIREMENTS FOR THE DEGREE

OF MASTER OF SCIENCE

DEPARTMENT OF ELECTRICAL ENGINEERING

EDMONTON, ALBERTA

FALL, 1983

THE UNIVERSITY OF ALBERTA

RELEASE FORM

NAME OF AUTHOR ..... THOMAS M. CURRAN .....

TITLE OF THESIS ..... R.F. HYPERTHERMIA APPLICATOR .....

..... USING ORBITING ELECTRODES .....

DEGREE FOR WHICH THESIS WAS PRESENTED

..... MASTER OF SCIENCE .....

YEAR THIS DEGREE GRANTED ..... 1983 .....

Permission is hereby granted to THE UNIVERSITY OF ALBERTA LIBRARY to reproduce single copies of this thesis and to lend or sell such copies for private, scholarly or scientific research purposes only.

The author reserves other publication rights, and neither the thesis nor extensive extracts from it may be printed or otherwise reproduced without the author's written permission.

(SIGNED) ..... T. Curran .....

PERMANENT ADDRESS:

..... #1407 11135-83 AVENUE .....

..... EDMONTON, ALBERTA .....

..... CANADA T6G 2C6 .....

DATED ..... Oct. 4 ..... 19 83

THE UNIVERSITY OF ALBERTA

FACULTY OF GRADUATE STUDIES AND RESEARCH

The undersigned certify that they have read, and recommend to the Faculty of Graduate Studies and Research, for acceptance, a thesis entitled

R.F. HYPERTHERMIA APPLICATOR USING ORBITING ELECTRODES submitted by

THOMAS M. CURRAN in partial fulfilment of the requirements for the degree of

MASTER OF SCIENCE in

ELECTRICAL ENGINEERING

.....
Supervisor

.....

.....

Date..... October 4 1982.....

ABSTRACT

This work examines hyperthermia as a cancer treatment and describes the development of a new hyperthermia applicator. The r.f. applicator produces more heat deep within a subject than on or near the surface according to the results obtained.

Experimental temperature distribution results in an agar cylinder were found to be in close agreement with computer-generated data. The effects of altering various applicator parameters were explored using the computer models. From this work an optimized applicator was found which should produce more heat deep within a dielectric than on the surface.

The hyperthermia applicator consists of parallel plate electrodes the same width as the heated medium (agar). Radio frequency energy at 3.75 MHz, or lower, is used because of its substantial penetration depth. A temperature controlled saline bath is utilized to cool the surface of the irradiated dielectric and improve energy coupling. Finally the electrodes are made to orbit the irradiated medium to reduce superficial energy exposure without affecting deep exposure within the medium.

Live animal experiments were performed but proved to be inconclusive.

TABLE OF CONTENTS

CHAPTER PAGE

INTRODUCTION

A HISTORY OF HYPERTHERMIA.....1

THE EFFECT OF HYPERTHERMIA ON TUMORS.....4

METHODS OF PRODUCING HYPERTHERMIA.....6

THEORY FOR R.F. HEATING

THE QUASI-STATIC APPROXIMATION.....19

HEATING WITH COILS AND PLATE ELECTRODES.....24

MEGAERA: THE FINITE DIFFERENCE APPROXIMATION...30

METHODS AND MATERIALS

VOLUMETRIC HEAT CAPACITY MEASUREMENT OF AGAR...36

THERMAL CONDUCTIVITY MEASUREMENT.....38

DIELECTRIC MEASUREMENTS.....42

TEMPERATURE DISTRIBUTIONS.....49

LIVE ANIMAL MEASUREMENTS.....64

DATA AND RESULTS

MEASUREMENT OF VOLUMETRIC HEAT CAPACITY OF AGAR.....66

THERMAL CONDUCTIVITY MEASUREMENT FOR AGAR.....70

ELECTRICAL CONDUCTIVITY MEASUREMENTS.....76

TEMPERATURE MEASUREMENTS IN THE AGAR.....81

MEASURED TEMPERATURE DISTRIBUTIONS.....84

MEGAERA SIMULATIONS.....91

SIMULATION OF MOVING ELECTRODE HEATING.....103

SIMULATED VARIATION OF APPLICATOR PARAMETERS..123

ROTATING ELECTRODES.....143

HYPERTHERMIA IN A LIVE ANIMAL.....149

DISCUSSION

EVALUATION OF ELECTRODE CONFIGURATIONS.....152

CLINICAL CONSIDERATIONS.....159

CONCLUSIONS.....160

BIBLIOGRAPHY AND REFERENCES.....161

APPENDIX 1.

COMPUTER PROGRAMS TO SIMULATE R.F. HEATING WITH ROTATING ELECTRODES.....174

APPENDIX 2.

CALCULATION OF POWER ABSORBED BY LOAD.....182

APPENDIX 3.

MAXIMUM TEMPERATURE ERROR RESULTING FROM 2-D SIMULATION.....185

APPENDIX 4.

PERMITTIVITY AND CONDUCTIVITY DERIVATIONS FOR DIELECTRIC MEASURING CELL[7].....187

LIST OF TABLES

TABLE		PAGE
3.1	Calibration fluids for dielectric measuring cell	48
3.2	Fitted and measured cooling curve points	55
4.1	Water temperature in calorimeter versus time	67
4.2	Temperature measured at three sites in agar cylinder for given voltage and current	71
4.3	Thermal conductivity, k, measured for various thicknesses of agar	71
4.4	Values used to plot straight line graph of agar thermal conductivity versus thickness	74
4.5	Assessment of dielectric measuring cell accuracy using saline solutions and published values	77
5.1	Summary of target specificities (η) for various applicators	155-156

LIST OF FIGURES

FIGURE		PAGE
1.1	Modalities for crossfire heating using r.f. or measured applicators	11
1.2	Heating pattern produced by pancake coil	12
2.1	E-fields inductively coupled into tissue by coil type hyperthermia applicator	25
2.2	E-fields capacitively coupled into tissue by parallel plates	27
2.3	Grid block spacing and numbering used by Megaera.	32
3.1	Apparatus used for heat capacity measurement	37
3.2	Chamber used for thermal conductivity measurements	39
3.3	Apparatus used for thermal conductivity measurements	41
3.4	Dielectric measurement cell	43

3.5 Apparatus used for dielectric measurements.....44

3.6 Plot of ϵ_s vs. $\sin\phi/\omega x$ for low conductivity materials in dielectric measuring cell.....47

3.7 Apparatus used for heating agar cylinder.....50

3.8 Apparatus used to move electrodes around heated medium.....52

3.9 Apparatus used to maintain saline bath temperature and heat agar cylinder.....53

3.10 Cooling curve with 99% confidence band.....55

3.11 One half of cylinder shown viewed from above. Electrodes each (1.95±0.1) cm from agar and situated along flat portion of semi-circle.....57

3.12 Plot of temperature vs. angle for various radii in r.f. irradiated cylinder.....58

3.13 Top view of agar cylinder showing radial lines along which temperatures were measured.....61

4.1 Cooling curve for calculating the heat capacity of agar.....68

4.2 Arrangement of materials and apparatus inside the thermal conductivity measurement chamber.....72

4.3 Calculated thermal conductivity for various agar slab thicknesses.....75

4.4 Temperature profile in agar cylinder showing temperatures directly between electrodes (top two curves) and perpendicular to this line (bottom two curves). Solid lines are for stationary electrodes and dashed are for electrodes orbiting between ±40°.....82

4.5 Temperature distribution inside agar cylinder heated with symmetric electrodes.....85

4.6 Top view of one half of 5 cm radius agar cylinder showing electrodes relative to x- and y-axes used for reference purposes in simulated temperature maps.....86

4.7 Hot spots produced in a dielectric by various electrode configurations.....87

4.8 Initial orientation of asymmetric electrodes relative to x- and y-axes in agar cylinder.....89

4.9 Temperature distribution inside agar cylinder heated with asymmetric electrodes.....90

4.10 Temperature profile measured in agar with high and limits calculated by Megaera.....92

4.11 Temperature profile measured in agar and calculated by Megaera.....94

4.12 Calculated temperature distribution produced inside agar by symmetric electrodes.....95

4.13 Temperature profile in agar irradiated with asymmetric electrodes.....97

4.14 Temperature along y-axis in agar irradiated by asymmetric electrodes.....99

4.15 Temperature profile along x-axis in agar cylinder.....100

4.16 Temperature profile along y-axis in agar.....101

4.17 Calculated temperature distribution produced inside agar cylinder heated with asymmetric electrodes.....102

4.18 Calculated temperature distribution inside agar cylinder heated with orbiting symmetric electrodes undergoing sinusoidal speed variation through ±40° arc.....104

4.19 Placement of numbered thermocouples in agar cylinder (top view).....105

4.20 Temperature profile along 0° radial.....106

4.21 Temperature profile along 45° radial.....107

4.22 Temperature profile along 90° radial.....108

4.23 Calculated temperature distribution inside agar cylinder heated with orbiting symmetric electrodes undergoing circular speed variation through ±40° arc.....109

4.24 Calculated temperature distribution inside agar cylinder heated with orbiting symmetric electrodes undergoing flattened sinusoidal speed variation through ±40° arc.....111

4.25 Placement of numbered thermocouples in agar cylinder (top view).....112

4.26 Calculated temperature distribution inside agar cylinder heated with asymmetric orbiting electrodes undergoing sinusoidal speed variation through ±40° arc.....113

4.27 Temperature profiles along 0° radial.....114

4.28 Temperature profiles along 45° radial.....116

4.29 Temperature profiles along 90° radial.....117

4.30 Temperature profiles along 135° radial.....118

4.31 Calculated temperature distribution inside agar cylinder heated with asymmetric orbiting electrodes. Electrodes undergoing circular speed variation through ±40° arc.....119

4.32 Calculated temperature distribution inside agar cylinder heated with asymmetric orbiting electrodes. Electrodes undergoing flattened sinusoid speed variation through ±40° arc.....120

4.33 Calculated temperature distribution using same parameters as in Figure 4.12 except twice the power.....124

4.34 Calculated temperature distribution using same parameters as in Figure 4.12 except four times the power.....126

4.35 Calculated temperature distribution using the same parameters as in Figure 4.34 except a 10° C saline bath.....127

4.36 Calculated temperature distribution using the same parameters as in Figure 4.33 except five times the bath electrical conductivity.....128

4.37 Calculated temperature distribution using the same parameters as in Figure 4.33 except one nineteenth the bath electrical conductivity...130

4.38 Calculated temperature distribution using the same parameters as in Figure 4.33 except the electrodes are farther (3.55 cm) apart.....131

4.39 Calculated temperature distribution in medium using 1 cm wide stationary symmetric electrodes.. 132

4.40 Three dimensional plot of Figure 4.39.....133

4.41 Calculated temperature distribution in medium

using 2 cm wide symmetric electrodes.....135

4.42 Three dimensional plot of Figure 4.41.....136

4.43 Calculated temperature distribution in medium using 4 cm wide symmetric electrodes.....137

4.44 Three dimensional plot of Figure 4.43.....138

4.45 Calculated temperature distribution using the same parameters as in Figure 4.33 except the electrodes are 9.7 cm wide.....140

4.46 Calculated temperature distribution using the same parameters as in Figure 4.33 except that the electrodes are 23.7 cm wide.....142

4.47 Calculated temperature distribution using the same parameters as in Figure 4.5 except that the electrodes revolve completely around the phantom. 144

4.48 Calculated temperature distribution using the same parameters as in Figure 4.9 (asymmetric electrodes) except that the electrodes revolve completely around the phantom.....146

4.49 Calculated temperature distribution using the same parameters as in Figure 4.45 (9.7 cm wide stationary symmetric electrodes) except that the electrodes rotate completely around the phantom.. 147

4.50 Temperature profile obtained in a live cat irradiated with symmetric electrodes orbiting between ±40°.....150

A.1.1 Sinusoidal electrode speed variation.....176

A.1.2 Circular electrode speed variation.....178

A.1.3 Flattened-sinusoidal electrode speed variation... 180

A.2.1 Equivalent circuit for hyperthermia applicator... 183

A.3.1 Electrode-insulating boundary configuration for uniform current density.....186

A.3.2 Electrode-insulating boundary configuration for non-uniform current density.....186

A.4.1 Equivalent circuit for dielectric measuring

apparatus.....188

A.4.2 Imaginary and real components of complex impedance.....188

INTRODUCTION

A HISTORY OF HYPERTHERMIA

Heat has long been used by man in the treatment of disease. Heat in the form of naturally occurring fever or inflammation was naturally used to help control many infections before man learned to produce it. Hippocrates once said,"Give me the power to produce fever and I will cure all disease" [cited in 54]. Many afflictions have been, or are, treated with heat. The list includes acne [66], arthritis [66], cancer [37], carbuncles and furuncles [15], diabetes [cited in 66], hemorrhoids [25], syphylis [11], and possibly the common cold [43].

As long ago as 3000 B.C., heat in the form of a smoldering stick was used to treat tumors [10]. In the 1890's Coley showed that pyrogens (Coley's Toxins) could produce regression or even cure neoplastic lesions [17]. Unfortunately he could not tell whether heat or some other immune response was responsible for the tumor regressions [20]. Around the same time D'Arsonval and Tesla suggested and examined the use of high frequency (h.f.) fields (1-10 MHz) in medicine [66]. Such effects as analgesia, vascular dilatation, and lower blood pressure were reported by D'Arsonval in 1893 [6]. A colleague of D'Arsonval's, Paul Oudin, used h.f. fields (a 'shower of sparks') for the

purpose of treating tumors [cited in 66]. In 1906 de Keating-Hart used h.f.fields in the form of an electrical discharge to destroy tumors [40].

Interest in hyperthermia as a cancer treatment was increased in 1918 by Rohdenburg. He published a literature review showing that half the recorded spontaneous tumor regressions were preceded by high fever, infection, or heat application [1]. This indicated that some cancers could be treated by any method which would increase the tumor temperature sufficiently.

In 1939 Denier explored the use of microwave (3.75 MHz) diathermy in conjunction with x-rays, as a tumor therapy [cited in 40]. In addition, the possibility of selective heating as a result of variations in frequency and dielectric properties of tumors and organs had been considered by 1941 [cited in 66]. Up to 1955 several papers were published dealing with the effects of heat and heat plus ionizing radiation on cancers. Interest in hyperthermia then waned until the early 1960's, when Crile published results showing that heat and especially heat plus ionizing radiation were effective in treating tumors [18]. More recently, work by Muckle and Dickson [20, 46], Pettigrew [51], LeVeen [38, 39], Cavaliere [12], and many others, have led to the present interest in hyperthermia as a cancer therapy.

To date numerous papers have been published on the use and effect of heat on cancer tumors. The overwhelming conclusion is that hyperthermia, particularly when used in conjunction with chemotherapy or ionizing radiation, has a detrimental effect on tumors while sparing healthy tissue [45, 52]. There are also accounts in the literature claiming hyperthermia can act as an analgesic and cause regression or eradication of tumors which were unresponsive to conventional therapy [50, 37]. The evidence shows that hyperthermia is a promising tool for cancer therapy and must by investigated further.

THE EFFECT OF HYPERTHERMIA ON TUMORS

At a biochemical level, Ludgate *et al* [41] have described the effect of hyperthermia on tumor cells. Heat destroys sensitive cells by scrambling molecular bonds. This leads to changes in the cytoplasm and DNA damage. The DNA damage is not repaired because of heat induced changes in repair enzymes and their production. The cell walls become leaky, releasing ions. Aerobic glycolysis gives way to anaerobic glycolysis resulting in a lower pH and subsequent lysosomal activity.

Tumors often consist of a well-vascularized periphery surrounding a poorly vascularized, semi-necrotic, centre [38,54]. The central portion of the tumor tends to be most vulnerable to heat therapy and resistant to ionizing radiation [47, 48]. The opposite is true for the well vascularized portion of the tumor. Growing cells in the S-phase of mitosis have been found most vulnerable to heat while resistant to ionizing radiation [1, 47, 72]. Hence, a fortunate synergism between hyperthermia and ionizing radiation exists [46, 45]. Some researchers have found that certain chemotherapeutic agents appear to increase the sensitivity of cells to heat and vice versa [45, 67]. In addition, there may be a tumoricidal immunological response associated with hyperthermia [65, 38, see p. 15].

Investigations by LeVeen *et al*[38] have shown that growing tumors will displace normal vasculature and produce their own blood vessels through angiogenesis. This process occurs primarily at the periphery of the tumor [54]. These new vessels tend to be a mass of small capillaries which offer a high resistance to heat dissipating and nutrient bearing blood flow. As a result, the centre of the tumor receives very little oxygen or nutrients which can lead to necrosis [54]. When heat is applied the surrounding healthy vessels dilate while the tumor vessels do not. This causes changes in pressure which further decrease the amount of blood flowing through the tumor relative to the healthy tissue [37, 38]. This can lead to higher temperatures in the tumor relative to the surrounding healthy tissue leading to tumor death.

LeVeen [38] has found that the microvasculature in lung tumors is destroyed after a few three-hour hyperthermia sessions involving tumor temperatures of 45°C or more. This may be the result of the capillaries becoming clogged with erythrocytes. The tumor tends to become acidic which can cause erythrocytes to become rigid, effectively increasing the viscosity of the blood. This effect was discovered and is being utilized by Von Ardenne [34]. He increases the glucose level in patients to decrease their blood pH before applying hyperthermia.

METHODS OF PRODUCING HYPERTHERMIA

Numerous methods have been found to produce whole body or local hyperthermia. Each one has its own strengths and weaknesses with no particular method best suited to every type of tumor. The following paragraphs describe various methods of producing hyperthermia and include some of the advantages and disadvantages of each technique.

Whole body hyperthermia has been produced by using molten wax baths [34], hot water baths [54], a heated enclosure or garment with or without radio frequency (r.f.) heating [54, 11], injection of pyrogenic agents [17], perfusion with heated blood [cited in 54], etc. This type of treatment has the potential to destroy unknown or widespread metastases if sufficiently high temperatures are obtained. A large amount of medical support is required because of the danger involved in raising an individual's body temperature to the 41.8°C generally used [54, 50]. An individual's heart beat increases at the rate of about 10 beats/°C. This can be fatal especially for those with cardiac problems [50, 54]. Using conduction to warm a person to therapeutic temperatures is a long and tedious process. The use of pyrogens is, at best, unsafe because the response can be difficult to control and unpredictable especially when used on a weakened cancer patient [20].

With local hyperthermia high tumor temperatures (45-50°C) can be tolerated by patients. Higher temperatures mean a shorter treatment time and a more effective tumor kill. Storm *et al* suggest 30 hours of treatment at 42°C, 3 to 4 hours at 45°C, and a matter of minutes at 50°C to cause thermal death of tumors [60].

Local hyperthermia has been produced by immersion in a heated liquid or perfusion of an affected area with heated chemotherapeutic drugs, blood, or saline [57, 41, 59]. Great care must be taken to avoid permanently damaging the heated area [57, 13]. These techniques have been successful in the treatment of melanomas of the extremities and of some success in treating bladder carcinomas [57, 41, 28]. Tumor location and accessibility limit the usefulness of these techniques.

Invasive applicators have been found useful for treating certain types of tumors. These devices are designed to be inserted into or near a tumor and, using microwave or r.f. fields, produce localized heating [62, 58, 68, 59]. Arrays of implantable electrodes have been used to localize heating [21]. Implanting metal "seeds" in a tumor and heating them with magnetic fields has also been tried for producing localized hyperthermia [56]. These devices are suitable only where the tumor is accessible either through a natural body cavity or by surgery.

Further, implanting a device in a tumor can produce metasteses as a result of mechanical disturbance. Some of these techniques are also unsatisfactory because they require the use of a general anaesthetic and surgery[36].

Ultrasound, r.f. fields, and microwaves can be used to non-invasively produce local or regional hyperthermia. Not every tumor is ideally suited to these modes of therapy and there can be a problem with producing excessive heating in the wrong area.

Ultrasound is useful because it does not heat fat preferentially; temperature measurements during treatment are simple to make which is not the case with r.f. fields. Deep heating is possible with focussing transducers, multiple transducers, or moving transducers [54, 36]. Stray leakage of ultrasound into the environment is not a problem. Air is strongly attenuating to ultrasound and the mismatch between soft tissues and air is such that 99.9% of the energy is reflected at the interface [27, 16]. This also means that gas-filled organs such as the lungs or intestines cannot be effectively heated with ultrasound. The use of a retention enema or the induction of a hydrothorax are possible solutions to this problem but may not always be satisfactory [36]. There are also large reflections produced at bone-tissue interfaces and bone absorbs ten times more ultrasound energy than muscle [54].

As a result, areas blocked by or close to bone cannot be treated [16].

Radiative microwave applicators operating from 433-2450 MHz have been used extensively over the last ten years. They don't heat fatty tissue preferentially except when tissue interfaces create large reflections. The applicators tend to be quite compact and the heated area can be easily localized. These applicators are usually rectangular or circular waveguides with, or without, dielectric loading or ridges [26, 14, 58, 42, 64]. With surface cooling, waveguide applicators operating at 915 MHz have been effective in producing deep heating in human thighs [35]. The use of multiple applicators can also improve the deep heating ability of microwaves to some extent [24, 14, 16]. Unfortunately microwaves have a very shallow penetration depth (skin depth 3.7 cm at 433 MHz and 2.1 cm at 2450 MHz) relative to r.f. (skin depth 17.4 cm at 27.12 MHz and 91.3 cm at 1 MHz) or ultrasound energy so they are not generally suited to deep heating[22]. Care must also be taken to ensure that resonant effects are not produced in organs, cavities, or limbs at the higher frequencies [63]. Another disadvantage with microwave applicators is that metal probes can interfere with the fields to give false temperature readings [27].

Radiative applicators in the r.f. range have been developed. Among these is a ridged waveguide dielectrically loaded with distilled water which operates at 27.12 MHz [49, 59]. This applicator can be used to heat a large, deep area of the thorax particularly when two are used in a 'cross-fire' mode [see figure 1.1(b)]. Another applicator uses a circle of sixteen transverse electromagnetic apertures operating at 50-110 MHz to produce deep heating [70]. This particular system utilizes water as a medium to cool superficial tissues and improve coupling [70].

R.F. energy can be coupled inductively to a dielectric. In this case magnetic fields are utilized to induce eddy currents in the dielectric. Often a flat pancake coil or a wound coil is used for this purpose [3, 61]. These applicators do not preferentially heat skin and subcutaneous fat as much as capacitive applicators do. Tissues with high electrical conductivity (*ie.* muscle) tend to heat up more than those with low conductivity (*ie.* fat) (see page 24).

The pancake coil produces a toroidal region of maximum heat just below the subcutaneous fat layer (Figure 1.2). Storm's [61] single winding coil appears to heat an object placed inside it uniformly because of thermal conduction. Eddy currents circulate around the central axis which means

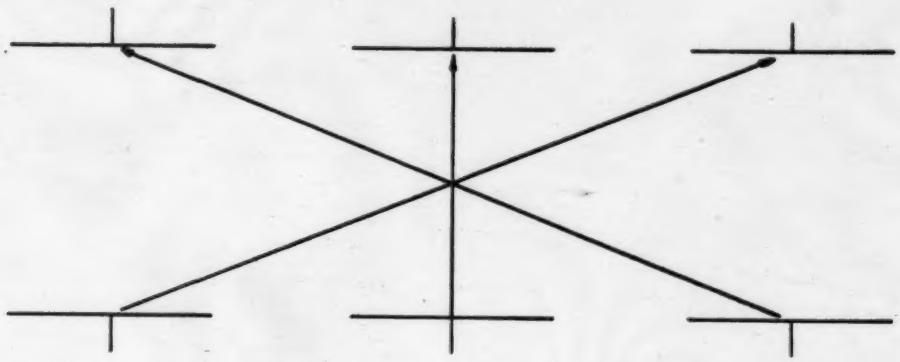

(a) Crossfire capacitive heating

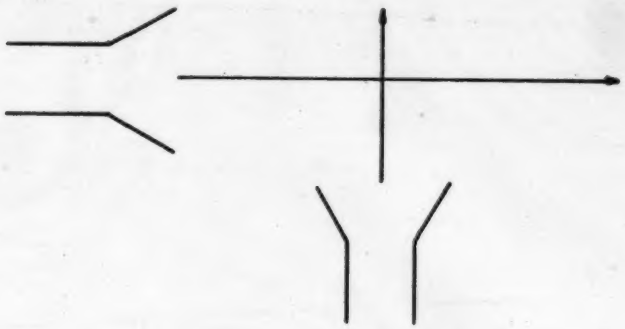

(b) Crossfire waveguides

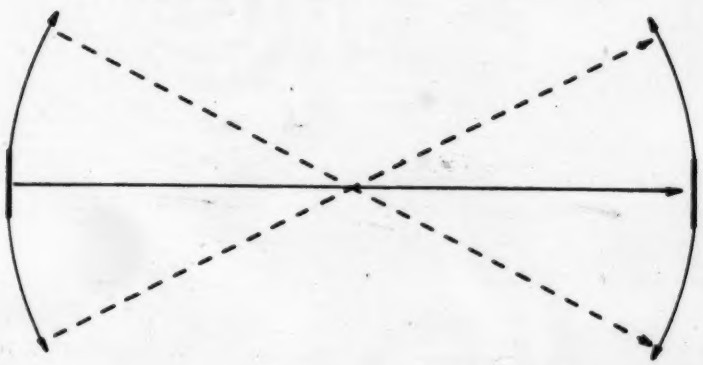

(c) Rotating electrodes

Figure 1.1 Modalities for crossfire heating using r.f. or microwave applicators.

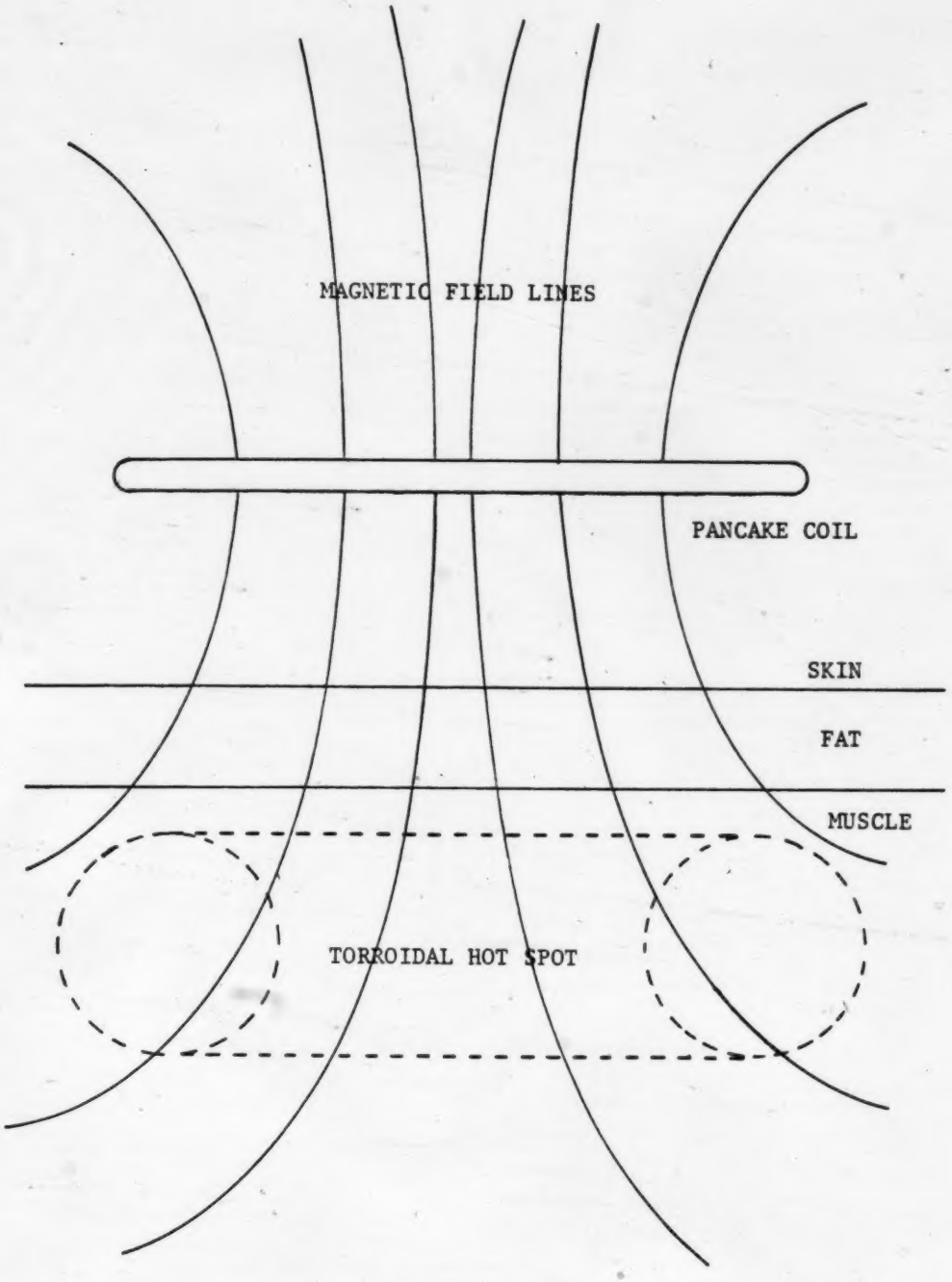

Figure 1.2 Heating pattern produced by pancake coil.

there is no current produced on the axis [16]. A plot of the H-field inside the coil indicates that the field increases drastically as one approaches the edge of the coil [16]. This implies that the strongest heating would occur in the superficial parts of the body if fat and skin had dielectric properties similar to muscle. Shaping fields is very difficult with inductive heating and metal probes can perturb the field giving false temperature readings [27, 16].

Capacitive heating with r.f. has been another popular method of inducing hyperthermia. Electric fields are produced which in turn cause current to flow in the dielectric. This method is simple and useful because electrode size and shape can easily be tailored to fit most applications [44, 4]. Multiple applicators produce deep heating and the applicators can be cooled to prevent skin overheating [37, 65]. Despite the high penetration depth of r.f. fields, subcutaneous fat tends to heat up more than deep tissues when capacitive heating is used. This can be a serious problem when only two stationary electrodes are utilized. In addition, the heating pattern can be difficult to predict and metal probes can perturb the r.f. field giving false temperature readings during irradiation [27].

At microwave frequencies phased arrays have been suggested as a means of focussing energy deep inside a tissue mass without over heating the surface [32]. Numerous radiators are used and the radiation from each phase shifted to produce constructive interference only at the tumor site [54]. In practice this technique is unsuitable because a human body is an extremely complicated, inhomogeneous, dielectric. As a result, attempts to focus energy in this way generally meet with failure [14].

As previously mentioned, multiple applicators have been used to produce deep heating. Generally researchers have devised applicators which operate in the 13-110 MHz range and have applicators oriented in a cross-fire manner [Figure 1.1(a,b)] [65, 59, 70]. These applicators take advantage of the large penetration depth of r.f. fields and spare surface tissue, but not the deep tumor site, from high radiation levels. As a result, skin and subcutaneous fat temperatures can be maintained at acceptable levels while deep tumor temperature is increased.

The cross-fire technique has been used with some success by LeVeen to treat lung tumors [38, 39, 65]. These tumors are very difficult to heat by most other means because they are deeply embedded in the thorax in an air-filled moving organ surrounded by a bony rib cage.

Sugaar and LeVeen have treated lung tumors with their cross-fire applicator and then surgically removed the tumors for histological examination [65]. These studies revealed damaged capillaries in the tumor's stroma leading to an immunological response. The immune response was similar to that seen in certain graft rejections.

LeVeen has had a good success rate, even using a non-cross-fire applicator, treating otherwise untreatable lung tumors [37, 38]. He found regression in one third of the cases treated, relief of pain and improved appetite in over 80% of the cases, and about 10% of the patients were apparently cancer-free for 2-3 years. LeVeen pointed out that his cross-fire applicator is vastly superior to the applicators used in the above trials [38].

An improvement to the cross-fire technique might result from using one moving applicator rather than two or more switched stationary applicators [Figure 1.1(c)]. The moving applicator acts like numerous switched applicators but is far simpler and cheaper to construct.

The use of moving electrodes has already been described and patented by LeVeen [39]. He has envisioned a system which moves two pancake coil electrodes in a semi-circular orbit around the patient. His design suffers from using air as the coupling medium between the

electrodes and skin. This could produce overheating of the surface layers. His design also shows electrodes which are so far apart that relatively small field gradients are present at the patient site. This may have the effect of spreading the fields more evenly over the patient which would tend to decrease the advantages of using moving electrodes. Further, any localization of fields would be practically impossible and stray radiation would become a serious problem.

For this project a hyperthermia applicator has been designed and built which uses moving electrodes as an extension of LeVeen's concept. This applicator utilizes parallel plate electrodes but could use any other kind of electromagnetic or ultrasonic radiators. Saline solution is used as the coupling medium between the electrodes and skin. This drastically reduces reflections at the skin boundary and helps keep superficial tissues cool during irradiation. The electrodes are kept within a few centimeters of the skin, producing higher field gradients, and taking full advantage of the electrode motion. The electrode-skin proximity and the large air-saline mismatch reduce stray radiation into the environment substantially.

Immersing a patient in chilled saline would not be acceptable as excessive cooling of the entire body would likely result. To cool the irradiated surfaces

sufficiently hypothermia could inadvertantly be produced in the patient. A doughnut shaped bag filled with chilled saline could be used to encircle the portion of the patient containing the tumor. This would require some form of thermal and electrical coupling medium between the bag and patient. The medium would have to be capable of penetrating the corified epithelium to be effective. Inside the bag electrodes travelling on tracks could be used to distribute the r.f. over the surface. With this type of applicator the heating and cooling could be localized and readily controlled.

Temperature patterns and profiles produced in agar cylinders by moving or stationary parallel plate electrodes were examined both experimentally and theoretically. In each case the surface of the agar was cooled by a saline bath. Computer programs HTAVE.0, HTAVE.1, and HTAVE.2 were written, and used, to predict moving electrode temperature distributions using stationary electrode data [Appendix 1]. Stationary electrode temperature distributions were closely predicted using the computer program MEGAERA developed by A. Hiebert of the University of Alberta Applied Electromagnetics Group [30]. MEGAERA simulated, under certain circumstances, the temperature distribution inside a dielectric exposed to r.f. energy from various electrodes. With this data one of the HTAVE programs could then be used to determine the effect of moving the

electrodes.

Temperature data obtained in this work clearly demonstrates the superiority of moving electrodes over stationary electrodes for producing deeper, more uniform heating.

THEORY FOR R.F. HEATING

THE QUASI-STATIC APPROXIMATION

The instantaneous electromagnetic heating in any dielectric can be calculated if the electric field intensity, $\vec{E}$, and dielectric conductivity, σ, are known everywhere inside the dielectric. The heating is calculated using the equation,

$$P = \sigma|\vec{E}|^2 \qquad 1$$

where P is the instantaneous power per unit volume dissipated in the medium. The electric field is described exactly by Maxwell's equations subject to appropriate boundary conditions. Maxwell's equations are,

$$\begin{aligned} \nabla\times\vec{E} &= -\mu\frac{\partial\vec{H}}{\partial t} \\ \nabla\times\vec{H} &= \vec{J}+\epsilon\frac{\partial\vec{E}}{\partial t} \\ \nabla\cdot\vec{E} &= \frac{\rho}{\epsilon} \\ \nabla\cdot\vec{H} &= 0 \end{aligned} \qquad 2$$

where $\vec{H}$ is the magnetic field intensity, μ is the permeability, ϵ is the permittivity, and $\vec{J}$ is the current density. Unfortunately these equations are very difficult, if not impossible, to solve exactly in all but a few simple

cases. As a result, approximations are usually made to simplify them.

Consider a medium with

$$\frac{\sigma}{\omega\varepsilon} >> 1 \qquad 3$$

where ω is the angular frequency. In this dielectric the conduction current is much larger than the displacement current. As a result, Maxwell's curl equations can be simplified to [71],

$$\nabla\times\vec{E} = -\mu\frac{\partial\vec{H}}{\partial t}$$

$$\nabla\times\vec{H} = \vec{J} \qquad 4$$

Further, assume that the system has dimensions much smaller than a wavelength λ in the dielectric where

$$\lambda = \frac{2\pi}{\omega}\left(\frac{\mu\varepsilon}{2}\left[1 + \left(\frac{\sigma}{\omega\varepsilon}\right)^2\right]^{\frac{1}{2}} + \frac{\mu\varepsilon}{2}\right)^{-\frac{1}{2}} \qquad 5$$

for a uniform plane wave [71, 50 on p. 335]. In such a case the eddy currents produced by the time varying magnetic field are insignificant. Hence, Maxwell's curl equations further simplify to [71],

$$\nabla\times\vec{E} = 0 \qquad 6$$

$$\nabla\times\vec{H} = \vec{J} \qquad 7$$

This is the quasi-static approximation. In fact, these equations are true only for static fields [71]. However, under the conditions outlined above they can be used to approximate time varying fields. Static fields are first evaluated then an $e^{j\omega t}$ time dependance is assumed to calculate heat deposition.

Equation 6 allows us to define a scalar potential $\Phi(x,y,z)$ such that

$$\vec{E} = -\nabla\phi \qquad 8$$

Substituting 8 into 6 gives,

$$\nabla\times(-\nabla\phi) = 0 \qquad 9$$

which is true because the curl of the gradient of a scalar is always zero [33]. Taking the divergence of 7 gives

$$\nabla\cdot\nabla\times\vec{H} = \nabla\cdot\vec{J} \qquad 10$$

The divergence of the curl of a vector is always equal to zero so we have [33]

$$\nabla\cdot\vec{J} = 0 \qquad 11$$

Now,

$$\vec{J} = \sigma\vec{E} \qquad 12$$

which substituted into 11 gives

$$\nabla\cdot(\sigma\vec{E}) = 0 \qquad 13$$

Substituting 8 into 13 gives

$$\nabla\cdot(\sigma(-\nabla\phi)) = 0$$

or

$$\nabla\cdot(\sigma\nabla\phi) = 0 \qquad 14$$

which is a form of the current continuity equation. This equation is solved numerically by MEGAERA to evaluate fields and temperature distributions inside lossy dielectrics.

Boundary conditions for Maxwell's equations are [33],

$$\hat{n}\times(\vec{E}_2 - \vec{E}_1) = 0 \qquad 15$$

and

$$\hat{n}\cdot(\varepsilon_2\vec{E}_2 - \varepsilon_1\vec{E}_1) = \rho_s \qquad 16$$

where $\vec{E}_1$ and $\vec{E}_2$ are the electric fields in media 1 and 2 respectively, $\hat{n}$ is the unit vector normal to the surface between the two media, and ρ_s is the surface charge on the boundary between 1 and 2. When the quasi-static approximation is applicable these boundary conditions are equivalent to

$$\sigma_1\vec{E}_{n_1} = \sigma_2\vec{E}_{n_2} \qquad 17$$

and

$$\phi_1 = \phi_2 \qquad 18$$

where σ_1 and σ_2 are the conductivities of media 1 and 2 respectively, $\vec{E}_{n1}$ and $\vec{E}_{n2}$ are the normal components of the electric field in media 1 and 2 respectively, and ϕ_1 and ϕ_2 are the potentials in media 1 and 2 respectively [30]. Equations 17 and 18 are used by MEGAERA when solving the current continuity equation 14 [30].

HEATING WITH COILS AND PLATE ELECTRODES

Tissues with high electrical conductivity (*ie.* muscle) tend to heat up more than those with low conductivity (*ie.* fat) when inductive coupling is used. This occurs because the applicators produce E fields which are usually parallel to the fat-muscle interface. Boundary conditions at the interface are such that,

$$\vec{E}_{tf} = \vec{E}_{tm} \qquad 19$$

where $\vec{E}_{tf}$ is the tangential field in the fat and $\vec{E}_{tm}$ is the tangential field in the muscle [figure 2.1]. The conductivity of the fat is lower than that in the muscle so the amount of power deposited in the fat is lower than that in the muscle. This can be expressed as,

$$\frac{P_f}{P_m} = \frac{\sigma_f |\vec{E}_{tf}|^2}{\sigma_m |\vec{E}_{tm}|^2} \qquad 20$$

where P_f is the power deposited in the fat, P_m is the power deposited in the muscle, σ_f is the fat conductivity, and σ_m is the muscle conductivity. From equation 19 we have

$$\frac{P_f}{P_m} = \frac{\sigma_f}{\sigma_m} \qquad 21$$

Since $\sigma_f < \sigma_m$ we have $P_f < P_m$.

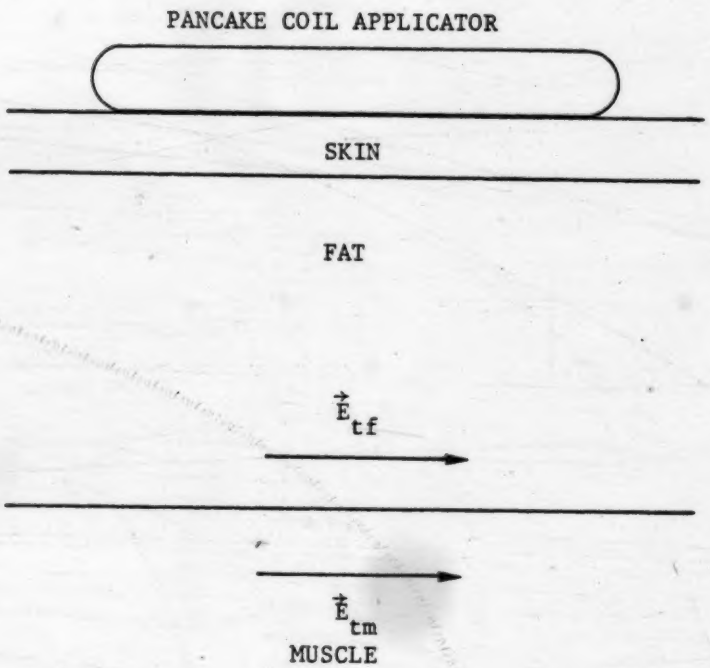

Figure 2.1 $\vec{E}$ - fields inductively coupled into tissue by coil type hyperthermia applicator.

The rationale for the high heat production by capacitive applicators in relatively low loss fat has been simply illustrated, as follows, by Christensen and Durney [16]:

Consider two long capacitor plates with fat and muscle dielectric layers between them (Figure 2.2). From Maxwell's equations we have

$$\nabla\times\vec{H} = \vec{J} + \frac{\partial(\varepsilon\vec{E})}{\partial t} = \sigma\vec{E} + j\omega\varepsilon\vec{E}$$

where an $e^{j\omega t}$ time dependence is assumed for $\vec{E}$, and σ is the dielectric conductivity which contains all loss terms. Taking the divergence of both sides gives

$$\nabla\cdot(\sigma + j\omega\varepsilon)\vec{E} = 0$$

Using Gauss' theorem and the usual pillbox argument ,across the boundary in Figure 2.2 [51 p. 95], it can be shown that

$$\varepsilon_f\vec{E}_{nf} = \varepsilon_m\vec{E}_{nm} \qquad 22$$

$\vec{E}_{nf}$ is the normal r.m.s. electric field in the fat, $\vec{E}_{nm}$ is the normal r.m.s. electric field in the muscle, ϵ_f is the permittivity in the fat and ϵ_m is the permittivity in the muscle. In the fat the average power absorbed per unit volume P_f is

$$P_f = \sigma_f|\vec{E}_{nf}|^2 \qquad 23$$

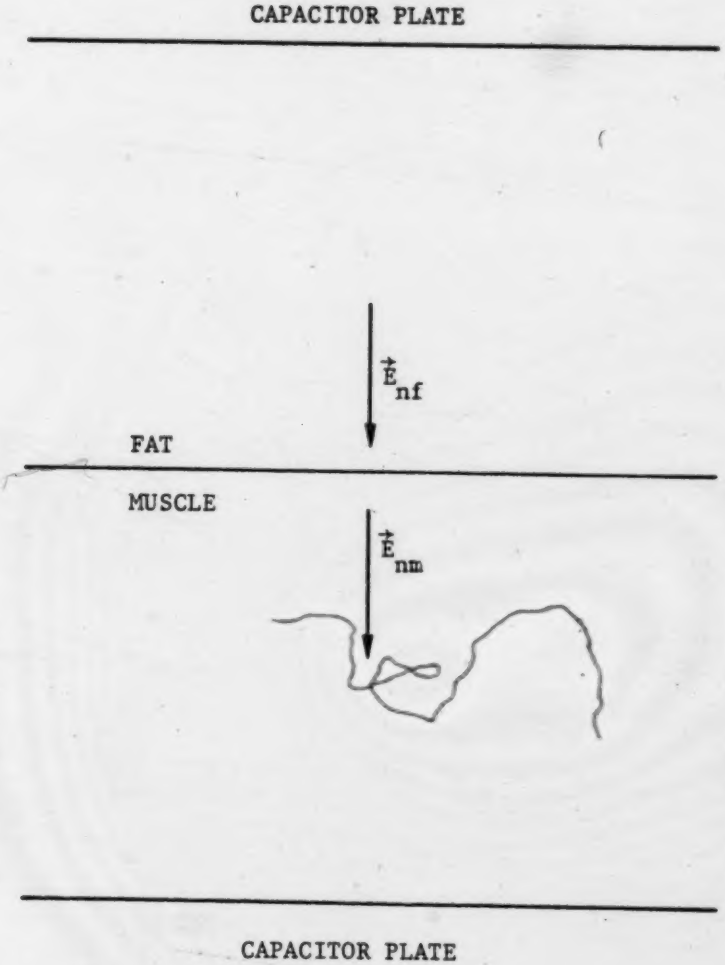

Figure 2.2 $\vec{E}$ - fields capacitively coupled into tissue by parallel plates.

where σ_f is the conductivity in the fat. Similarly, in the muscle P_m is

$$P_m = \sigma_m |\vec{E}_{nm}|^2 \qquad 24$$

where σ_m is the conductivity in the muscle. The ratio

$$\frac{P_f}{P_m} = \frac{\sigma_f |\vec{E}_{nf}|^2}{\sigma_m |\vec{E}_{nm}|^2} \qquad 25$$

describes the amount of power absorbed in a unit volume of fat relative to a unit volume of muscle. From equation 22 we have

$$\frac{|\vec{E}_{nf}|^2}{|\vec{E}_{nm}|^2} = \frac{|\epsilon_m|^2}{|\epsilon_f|^2} \qquad 26$$

At a frequency of 27.12 MHz we have for fat and muscle $\epsilon_m = 113 - j405.82$, $\epsilon_f = 20.0 - j7.23$, $\sigma_f = 1.09 \times 10^{-2}$ S/m, and $\sigma_m = 0.612$ S/m [16]. Thus,

$$\frac{\sigma_f}{\sigma_m} = 0.02 \qquad 27$$

which indicates more heating in muscle for

$$\vec{E}_{nf} = \vec{E}_{nm} \qquad 28$$

However,

$$\frac{|\vec{E}_{nf}|^2}{|\vec{E}_{nm}|^2} = \frac{|113-j405.82|^2}{|20.0-j7.23|^2} = 392.37 \qquad 29$$

Therefore,

$$\frac{P_f}{P_m} = (0.02)(392.37) = 7.85 \qquad 30$$

Or, there is more heat in the fat than in the muscle.

MEGAERA: THE FINITE DIFFERENCE APPROXIMATION

The following section, content and notation are drawn from the work of Hiebert [30].

MEGAERA uses a finite difference approximation to solve the current continuity equation

$$\nabla\cdot(\sigma\nabla\phi) = 0 \qquad 31$$

In two dimensions this equation is:

$$\frac{\partial}{\partial x}\left(\sigma\frac{\partial\phi}{\partial x}\right) + \frac{\partial}{\partial y}\left(\sigma\frac{\partial\phi}{\partial y}\right) = 0 \qquad 32$$

For the first term in eqn. 32 the finite difference approximation is:

$$\frac{\partial}{\partial x}\left(\sigma\frac{\partial\phi}{\partial x}\right) \simeq \left(\frac{2}{h_i+h_{i-1}}\right)\left\{\left(\frac{\sigma_{i+1}+\sigma_i}{2}\right)\left(\frac{\phi_{i+1}+\phi_i}{h_i}\right) - \left(\frac{\sigma_{i-1}+\sigma_i}{2}\right)\left(\frac{\phi_i-\phi_{i-1}}{h_{i-1}}\right)\right\} \qquad 33$$

where σ_i and ϕ_i are the conductivity and potential at the i^{th} location, and h_i is the distance between the i^{th} and the $(i+1)^{th}$ location [Figure 2.3]. A similar equation exists for the second term in eqn. 32.

The area of interest is divided up into numerous rectangular blocks with centres defined by (i,j) coordinates. Each block is assumed to be completely homogeneous with regard to electrical and thermal properties. If one applies the two dimensional finite difference equation to grid block number (i,j) and the four neighboring grid blocks [figure 2.3] an equation of the form

$$R_{i,j}\phi_{i,j+1}+S_{i,j}\phi_{i+1,j}+A_{i,j}\phi_{i,j}+C_{i,j}\phi_{i-1,j}+F_{i,j}\phi_{i,j-1} = 0 \qquad 34$$

results, where

$$\begin{aligned} R_{i,j} &= (\sigma_{i,j+1}+\sigma_{i,j})/\{k_j(k_j+k_{j-1})\} \\ S_{i,j} &= (\sigma_{i+1,j}+\sigma_{i,j})/\{h_i(h_i+h_{i-1})\} \\ A_{i,j} &= -R_{i,j}-S_{i,j}-C_{i,j}-F_{i,j} \qquad 35 \\ C_{i,j} &= (\sigma_{i-1,j}+\sigma_{i,j})/\{h_{i-1}(h_i+h_{i-1})\} \\ F_{i,j} &= (\sigma_{i,j-1}+\sigma_{i,j})/\{k_{j-1}(k_j+k_{j-1})\} \end{aligned}$$

and k_j is the distance between the (i,j) and (i,j+1) positions. These five equations, 35, in five unknowns are solved to find the coefficients in equation 34.

An equation similar to eqn. 34 is found for each grid block in the domain. The resulting system of equations forms a matrix which MEGAERA solves with the aid of an iterative relaxation method known as the Alternating

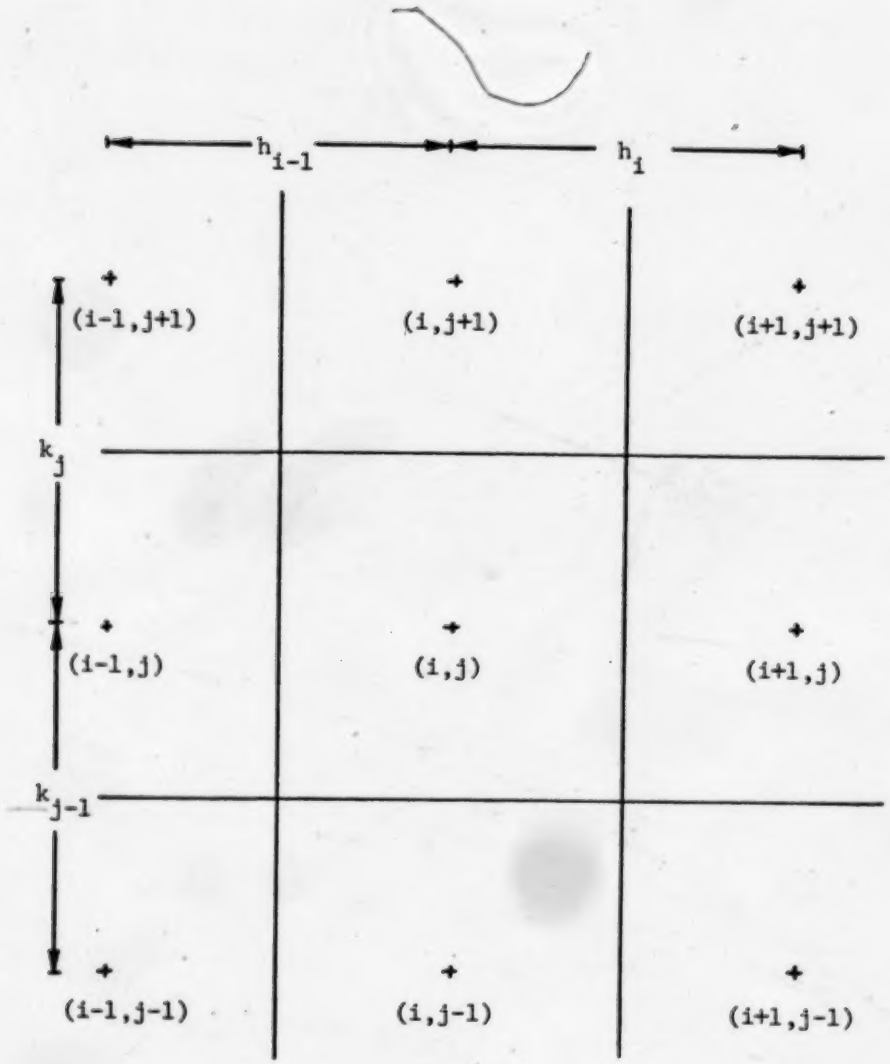

Figure 2.3 Grid block spacing and numbering used by MEGAERA.

Direction Implicit Procedure.

At the boundary between an insulator in grid (i-1,j) and a dielectric in grid block (i,j) the boundary condition,

$$\frac{\partial \phi}{\partial n} = 0 \qquad 36$$

where n is the normal, is satisfied by setting

$$\phi_{i-1,j} = \phi_{i,j} \qquad 37$$

If grid block (i-1,j) is an electrode then $\phi_{i-1,j}$ is known and a modification is made to its coefficient to allow for the assumed infinite conductivity. When grid block (i-1,j) has a different conductivity than block (i,j), the boundary conditions

$$\sigma_1 \vec{E}_{n_1} = \sigma_2 \vec{E}_{n_2} \qquad 38$$

and

$$\phi_1 = \phi_2 \qquad 39$$

are utilized to modify the coefficients.

As previously noted, the average heating rate produced by a sinusoidally varying electric field is given by

$$P = \sigma |\vec{E}|^2 \qquad 40$$

When evaluating the temperature distribution inside a dielectric the only heat transfer mechanism taken into account by MEGAERA is conduction. While convection and radiation play a part when heating an immersed agar cylinder their effect is small. Infra-red radiation does not penetrate far in water and convection does not take place in the agar gel at the temperatures used. The water bath is sufficiently large that it can be approximated by an infinite heat sink. Water jets are used to direct a flow of saline over the agar surface so convective effects between the agar and and water bath can be ignored.

The equation used by MEGAERA to model heat production and flow is

$$\frac{M\partial T}{\partial t} = \nabla\cdot(k\nabla T) + \sigma|\vec{E}|^2 \qquad 41$$

where M is the volumetric heat capacity in J/°Cm³, k is the thermal conductivity in W/m°C, T is the temperature in°C, and t is time in seconds. The finite difference approximation for the spatial portion of eqn. 41 is similar to that for the current continuity equation. For example, the term

$$\frac{\partial}{\partial x}\left(k\frac{\partial T}{\partial x}\right) \approx \frac{2}{h_i+h_{i-1}}\left(\left(\frac{k_{i+1,j}+k_{i,j}}{2}\right)\left(\frac{T_{i+1,j}+T_{i,j}}{h_i}\right)\right.$$

$$\left. - \left(\frac{k_{i-1,j}+k_{i,j}}{2}\right)\left(\frac{T_{i,j}-T_{i-1,j}}{h_{i-1}}\right)\right) \qquad 42$$

Boundary conditions are handled in a manner analogous to the electrical case. The time derivative in 41 is evaluated using the forward difference approximation,

$$\frac{M\partial T}{\partial t} \simeq M_{i,j}\frac{(T_{i,j}^{n+1} - T_{i,j}^{n})}{\Delta t^{n}} \qquad 43$$

where n refers to the number of the timestep and Δt is the size of the timestep. The heating rate term in eqn. 41 is calculated using the current continuity equation for the finite difference equation.

The thermal finite difference equation is solved by using the Alternating Direction Implicit Method. This method is used for parabolic partial differential equations while the previously mentioned Alternating Direction Implicit Procedure is used to solve elliptic equations.

Using the above methods and approximations Megaera is able to simulate r.f. heating. The power of the program is its ability to simulate the heating produced by any shape or combination of electrodes. The accuracy of this program is demonstrated in following sections and used extensively to model different electrode configurations.

METHODS AND MATERIALS

VOLUMETRIC HEAT CAPACITY MEASUREMENT OF AGAR

The temperature of a (2.6±0.05) cm diameter by (3.6±0.05) cm long agar cylinder was measured then placed in a thermos containing (230.0±3.0) gm of heated water (Figure 3.1). The thermos was capped with styrofoam which was securely taped in place. A wood handled stirring paddle and a thermocouple extended through the styrofoam cap into the heated water. A Fluke 2190A Digital Thermometer was connected to the copper-constantan thermocouple. Water bath temperature was monitored over a period of time to determine the amount of energy absorbed by the agar and the amount lost through the calorimeter. With the volume of agar and amount of energy it absorbed known the volumetric heat capacity C_v could be calculated.

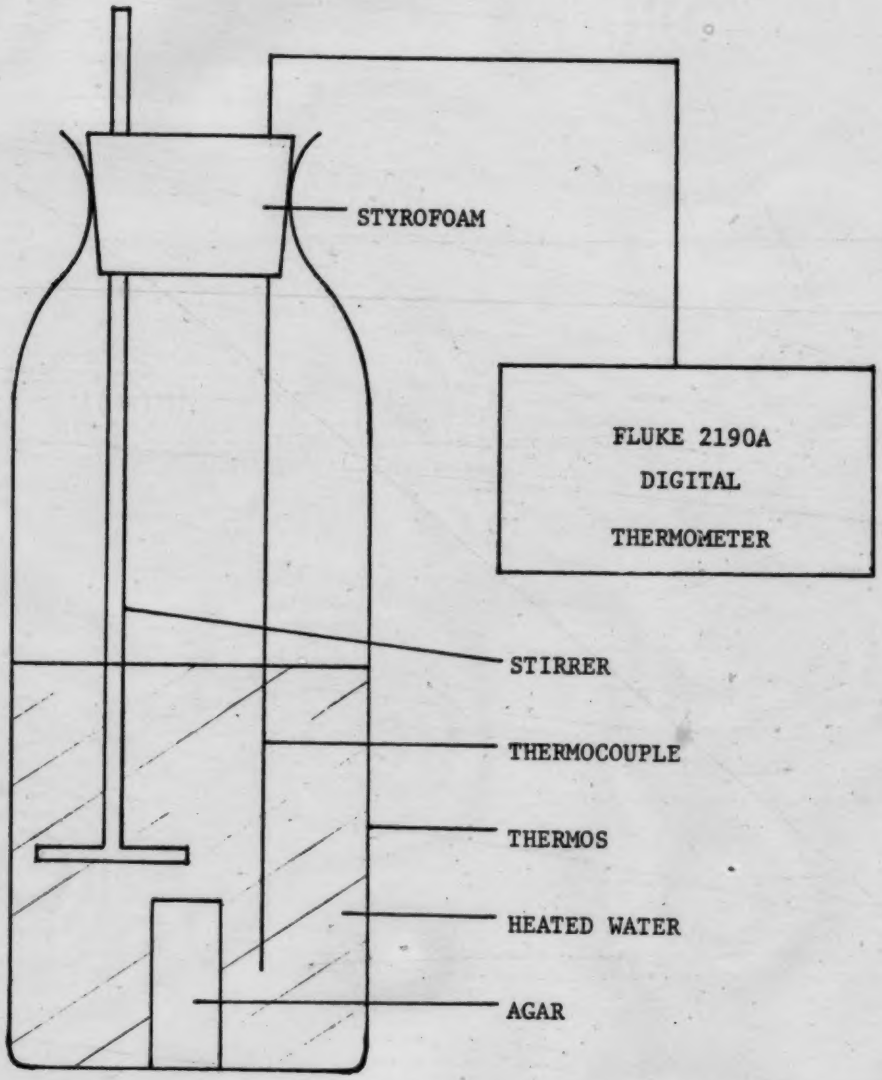

Figure 3.1 Apparatus used for heat capacity measurements.

Thermal Conductivity Measurement

To calculate the temperature distribution in r.f. heated agar the thermal conductivity k had to be measured. This was done using a measurement chamber belonging to the University of Alberta Applied Electromagnetics Group.

Two (15.2±0.3) cm diameter cylindrical sections of agar dielectric (0.9% NaCl, reagent grade, and 3% agar by weight dissolved in distilled water) were sandwiched between three brass disks (Figure 3.2). The upper agar slab was (1.15±0.03) cm thick and the lower slab (3.55±0.03) cm thick. The upper brass disk contained an electric heater coil and a copper-constantan thermocouple. Between the two agar slabs was a thin brass disk containing a thermocouple. The lower brass disk contained a water-flow heat sink and a thermocouple. Contact surfaces between the brass disks and agar were lightly coated with silicon Thermal Compound #120-8 (Wakefield Engineering Company) to ensure good heat transfer. Plastic film was wrapped around the sides of the agar slabs to retard evaporation. The agar and brass disks were insulated by 10 cm of styrofoam, top and bottom, and a minimum of 13 cm of styrofoam on the sides. For added support and insulation the whole chamber was contained in a tightly fitting plywood box.

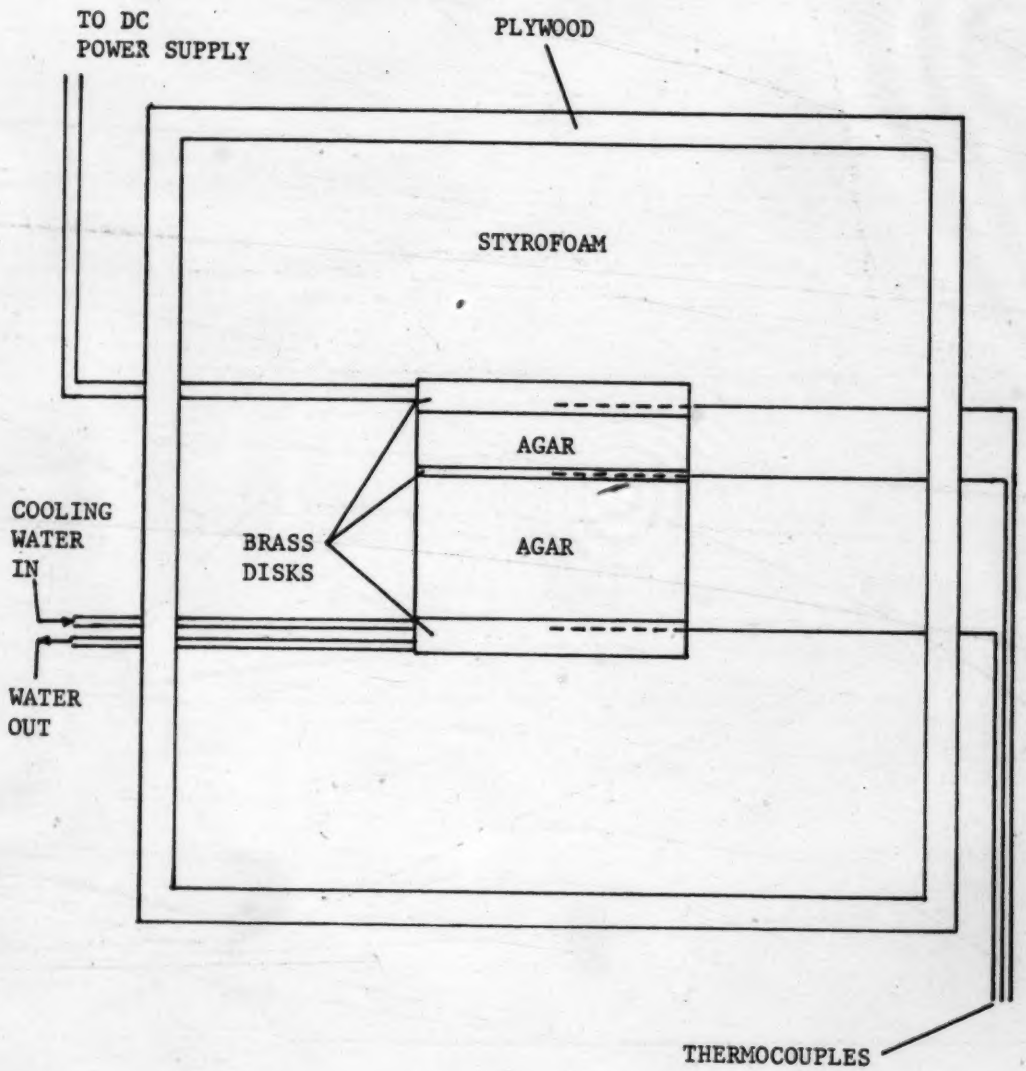

Figure 3.2 Chamber used for thermal conductivity measurements.

Power was supplied to the upper brass disk via an HP6439B D.C. Power Supply (Figure 3.3). A Keithley 168 Auto-ranging DMM and a Universal AVO Meter (10 amp scale) were used to measure voltage and current respectively. A Fluke 2176A Digital Thermometer was used to measure temperatures.

The middle brass disk allowed temperature measurements to be made between the heat source and heat sink. In this way three thermal conductivity measurements could be made at the same time. Measurements of k with the thin agar slab, the thick slab, and both slabs together compensated for convection along the sides of the agar.

The Fourier heat conduction equation [27]

$$Q=k\ A(T_1-T_2)/x$$

where, Q-input power (Watts)

A-surface area of agar cylinder top (m^2)

x-thickness of the agar slab (m)

T_1-temperature of the heated agar face (°C)

T_2-temperature of the cooled agar face (°C)

k-thermal conductivity (Watts/m°C),

was used to evaluate the thermal conductivity of the agar.

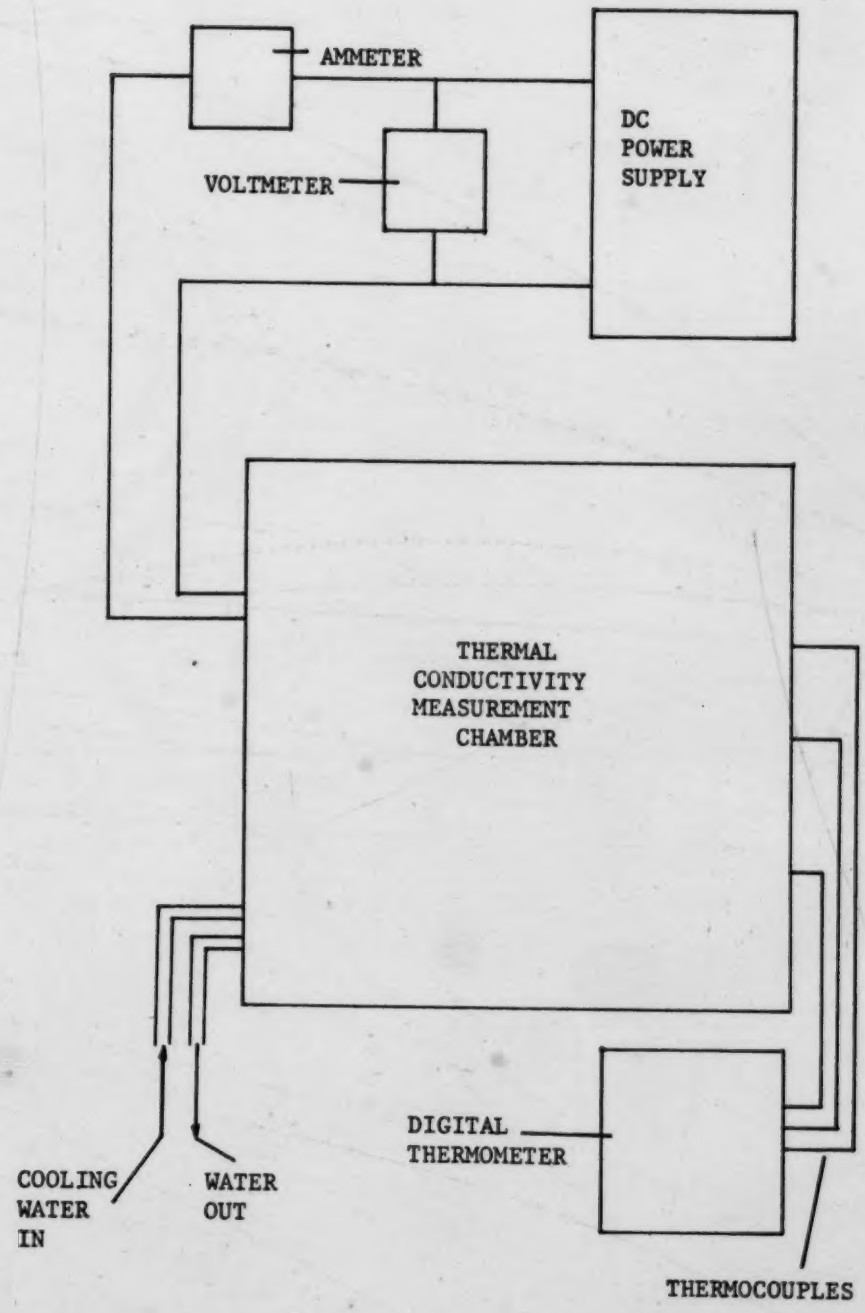

Figure 3.3 Apparatus used for thermal conductivity measurements.

Dielectric Measurements

The dielectric properties of the saline bath and agar cylinder were determined using a method described by Bottomley [7]. A nylon disk, 6 cm in diameter by 1 cm thick, had a 1 cm diameter hole drilled through its centre (Figure 3.4). The hole was countersunk on either end by concentric, 2 cm diameter, holes 0.35 cm deep. Two small holes, 1 mm in diameter, were drilled in opposing sides of the nylon disk, through to the central chamber. These holes were fitted with 19 gauge hypodermic needles and 10 cc syringes. The measuring cell was oriented so that the syringes were at the top and bottom of the disk. The lower syringe initially held the fluid to be measured and the top syringe acted as an overflow reservoir and drain for air bubbles. Non-liquid samples had to be carefully cut to size for the cell.

A silver plated copper disk, 2 cm in diameter, was placed in each countersunk hole and held in place by styrofoam blocks and plastic tie-straps. The area of contact between the nylon and electrodes was made waterproof with Dow Corning High Vacuum Grease. Short wires (5 mm long) were soldered to the electrodes and connected through an HP00601A component mounting adapter to an HP4815A Vector Impedance Meter (Figure 3.5). Frequency

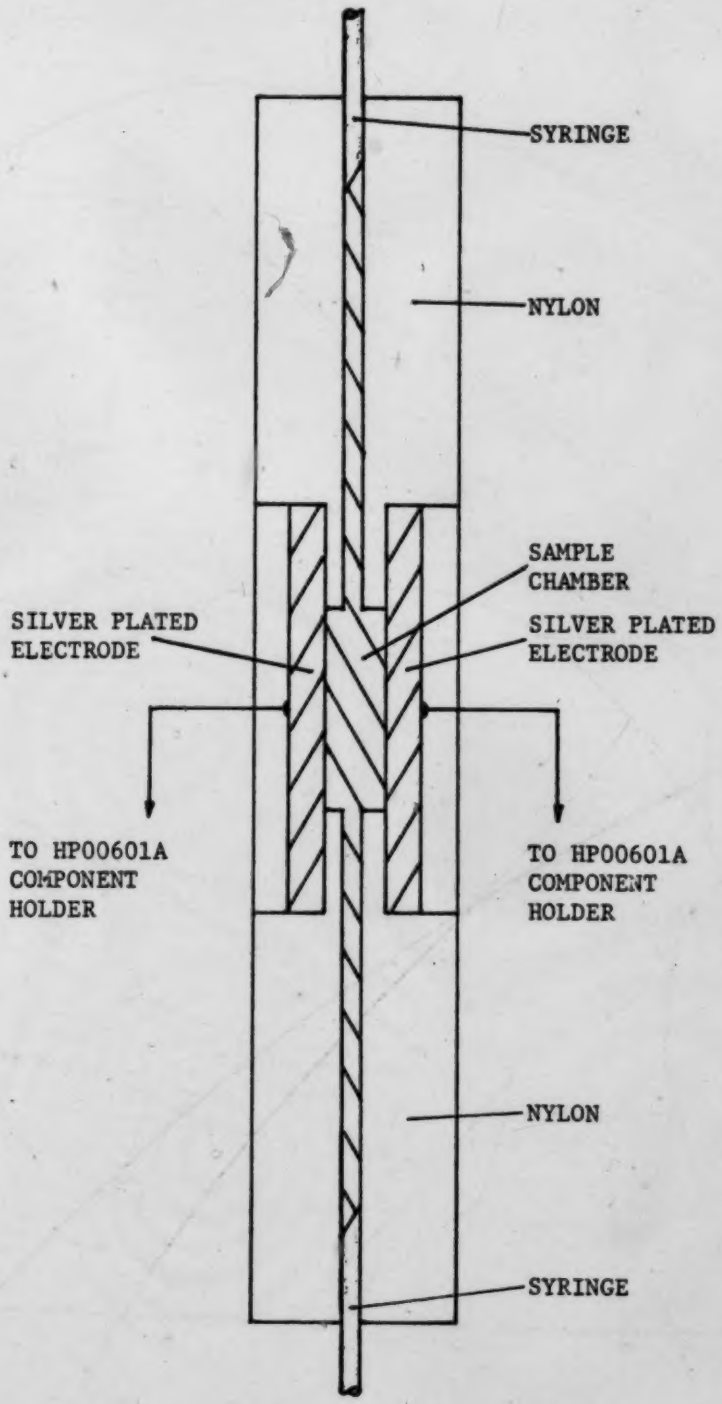

Figure 3.4 Dielectric measurement cell.

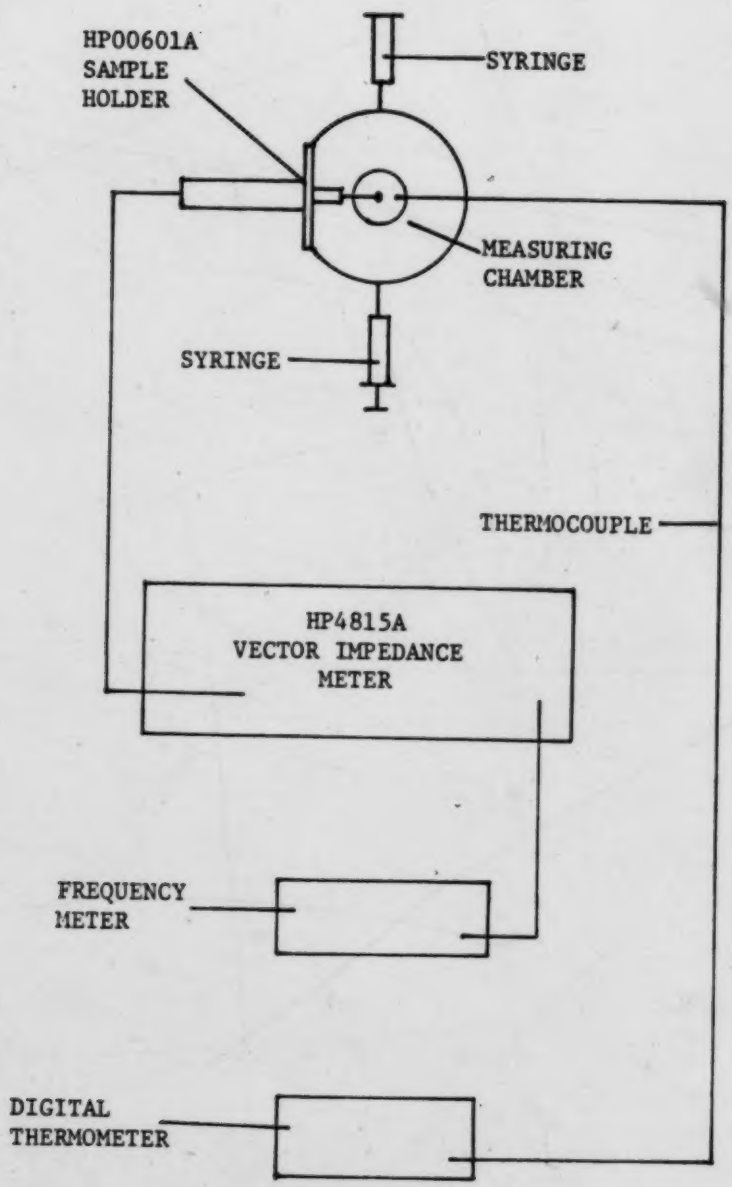

Figure 3.5 Apparatus used for dielectric measurements.

was monitored with a Fluke 1900A Multi-Counter. The sample temperature was monitored with a copper-constantan thermocouple, in contact with the ground electrode, and a Fluke 2100A Digital Thermometer.

The conductivity and relative dielectric constant of a sample in the cell can be shown to be [Appendix #4]

$$\sigma = \frac{z\cos\phi}{\ell(z^2-2\omega L_p \sin\phi+\omega^2 L_p^2)}$$

and

$$\varepsilon_r = \{\frac{\omega L_p - z\sin\phi}{\omega(z^2-2\omega L_p z\sin\phi+\omega^2 L_p^2)} - (C_o+C_p)\frac{1}{\varepsilon_o \ell}$$

where, σ-the sample conductivity

z-the magnitude of the measured impedance

ϕ-the phase angle of the vector impedance

ℓ-the cell constant

ω-the angular frequency

L_p-the probe inductance

C_o-the empty cell capacitance

C_p-the probe capacitance

ϵ_r-the sample relative dielectric constant

ϵ_o-the permittivity of free space.

The cell was calibrated by measuring the impedance of low conductivity liquids, with known dielectric properties.

A frequency of less than 5 MHz was used so that L (about 10 nH) could be neglected. In this case the simplified expressions

$$\sigma \simeq \frac{\cos\phi}{\ell z}$$

and

$$\varepsilon_r \simeq -\{\frac{\sin\phi}{\omega z} + (C_o+C_p)\}\frac{1}{\varepsilon_o \ell}$$

could be used. A graph of ϵ_r vs. $-(\sin\phi)/\omega z$ was plotted giving a straight line with a slope of $(\epsilon_o \ell)^{-1}$ and a y-intercept of $-(C_o+C_p)/\epsilon_o \ell$ (Figure 3.6 and Tables 3.1 and 3.2). Values of $(\epsilon_o \ell)^{-1}=6.11\times10^{12}F^{-1}$ and $(C_o+C_p)=4.73$ pF were obtained.

PLOT OF ε_r vs. $\frac{\sin\phi}{\omega z}$ FOR LOW CONDUCTIVITY MATERIALS IN DIELECTRIC MEASURING CELL

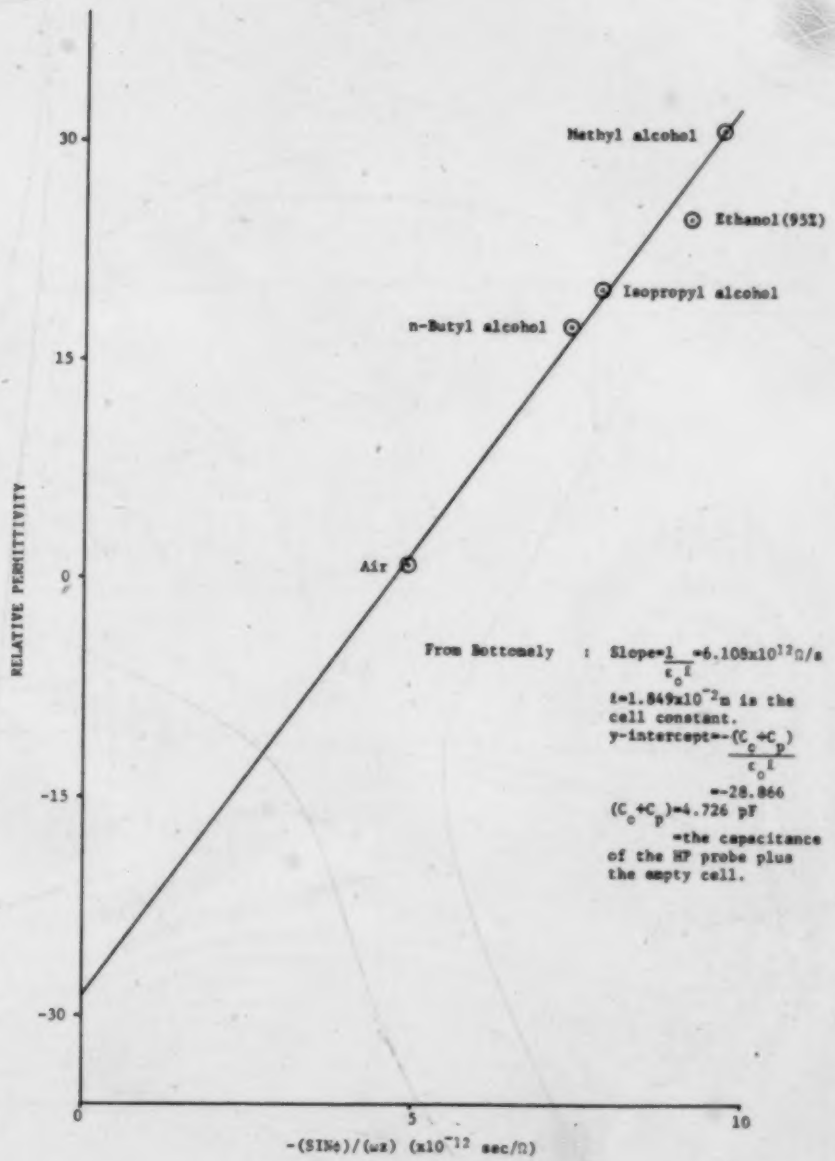

FIGURE 3.6

TABLE 3.1 Calibration Fluids For Dielectric Measuring Cell

DIELECTRIC	FREQ. (MHz)	$\epsilon_r[30]$*	$\frac{\sin\phi}{\omega z}$ ($\times 10^{-12}$) (s/Ω)
METHYL ALCOHOL	1.0	31.0	9.705
	10.0	31.0	9.531
ETHANOL (95%)	1.0	24.5	9.043
	10.0	24.1	8.992
ISOPROPYL ALCOHOL	1.0	20.1	7.860
	10.0	20.1	7.726
n-BUTYL ALCOHOL	1.0	17.4	7.437
	10.0	17.4	7.368
AIR	1.0	∿1.0	4.974

*AT 25°C.

Temperature Distributions

An agar cylinder (0.9% NaCl, reagent grade, and 3% agar, by weight dissolved in distilled water), 10 cm in diameter by 3 cm thick, was immersed in 300 litres of saline solution (0.9% NaCl, by weight, dissolved in tap water) contained in a large polyethylene tank. The saline and agar were found to have similar dielectric properties. The conductivity of the saline at 3.75 MHz was measured to be $\sigma_s = (2.01 \pm 0.03)$ S/m. For agar the conductivity was $\sigma_A = (1.99 \pm 0.03)$ S/m. From published literature the relative permittivities of the agar and saline, at 3.75 MHz, were estimated to be $\epsilon_s = \epsilon_A = 80 \pm 2$ [31, 32]. The similarity in electrical properties permitted good coupling of the r.f. to the agar and decreased the sensitivity of r.f. absorption to any irregularities in the agar shape. Saline prevented salt leaching from the agar, kept the dielectric homogeneous, and acted as a heat sink to cool the agar surface. The cylinder was thermally insulated on its top and bottom faces by styrofoam caps which reduced heat loss except in the radial direction. The caps were wrapped in plastic film and sealed with Dow Corning Silicone Sealer to keep water absorption from compromising their insulating ability. A plexiglass clamp held the agar cylinder and styrofoam caps securely below the saline surface (Figure 3.7).

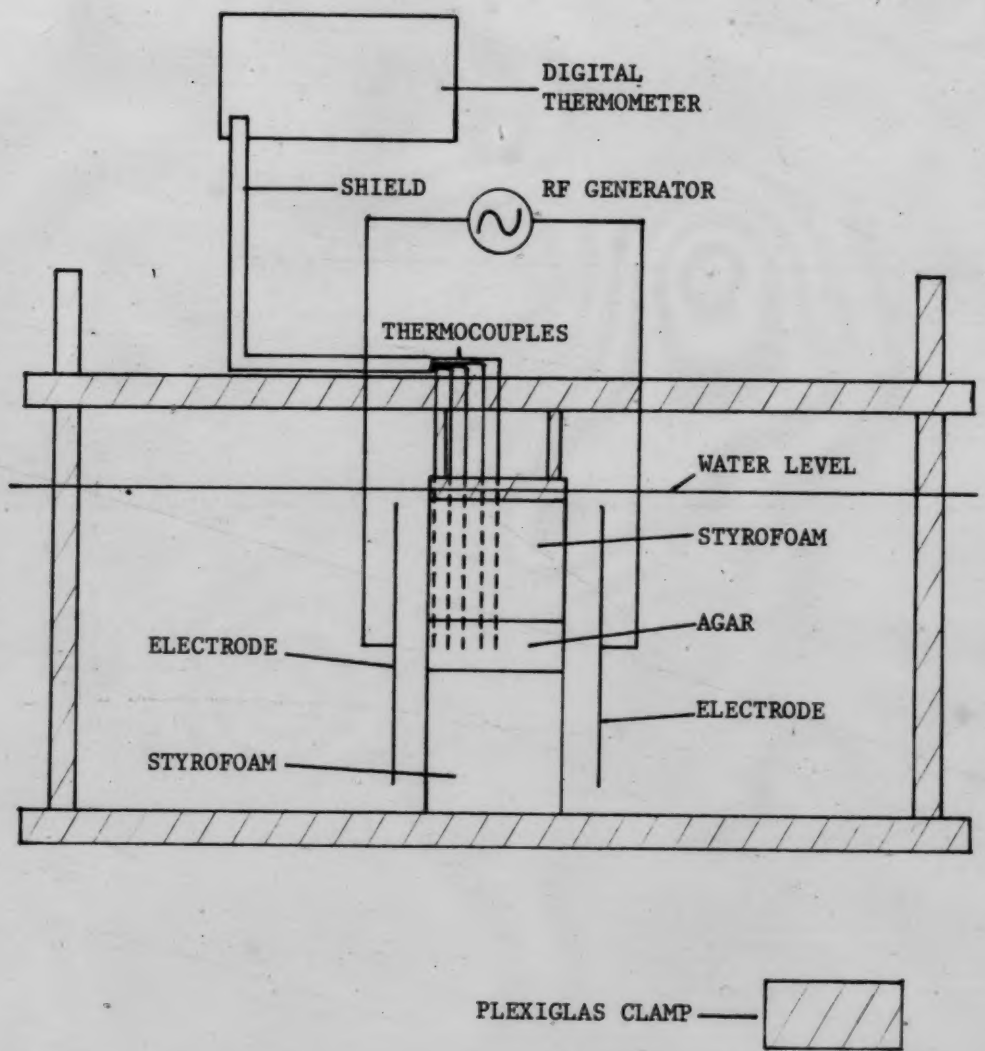

Figure 3.7 Apparatus used for heating agar cylinder.

The irradiating electrodes were each 1 cm wide by 15 cm high and made from flat silver-plated copper. Tall electrodes produced an $\vec{E}$-field in the 3 cm high agar cylinder. The $\vec{E}$-field did not vary greatly in the axial direction (Appendix #3). This permitted two dimensional simulation of the heating to be made. The electrodes were supported by nylon posts and could be made to revolve around the agar in an oscillatory manner, or held stationary. Amplitude and speed of oscillation as well as electrode distance from the agar surface could be varied (Figure 3.8).

R.F. power was provided by an HP615A Test Oscillator and amplified by an Electronic Navigation Industries Inc. ENI A-300 R.F. Power Amplifier. The oscillator was powered through a GraLab 600 Timer. A Decca KW-109 Supermatch was used to match the amplifier to the load (Figure 3.9). 'Low' frequency matching was optimized by the KW-109, and the electrode configuration used, at (3.75±0.02%) MHz. Frequency was monitored with a Fluke 1900A Multi-Counter.

Temperatures were measured at nine points in the agar and one in the water bath. Copper-constantan thermocouples (1 mm diameter), a Fluke 2190A Digital Thermometer and a Fluke Y2100 Thermocouple Selector were used to make temperature measurements. The thermocouples were oriented

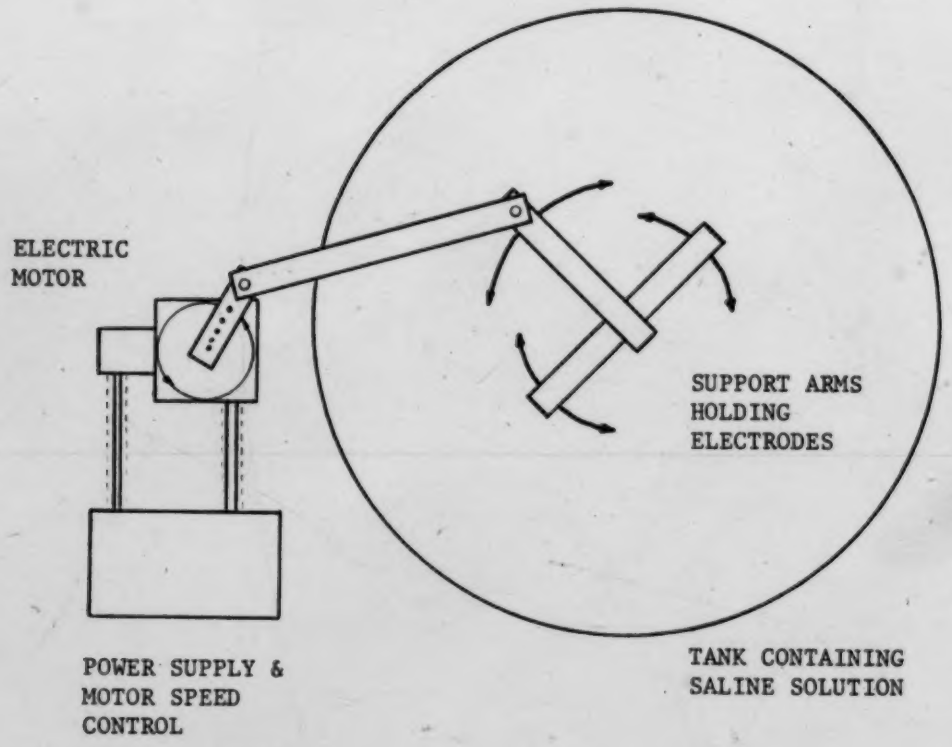

Figure 3.8 Apparatus used to move electrodes around heated medium.

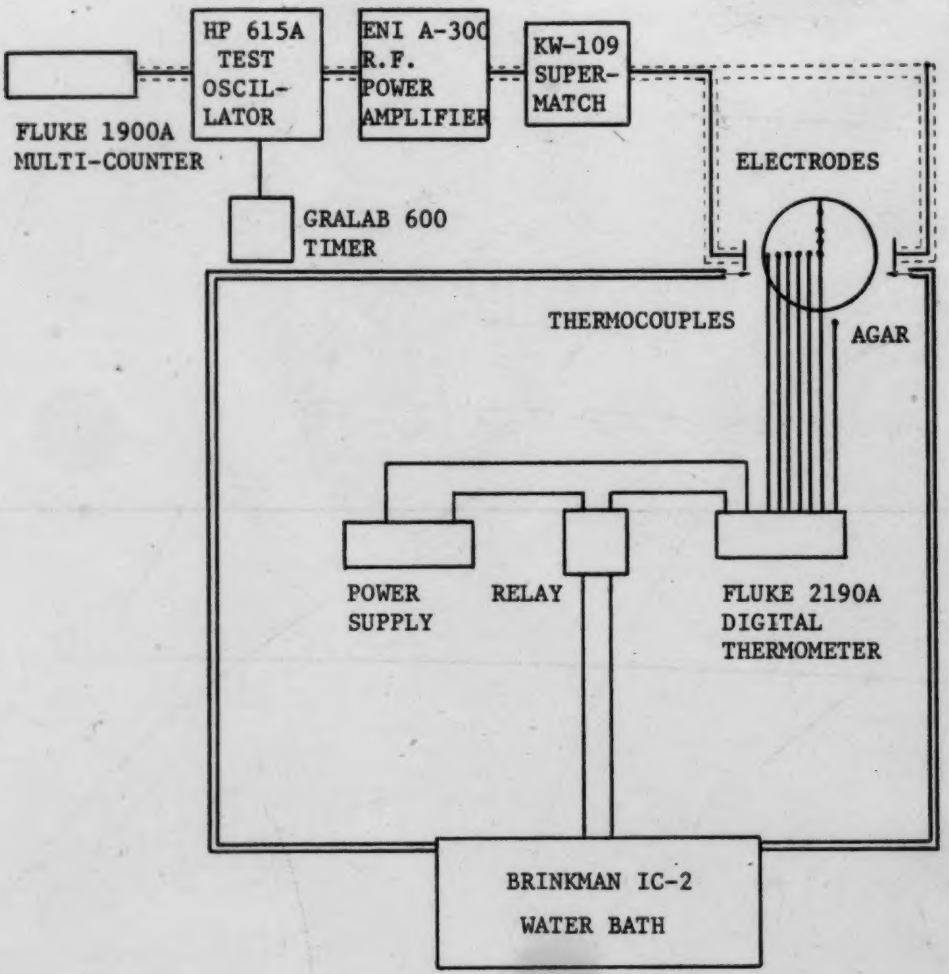

Figure 3.9 Apparatus used to maintain saline bath temperature and heat agar cylinder.

perpendicular to the $\vec{E}$-field to minimize current induction and artifactual heating. They were implanted to a depth mid-way down the length of the agar cylinder and along two radial lines perpendicular to each other. One line was set parallel to the stationary electrode $\vec{E}$-field (Figure 3.9).

The -water bath and agar were maintained at a temperature of (22.1±0.1)°C by a Brinkman IC-2 water bath pump/heater. The Brinkman was controlled by the Fluke 2190A through a relay, forming a feedback loop. A water bath temperature just above room temperature was chosen to avoid the need for a heater/refrigerator unit. Water jets located beside each electrode directed the flow of saline over the surface of the agar to aid cooling.

With thermocouples in place and the digital thermometer switched off, the agar was irradiated for 10 minutes at an output power of 200±10 Watts. The r.f. amplifier was then turned off and all ten temperature sites monitored over a period of about 6 minutes.

A curve fitting computer program was used to extrapolate the cooling curve data for each thermocouple back to the time the r.f. was terminated [23]. The program gave various statistics to indicate the reliability of each extrapolated point (Figure 3.10 and Table 3.2). The curve-fitting program was used to avoid

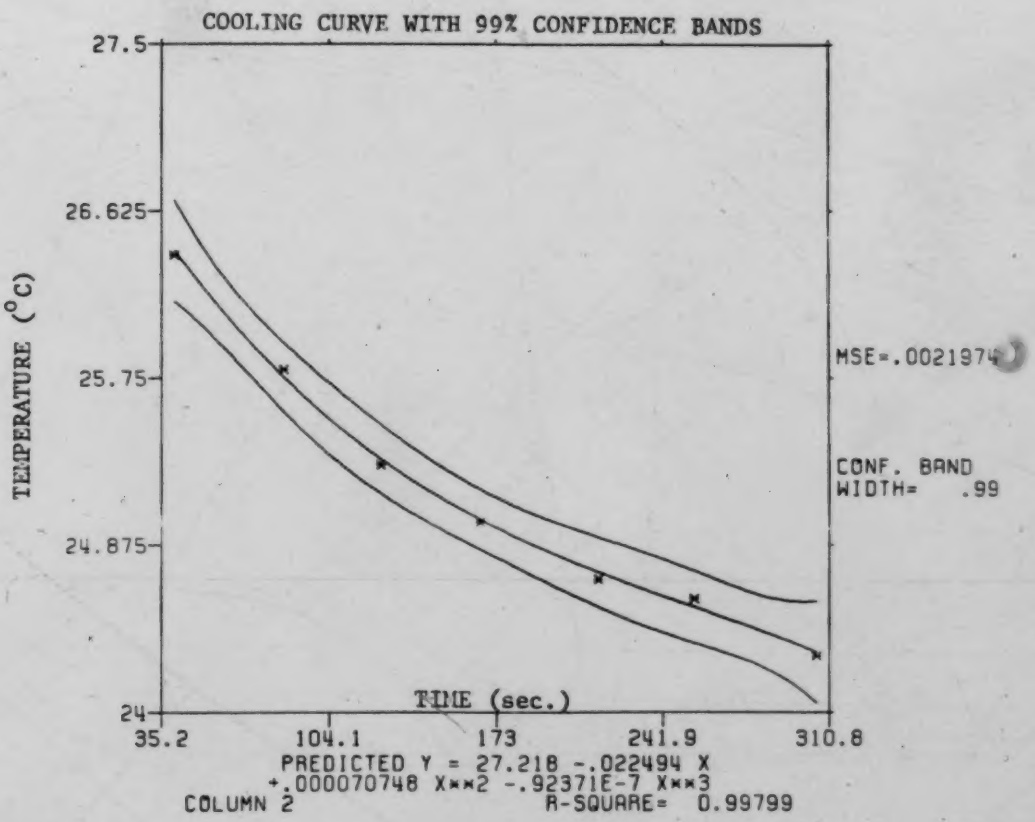

FIGURE 3.10

TABLE 3.2 Fitted and Measured Cooling Curve Points

FITTED Y	RESIDUAL	MEASURED Y
26.417084	-0.017104242	26.4
25.754410	0.045592960	25.8
25.322357	-0.022365056	25.3
25.007858	-0.007870853	25.0
24.731842	-0.031847052	24.7
24.550949	0.049049184	24.6
24.315445	-0.015454937	24.3

any bias in plotting the cooling curves. This procedure was repeated for several different orientations between the electrodes and thermocouples. Then the agar cylinder was cut in half to determine more accurately the position of each thermocouple. These data were then used to plot the temperature distribution inside the agar cylinder after 10 minutes of exposure to the r.f.

Data points obtained as above resulted in a fairly coarse temperature distribution (Figure 3.11). Plots of temperature vs. angle were made for various radii from the centre of the agar phantom (Figure 3.12). From these curves temperatures at points which were not measured could be estimated. In this way a denser field of temperature data could be obtained for improved plot production.

To predict temperature distributions resulting from moving electrodes, computer programs were written which used static-electrode temperature distributions as data (Appendix #1). These programs calculated a weighted average temperature over a specific radius and arc length inside the agar. Radii of 0,1,2,3,4, and 4.85 cm were used. The arc length corresponded to the orbit of the electrodes and the calculation considered the variation in temperature along its length. For the measurements considered here the arc length was $\pm 40°$ or $80°$ total.

TEMPERATURES MEASURED INSIDE AGAR CYLINDER

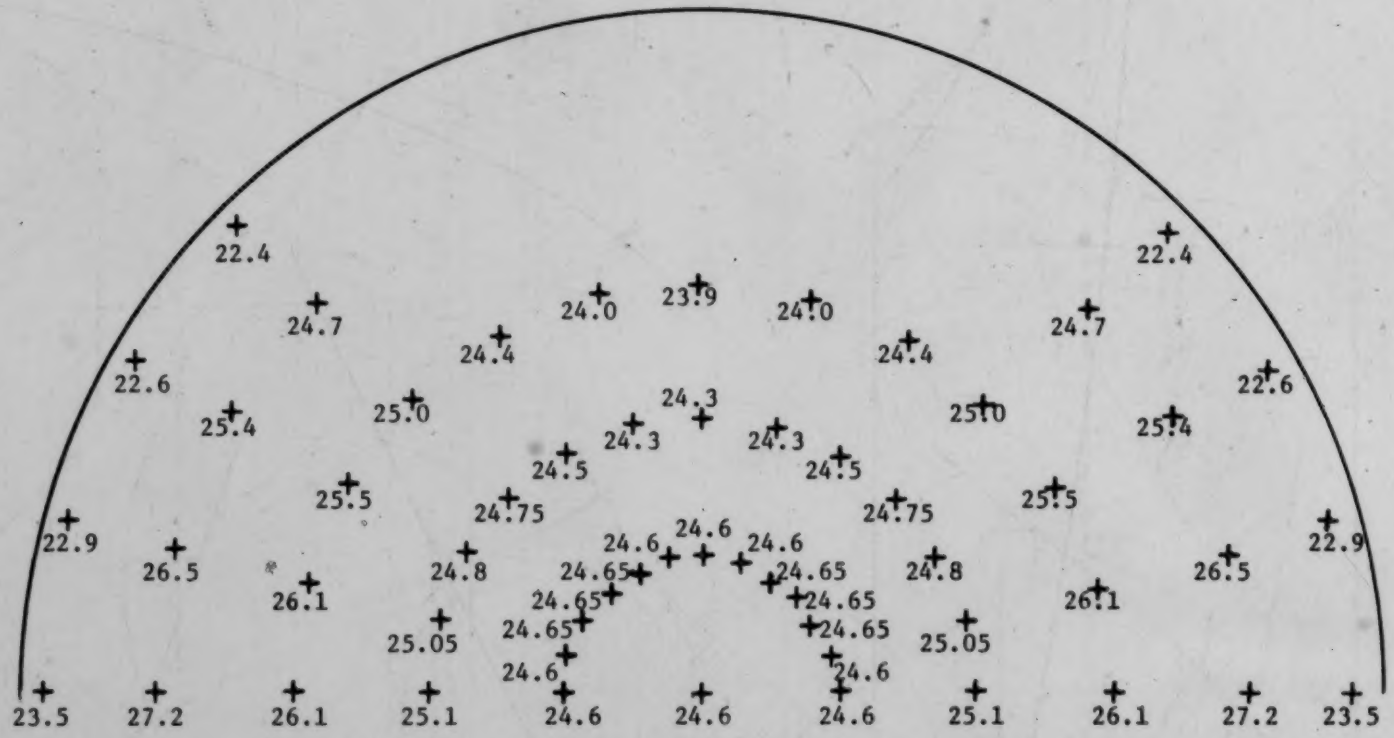

FIGURE 3.11 - One half of cylinder shown viewed from above. Electrodes each (1.95±0.1) cm from agar and situated along flat portion of semi-circle.

PLOT OF TEMPERATURE vs ANGLE FOR VARIOUS RADII IN R.F. IRRADIATED CYLINDER

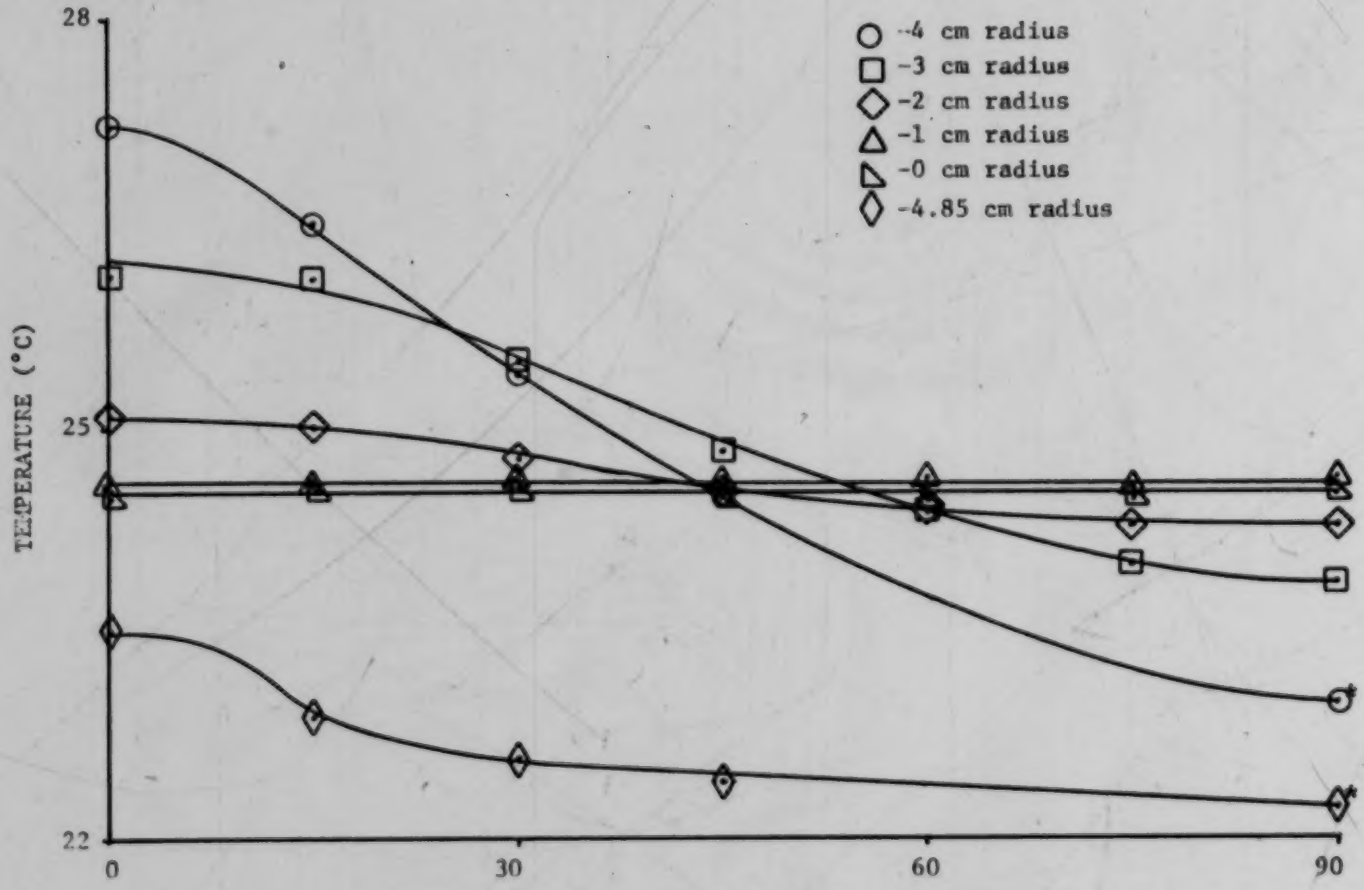

FIGURE 3.12

*Extrapolated from previous experiments

The weighting functions used to calculate the average temperatures were based on the electrode motion. This resulted from the fact that the temperature increase at a given point was inversely proportional to the speed of the electrode past that point. In other words the temperature increase varied proportionally with exposure time to a particular $\vec{E}$-field.

Assuming that the electrode speed varied sinusoidally from 0 m/s at the beginning of its swing, to some maximum at the centre of the swing, and back to 0 m/s at the end of its swing the following weighting function would result:

$$T=0.0470T_0+0.0501(T_1+T_{-1})+0.0614 (T_2+T_{-2})+0.0941(T_3+T_{-3}) +0.2709(T_4+T_{-4}) \quad 44$$

where, T-the averaged temperature, in °C, which would occur at the centre of an 80° arc

T_0-the temperature, in °C, measured at the centre of the arc.

T_n -the temperatures, in °C, measured at ±(10xn)° respectively, from the centre of the arc.

n=0,1,2,3, or 4.

The constants in equation 44 are inversely proportional to the velocity of the electrodes over that point in the arc. The sum of the constants over one entire

arc is normalized to unity. By applying the weighting function to the static electrode temperature data a plot of temperatures (which would result from electrodes with a sinusoidally varying speed) was obtained.

Water resistance and play in the electrode moving assembly prevented a true sinusoidal variation in electrode speed from occurring. The electrode speed variation closely resembled a flattened sinusoid or half circle. For the circular speed variation the weighting function was

$$T=0.0811T_0+0.0832(T_1+T_{-1})+0.0905$$
$$(T_2+T_{-2})+0.1088(T_3+T_{-3})+ 0.1770(T_4+T_{-4})$$

The flattened sinusoid was approximated by averaging the circular and sinusoidal functions. This weighting function was

$$T=0.0641T_0+0.0666(T_1+T_{-1})+0.0760$$
$$(T_2+T_{-2})+0.1014(T_3+T_{-3})+ 0.2240(T_4+T_{-4})$$

Temperature distributions calculated using the weighting functions were compared with measured data. The data was measured in the agar along 0°, 45°, 90°, and 135° radial lines (Figure 3.13).

Figure 3.13 Top view of agar cylinder showing radial lines along which temperatures were measured.

Great care had to be taken to ensure that the agar phantom did not move during a set of measurements. Further, the phantom had to be carefully positioned so that it was concentric with the electrode axis of rotation. If the phantom moved off centre the stationary electrode heating data would not be useful. As the electrodes moved their distance from the phantom would change. This would cause a change in the $\vec{E}$-field with electrode position which would invalidate the technique used to produce static electrode temperature maps. As a result, only temperature patterns obtained from electrodes moving along a path concentric with the phantom were used.

Non-concentric electrode motion could have been considered if provision was made for rotating the phantom. Care would have to be taken to ensure that the thermocouples did not move inside the agar. Complete temperature maps of the inside of the agar would have to be made for many electrode positions. These maps could then provide the data necessary to predict the moving electrode temperature distribution. Computer simulation of the above case would require numerous Megaera runs to simulate the various electrode positions. This entire amount of data would then be averaged together and weighted according to the electrode speed to produce a moving electrode temperature map.

The non-concentric electrode motion could prove useful with regard to moving and shaping an internal hot spot in agar. It was not examined in this work primarily because of the increased cost in computer time that would have resulted. In addition, the geometry of the problem indicates that concentric electrode movement would result in a higher centre temperature to peak temperature ratio than non-concentric motion. Further, the inhomogeneity of humans would be such that accurately shaping and steering an r.f. induced hot spot would be nearly impossible. So the concentric motion case would be of greatest interest for producing deep heating in a clinical situation without overheating superficial tissues.

Live Animal Measurements

A 3.5 kg male cat was anaesthetized (Nembutol) and shaved around the lower half of its torso. A midline incision was made in the ventral surface and the right kidney exposed by dissection. The right renal artery and vein were tied off to stop blood flow to the kidney. In this way the kidney roughly modelled a solid tumor. A stab wound was made just below the animal's right shoulder blade. Copper sheathed copper-constantan thermocouples were passed through the wound to the kidney site. Thermocouples were embedded in tissue along a line intersecting the centre axis of the cat and the right kidney. Thermocouples were also placed along a line perpendicular to this. As much as possible, the thermocouples were kept perpendicular to the $\vec{E}$-field. The incision was closed using 3-0 silk and waterproofed with vaseline. A cylindrical cloth harness held the animal upright with its head above the saline. The harness held the cat between the rotating electrodes and kept the animal's torso cylindrical. The electrodes were each 2 cm wide by 4 cm high and made from silver plated copper. The animal was approximately 12 cm in diameter and the electrodes about 4 cm from its skin. To avoid producing hypothermia in the cat the saline bath was maintained at 37.5°C. The animal was irradiated for 20 minutes at an

output power of (250±10) watts. Electrodes orbited around the cat in an oscillatory manner through an arc of 80°. Temperatures were measured as with the agar.

DATA AND RESULTS

MEASUREMENT OF VOLUMETRIC HEAT CAPACITY OF AGAR

Data obtained from volumetric heat capacity measurements are shown in Table 4.1. The water was initially at (66.3±0.1)°C and the agar cylinder at (20.1±0.1)° C. When the agar was placed in the calorimeter the water temperature began decreasing exponentially [Figure 4.1]. After 1000 seconds the temperature began decreasing linearly. The exponential decrease was the result of energy absorption by the agar. Energy leaking from the calorimeter produced the linear portion. By extrapolating the straight portion of the curve to t=0 seconds the loss of heat through the calorimeter could be accounted for. Figure 4.1 indicates that the water decreased (3.5±0.2)°C as a result of the agar, conversely the agar increased (42.7±0.2)°C as a result of the water. The total amount of energy absorbed by the agar was

$$U_{AGAR} = (3.5\pm0.2)°C \times (230.0\pm3.0)gm = (805\pm33.8)cal$$
$$= (805\pm33.8)cal \times 4.184\ J/cal = (3368.1\pm141.4)J$$

Heat capacity is the amount of energy (J) absorbed by a material, divided by the change in temperature (°C) of the material. So, the heat capacity for the agar was

$$C = (3368.1\pm141.4)J/(42.7\pm0.2)°C = (78.9\pm3.7)J/°C$$

TABLE 4.1 Water temperature in calorimeter versus time.

TIME (seconds)	TEMPERATURE (±0.1 °C.)
0.	66.3
60.	65.6
100.	65.4
180.	64.5
300.	63.8
420.	63.2
600.	62.8
660.	62.7
720.	62.6
780.	62.55
840.	62.4
960.	62.4
1020.	62.3
1080.	62.3
1140.	62.25
1500.	62.1
2000.	61.8

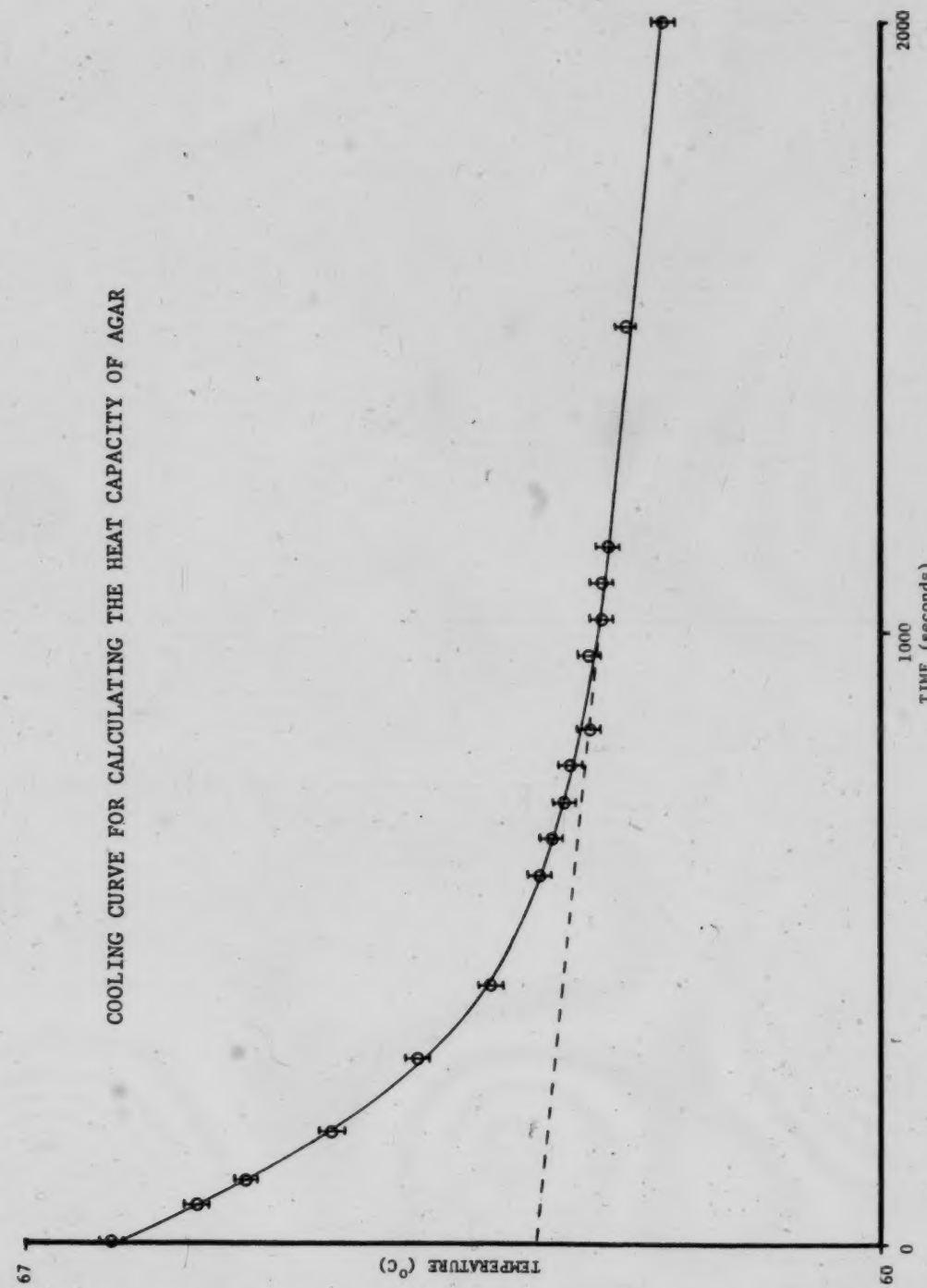
COOLING CURVE FOR CALCULATING THE HEAT CAPACITY OF AGAR
TEMPERATURE (°C)
67
60
0
1000
2000
TIME (seconds)

FIGURE 4.1

The volumetric heat capacity, used by Megaera, is the heat capacity of the material per unit volume (m^3). For the agar sample used, this gave a volumetric heat capacity of

$$C_v = (78.9 \pm 3.7) J/°C \times (5.2 \pm .03) \times 10^6 m^3$$
$$= (4.1 \pm 0.4) \times 10^6 J/°C\ m^3$$

THERMAL CONDUCTIVITY MEASUREMENT FOR AGAR

From the Fourier heat conduction equation

$$k=(Q\ x)/A(T_1-T_2)=(I\cdot V\cdot x)/A(T_1-T_2).$$

For the (1.15±0.03)cm thick slab of agar, using the data in Table 4.2,

$$k=(0.52\pm0.03)W/m°C$$

Table 4.3 shows values obtained for different thicknesses of agar.

Inaccuracy in the k measurement increased with increasing slab thickness. This occurred because energy was more readily lost through air convection around a thick slice of agar and imperfect insulation. Unfortunately the precision with which the thermal conductivity could be calculated was inversely proportional to the agar slab thickness. This was a result of uncertainty in the slab thickness. To arrive at a reasonable approximation for the thermal conductivity of the agar, regression analysis was used to find the thermal conductivity for a "0.0 cm" thick slab (Figure 4.3).

The straight line graph in figure 4.3 was determined using [8],

TABLE 4.2 Temperature measured at three sites in agar cylinder for given voltage and current .

SITE *	TEMPERATURE (^{o}C)
1	39.4
2	32.2
3	11.1

Voltage = (3.505±0.005) V.

Current = (1.7±0.01) A.

* See Figure 4.2.

TABLE 4.3 Thermal conductivity, k, measured for various thicknesses of agar.

AGAR THICKNESS (cm)	T_1-T_2 (^{o}C)	k (W/m^{o}C)
1.15±0.03	7.2±0.1	0.52±0.03
3.55±0.03	21.1±0.1	0.55±0.015
4.70±0.03	28.3±0.1	0.55±0.01

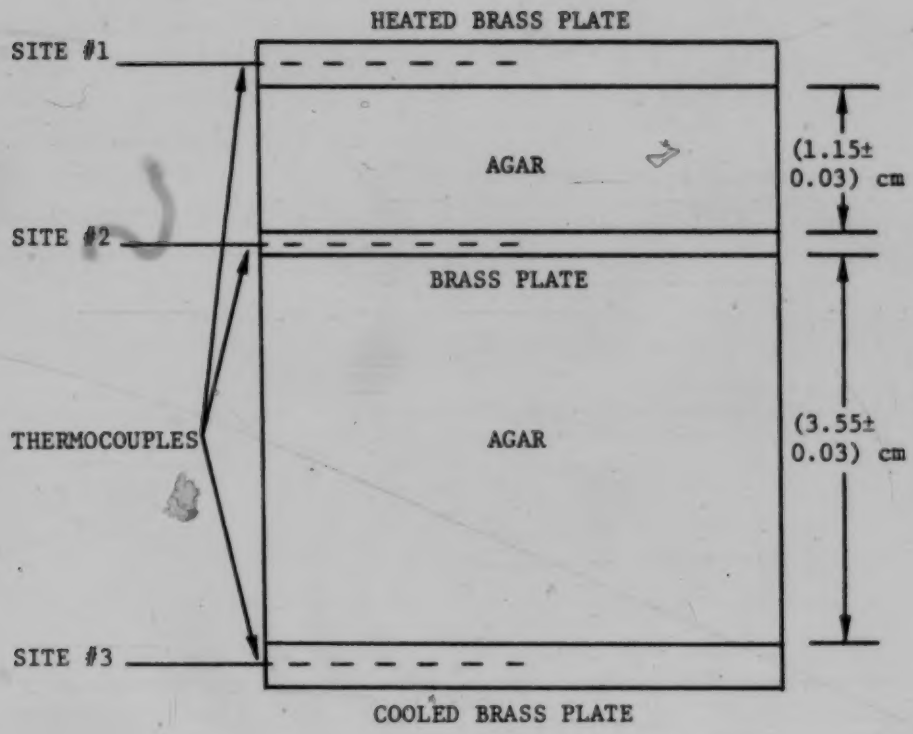

Figure 4.2 Arrangement of materials and apparatus inside the thermal conductivity measurement chamber.

$$a = \frac{\Sigma x^2 \Sigma y - \Sigma x \Sigma xy}{n\Sigma x^2 - (\Sigma x)^2}$$

$$b = \frac{n\Sigma xy - \Sigma x \Sigma y}{n\Sigma x^2 - (\Sigma x)^2}$$

where n=3 and, for a line of the form y=a+bx, the terms x,y,x^2 and xy given in Table 4.4. From the above,

$$a=0.51$$

and

$$b=0.0098$$

Taking the worst case limits, as shown in figure 4.3, the thermal conductivity for agar was found to be,

$$k=(0.51\pm0.04)\ W/m°C.$$

TABLE 4.4 Values used to plot straight line graph of agar thermal conductivity versus agar thickness.

x	y	x^2	xy
1.15	0.52	1.32	0.60
3.55	0.55	12.60	1.95
4.70	0.55	22.09	2.59
$\Sigma x=9.4$	$\Sigma y=1.62$	$\Sigma x^2=36.01$	$\Sigma xy=5.14$

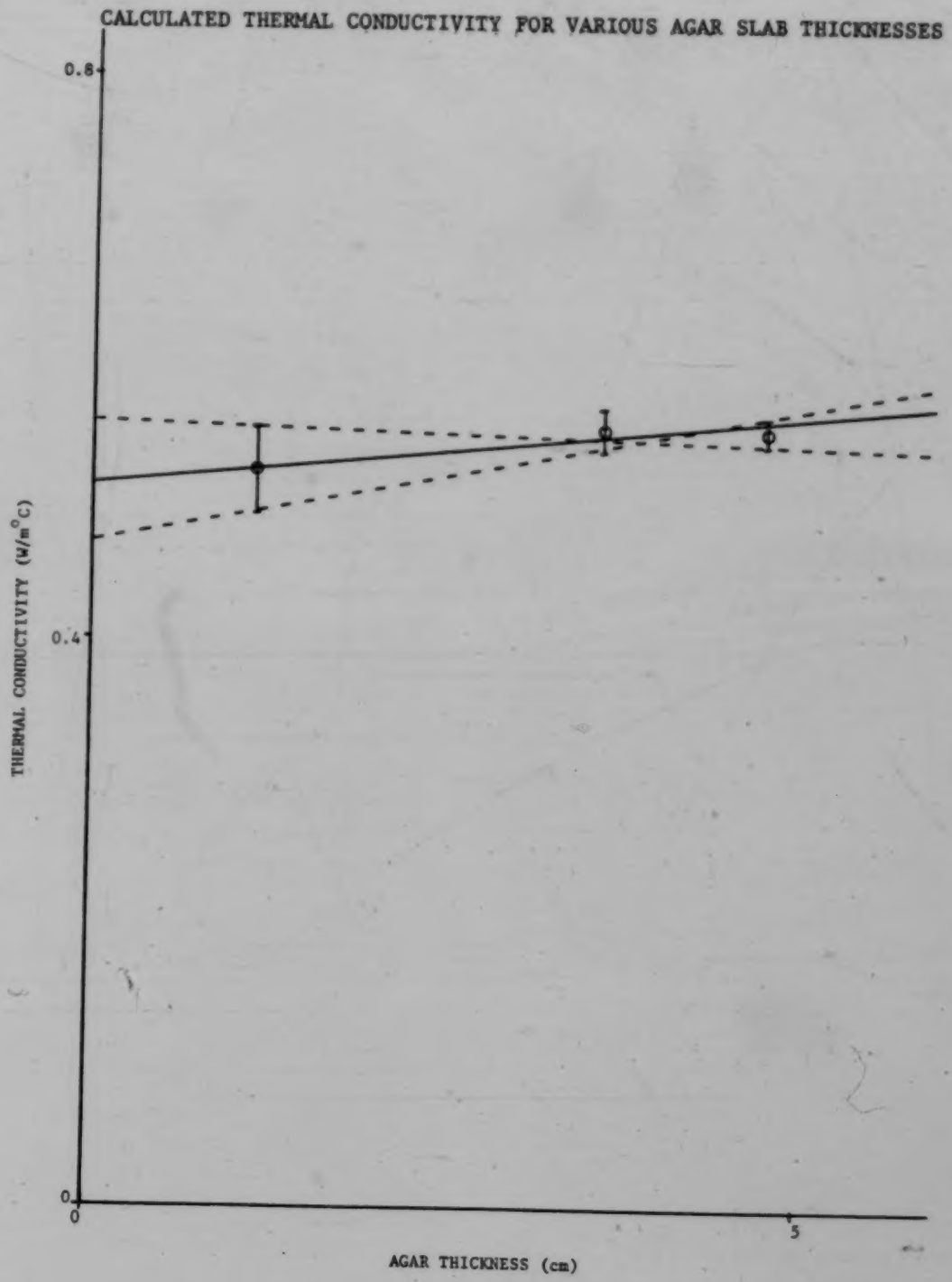
CALCULATED THERMAL CONDUCTIVITY FOR VARIOUS AGAR SLAB THICKNESSES
0.6
0.4
0
0
5
THERMAL CONDUCTIVITY (W/m °C)
AGAR THICKNESS (cm)

FIGURE 4.3

ELECTRICAL CONDUCTIVITY MEASUREMENTS

Saline solutions of known molarities and dielectric properties were used to determine the accuracy of the dielectric measuring cell. The cell proved accurate for measuring the conductivity but not the permittivity of highly conducting solutions [Table 4.5]. This was most pronounced at lower frequencies and in solutions with higher molarities. The source of this error lay in the inability of the HP 4815A to accurately measure very small phase angles. This led to a large amount of uncertainty, or lack of precision, in the permittivity measurements. The relation used to calculate the permittivity was far more sensitive to changes in a small phase angle than was the equation for conductivity. *i.e.*

$$\sigma \simeq \frac{\cos\phi}{\ell z} \qquad 45$$

$$\varepsilon_r \simeq -\{\frac{\sin\phi}{\omega z} + (C_o+C_p)\}\frac{1}{\varepsilon_o \ell} \qquad 46$$

The reason for this can be seen when the sine and cosine of two small angles, like 1° and 0.5°, are compared. *i.e.*

$$\sin(1.0°)=0.01745$$

TABLE 4.5 Assessment of dielectric measuring cell accuracy using saline solutions and published values.

SALINE MOLARITY (M)	FREQUENCY (MHz)	CONDUCTIVITY[(a)] ($10^{-4}\Omega^{-1}cm^{-1}$)	ε_r[(a)]	CONDUCTIVITY[(b)] ($10^{-4}\Omega^{-1}cm^{-1}$)	ERROR	ε_r[(b)]	ERROR	TEMPERATURE ($^{\circ}C$)
0.02	1.0	23.67±0.11	80.54±1.7	22.89±0.11	2%	150.80±36.82	39%	23.0
0.02	10.0	23.82±0.21	80.50±1.0	23.51±0.14	0%	78.07±2.70	0%	23.2
0.004	1.0	5.04±0.04	79.18±0.3	5.10±0.10	0%	99.98±9.02	14%	23.65
0.004	10.0	5.00±0.02	79.34±0.2	5.17±0.04	2%	85.95±0.67	7%	23.5

(a) Rosen, et al [53]. Corrected for measured sample temperatures. i.e. +2%/$^{\circ}C$ for conductivity and -0.5%/$^{\circ}C$ for relative permittivity, ε_r [69].

(b) Measured values.

$$\sin(0.5°)=0.00873$$

$$\cos(1.0°)=0.99985$$

$$\cos(0.5°)=0.99996$$

A 0.5° change in angle produced a 50% change in the value of the sine function. The same change in angle produced a 0.01% change in the cosine function. Clearly, equation 46, with its sine dependance on ϕ, should be more sensitive to variations in small angles than equation 45.

The water bath, used in the r.f. heating experiment, had a molarity of about 0.15 and the significant measurements made at 3.75 MHz. This combination produced a phase angle which was unacceptably small for accurate permittivity measurements. As a result, extrapolations of published values were used to estimate the relative permittivity of the water bath, and agar, as 81±2 [31,32]. Conductivity measurements were quite acceptable.

The conductivities measured for the agar and water bath proved to be very consistent giving average values of

$$\sigma_{bath} = (2.01\pm0.03)\Omega^{-1}m^{-1}$$

and

$$\sigma_{agar} = (1.99\pm0.03)\Omega^{-1}m^{-1}$$

These two values would be expected to be very similar as

ions could easily diffuse into, or out of, the agar bringing it into equilibrium with the bath [32]. The measured conductivities were high for normal saline solutions. This was expected as tap water was used in the bath. Further, the experiments were performed during early spring which, in Edmonton, means the water had a higher impurity content than usual. As long as the conductivities of the bath and agar were measured the problems posed by using tap water were deemed acceptable. This was especially true in view of the difficulty in obtaining and maintaining large quantities of distilled water. As an added bonus colonies of bacteria and mold were unwilling to grow on agar immersed in the tap water. With distilled water in the bath black patches would become visible on the agar after a few days.

For very poor conductors the large phase angle would lead to an unreliable conductivity measurement and an accurate permittivity measurement. Dielectric measurements on materials, and at frequencies, which gave a phase angle around 45° would produce the most accurate conductivity and permittivity.

From the above data the loss tangent for the agar was

$$\tan\delta = 117 \pm 5 \ .$$

The wavelength of 3.75 MHz r.f. in the agar was

$$\lambda = (1.16+0.04)m$$

With $\tan\delta >> 1$, and the agar cylinder much less than a wavelength across, the quasi-static approximation could be used.

TEMPERATURE MEASUREMENTS IN THE AGAR

One source of uncertainty with the temperature measurements was that resulting from curve fitting and extrapolation. The statistical error associated with fitting curves to the cooling data and extrapolating back to the time the r.f. was terminated was evaluated using [55]

$$\hat{S}_{\hat{y}} = \left(\frac{\Sigma y^2 - \Sigma \hat{y}^2}{n-2}\right)\left(1 + \frac{1}{n} + \frac{\bar{x}^2}{\Sigma x^2}\right)^{\frac{1}{2}}$$

where,

y-the measured temperature,

$\hat{y}$-the temperature predicted by curve fitting,

x-the time of each measurement,

$\bar{x}$-the average of the times the temperatures were measured,

n-the number of data points obtained for each curve.

Typically this error never exceeded ±0.15°C for any data point (Figure 4.4). Drift in the power source (±5%), variations in agar radius (±3%), and error inherent in the use of copper-constantan thermocouples (±0.1°C) were three other majour sources of error. Maximum drift in temperature data taken from the centre of the agar phantom amounted to no more than ±4%. This was more indicative of

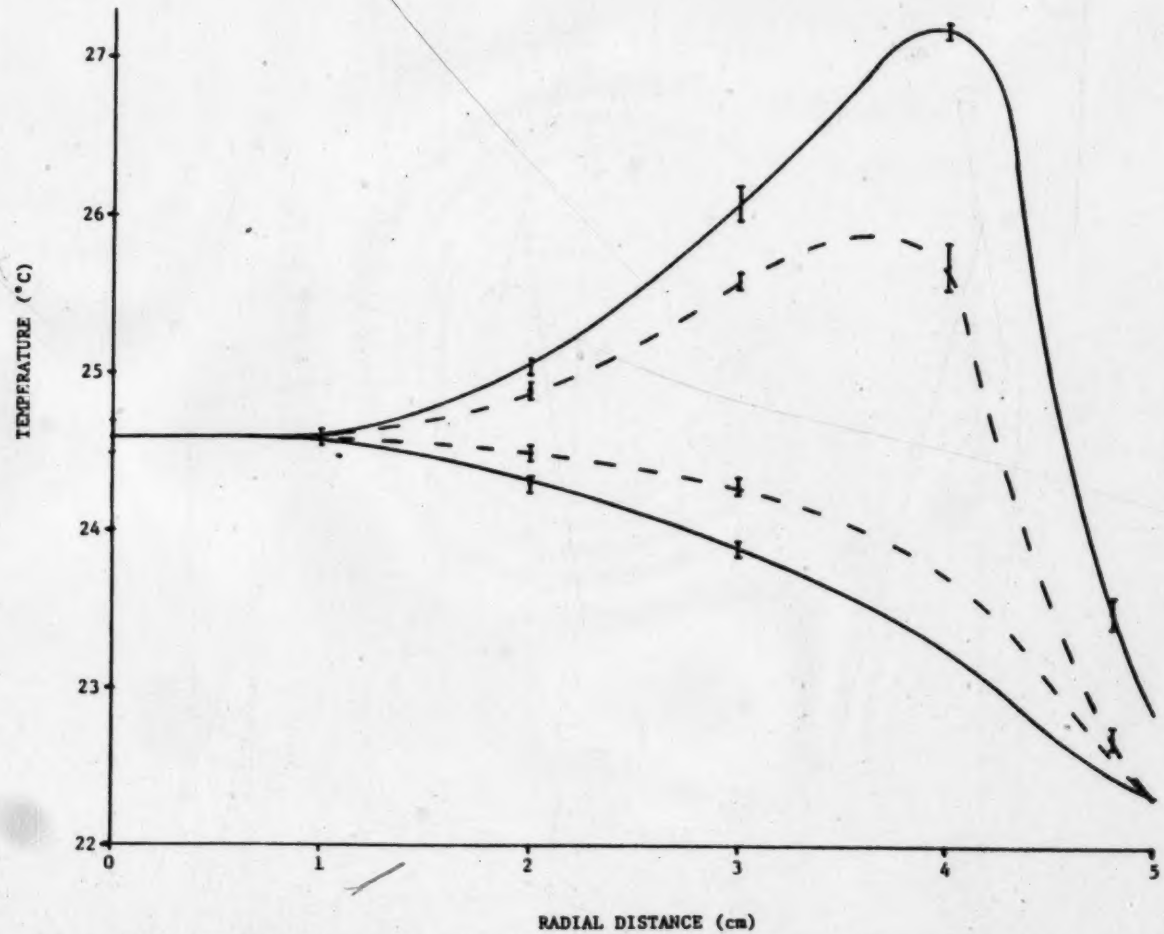

FIGURE 4.4 Temperature profile in agar cylinder showing temperatures directly between electrodes (top two curves) and perpendicular to this line (bottom two curves). Solid lines are for stationary electrodes and dashed are for electrodes orbiting between ±40°.

the reliability and accuracy of the measurements than the sum of all previously mentioned uncertainties.

Drift in the digital thermometer was insignificant over the course of the experiment. The resolution of the Fluke 2190A was limited to $\pm 0.05°C$.

The water bath temperature was controlled to within $\pm 0.1°C$ for each experiment. The volume of saline was great enough that no temperature increase due to r.f. absorption was detected.

Uncertainty in thermocouple position was rendered insignificant by laterally slicing the agar cylinder to find the thermocouple holes. This could not be done with the cats. Handling of the animals would likely have shifted the thermocouple positions a considerable amount. This uncertainty was estimated to be about ± 0.5 cm for most points.

In addition to the above uncertainties, the measurements made in live cats suffered from another problem. Thermocouples in the cat were not always perpendicular to the $\vec{E}$-field, hence an unknown amount of error could have been introduced.

MEASURED TEMPERATURE DISTRIBUTIONS

The temperature distribution produced by stationary electrodes, each (1.95±0.05)cm from the agar surface, is shown in Figure 4.5. Figure 4.6 indicates the relative location of the electrodes to produce this distribution plus x and y axes for reference purposes. As expected there are two symmetrically placed temperature peaks, one near each electrode. The peaks occur about 1 cm deep inside the agar because of the cool saline bath. If the saline was replaced by a thermal insulator the temperature peak would be much larger, occur at the agar surface, and decay exponentially toward the centre. Clearly, the advantage of using a cool bath or bolus is apparent for cooling superficial dielectric or tissue.

Two identical stationary electrodes placed about 2 cm from the subject would be unsatisfactory for hyperthermia therapy. There are two temperature peaks produced, one of which could over heat healthy tissue while a tumor was being treated with the other (Figure 4.7(a)). The solution would be to use one very large electrode (Figure 4.7(b)) or else asymmetrically spaced electrodes (Figure 4.7(c)). The latter case was examined in a manner similar to the symmetric electrode case.

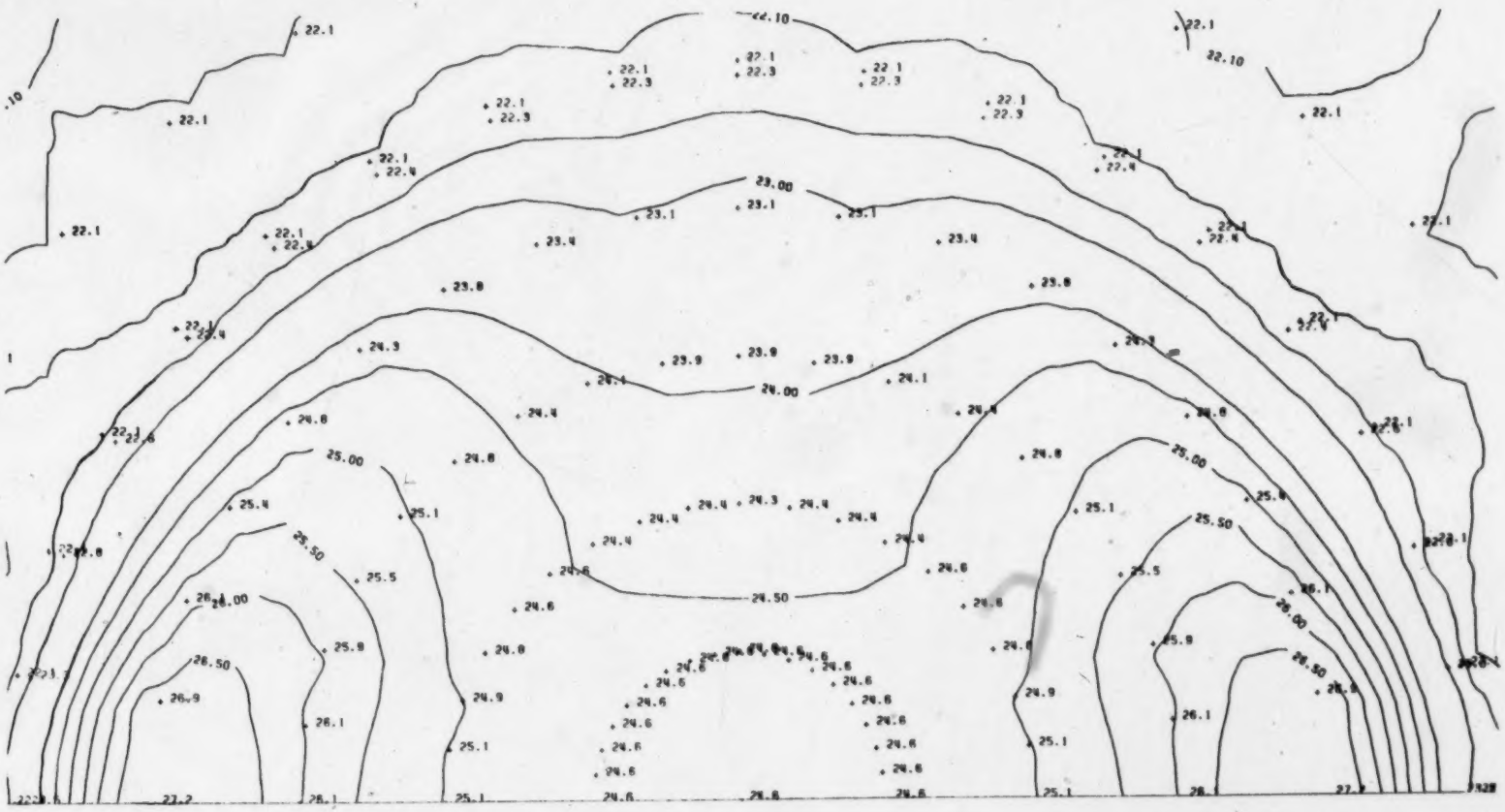

FIGURE 4.5 Temperature distribution inside agar cylinder heated with symmetric electrodes.

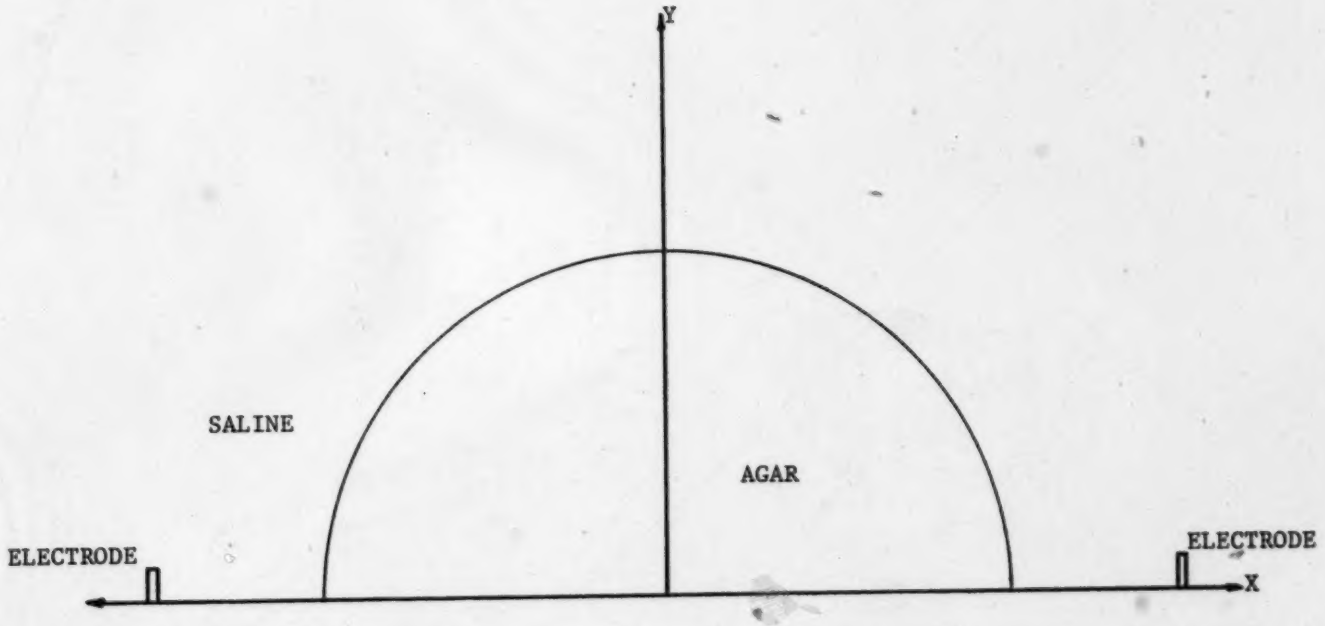

FIGURE 4.6 Top view of one half of 5 cm radius agar cylinder showing electrodes relative to x- and y-axes used for reference purposes in simulated temperature maps.

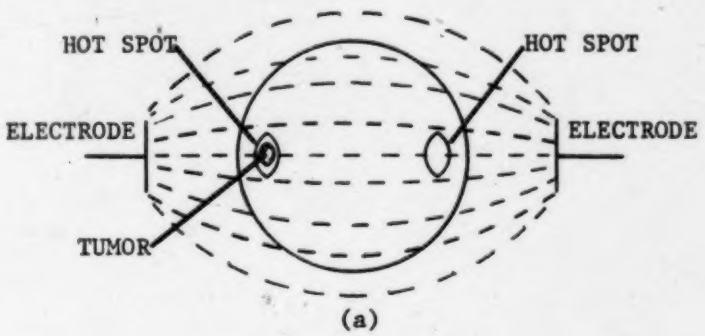

(a)

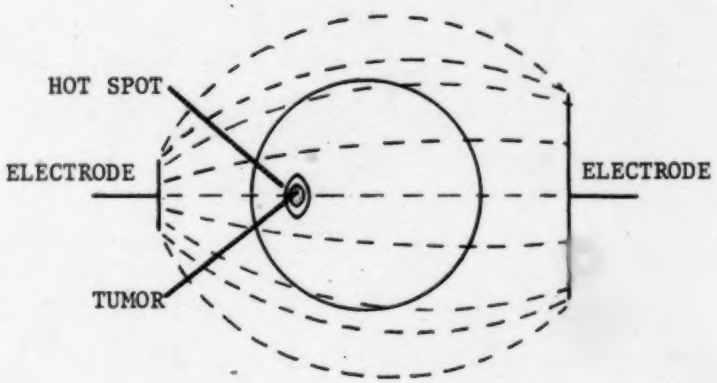

(b)

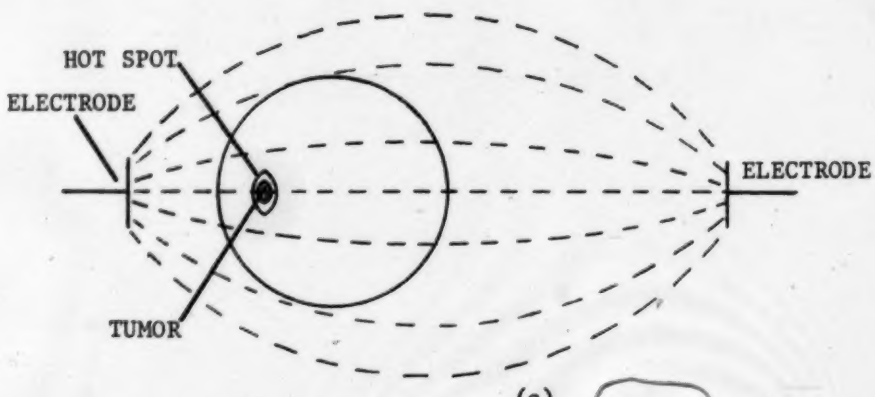

(c)

FIGURE 4.7 Hot spots produced in a dielectric by various electrode configurations.

The temperature distribution inside an agar cylinder irradiated with one electrode (2.0±0.1) cm, and the other (7.0±0.25) cm, from its surface (Figure 4.8) is shown in figure 4.9. There is only one large temperature peak produced with this configuration. For a shallow tumor this would be a superior applicator to the symmetrically placed electrode type. There would be no danger of producing an unwanted hot spot on the far electrode side of the subject.

The asymmetric electrodes produce a slightly lower peak temperature (0.2°C less) than the symmetric electrodes and a 0.9°C lower centre temperature. Far less energy is being deposited in the agar while little change is made in the peak temperature. Obviously the asymmetric electrodes are very efficient with regard to heating a shallow tumor and not imposing an unduly large heat load on the patient.

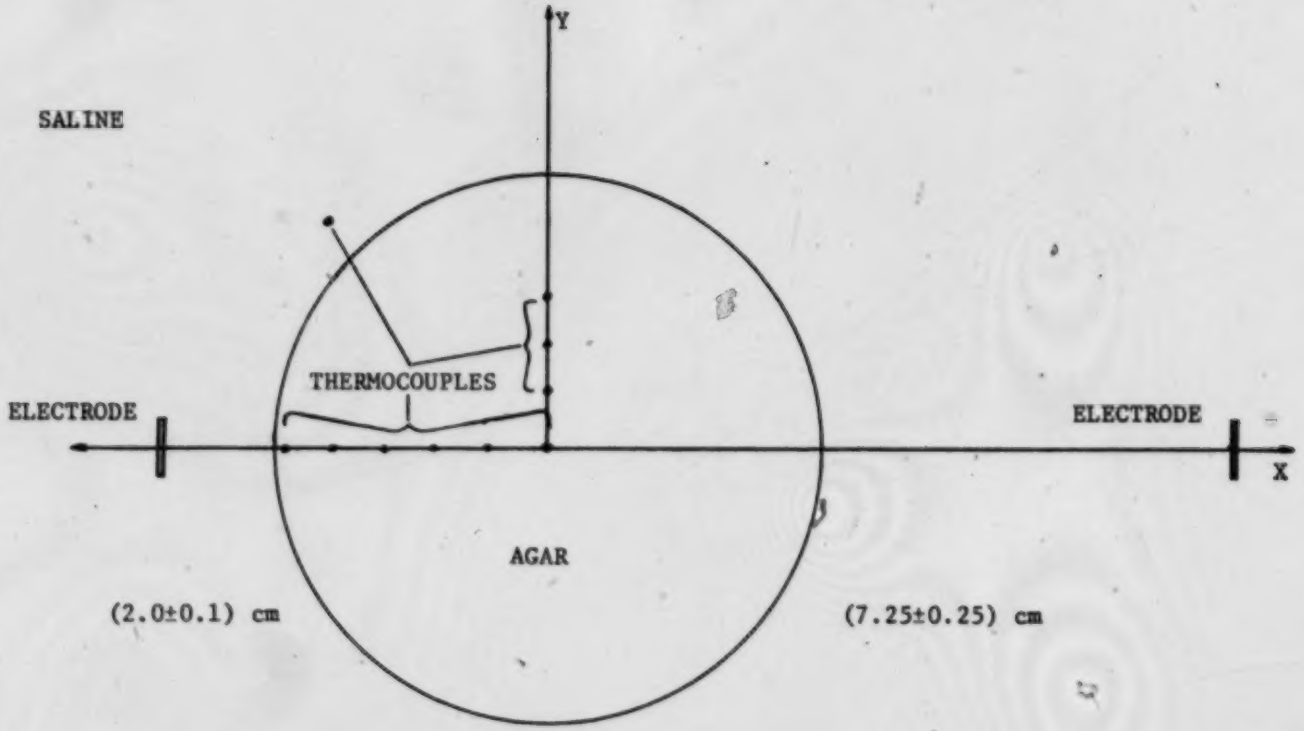

FIGURE 4.8 Initial orientation of asymmetric electrodes relative to 'x' and 'y' axes in agar cylinder.

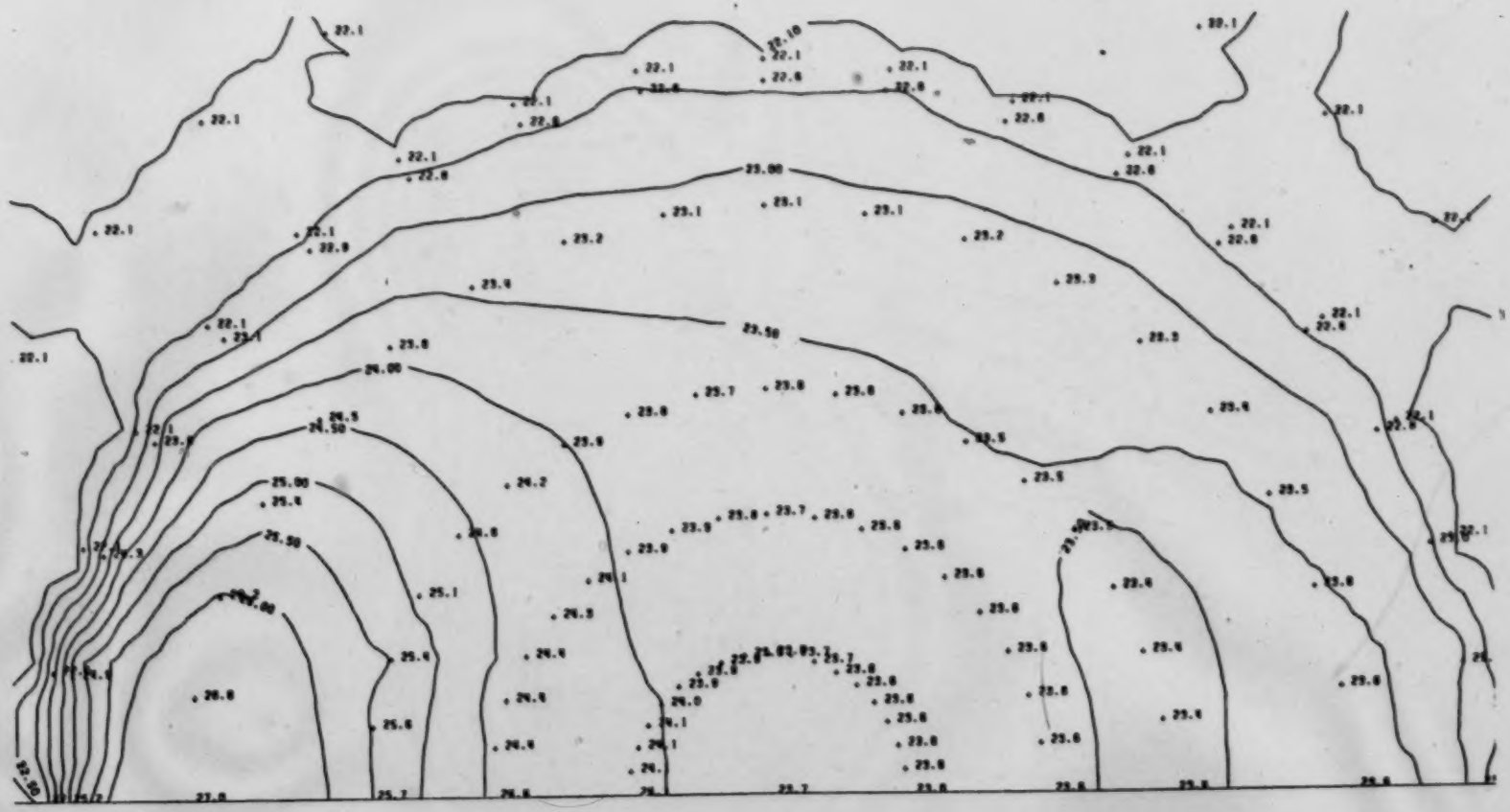

FIGURE 4.9 Temperature distribution inside agar cylinder heated with asymmetric electrodes.

MEGAERA SIMULATIONS

A considerable amount of labour was involved in producing each of figures 4.5 and 4.9. To expedite matters Megaera was used to simulate the temperature distributions in r.f. irradiated agar. The effects of varying experimental parameters were quickly seen with computer simulation. To validate the use of Megaera in place of actual experiments comparisons were made between measured and calculated temperature distributions.

Results of symmetric electrode simulations made using Megaera are shown in figure 4.10. Figure 4.10 (a) and (c) are the maximum and minimum temperature limits calculated by Megaera when uncertainties in measured power, thermal and electrical conductivities, electrode spacing, temperature measurements, and volumetric heat capacity are taken into account. Figure 4.10 (b) is the actual measured temperature profile. The measured profile sits well within the maximum and minimum limits. The temperature distribution is very sensitive to electrode spacing, power, and heat capacity. As a result, the maximum and minimum temperature limits are widely spaced.

A close approximation to the measured temperature profile is obtained from Megaera when the following

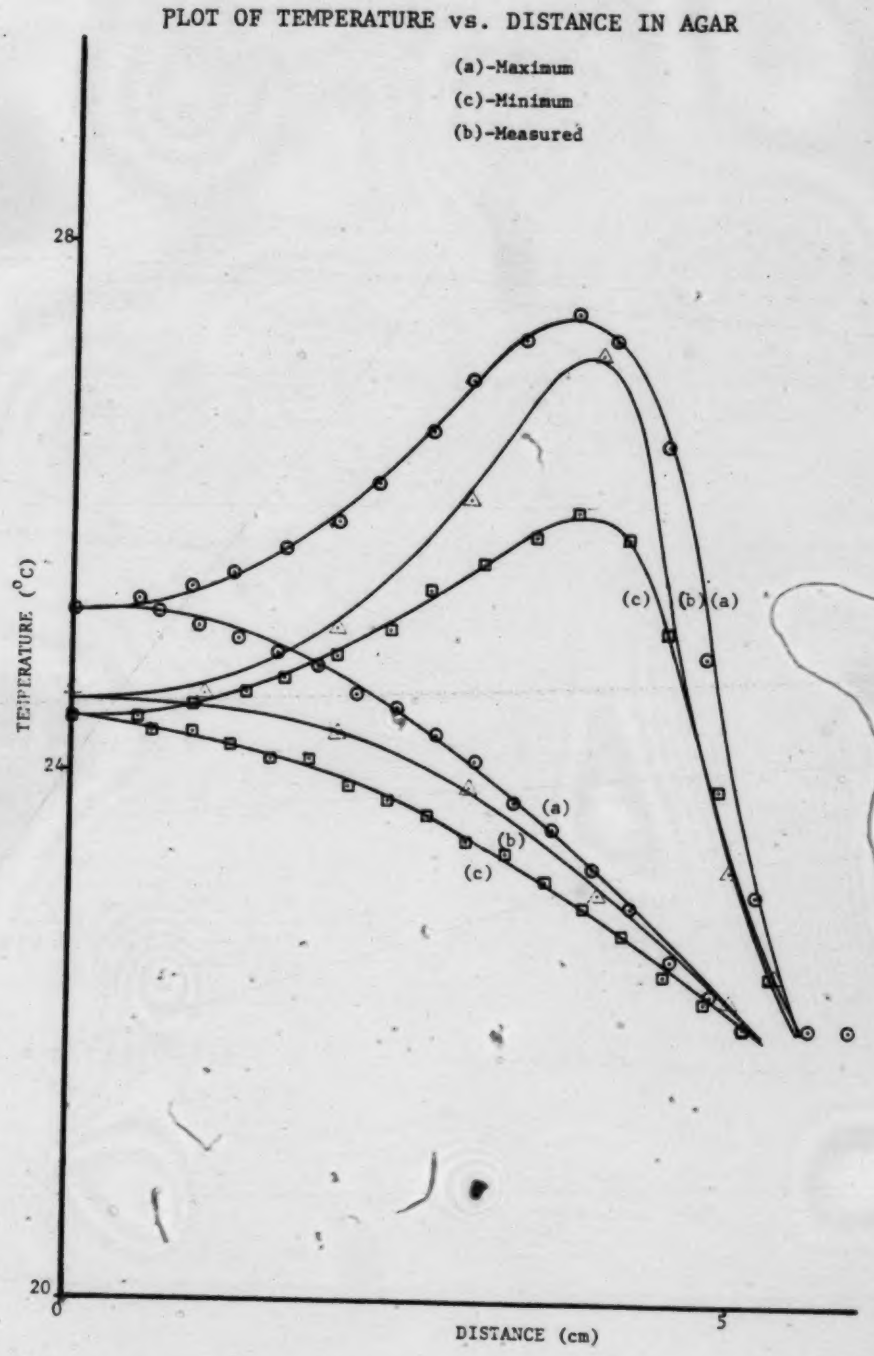

FIGURE 4.10. Temperature profile measured in agar with high and low limits calculated by Megaera.

parameters are used (Figures 4.11 and 4.12),

$\sigma_{\text{water bath}}$ -1.98 S/m

σ_{agar} -1.96 S/m

C_v -4.1x10⁴ J/°C m³

k-0.47 W/m°C

Power-12.6 W (see Appendix #2)

Electrode distance from agar surface-1.85 cm

These values are all within the measured bounds of uncertainty. Temperatures near the centre of the agar are calculated high by Megaera because the program assumes infinitely long electrodes. At the centre of the agar cylinder this assumption of no field spreading in the axial direction could amount to a 7% increase in temperature (Appendix #3). The error associated with using a two dimensional model decreases closer to the electrodes. This trend is evident in figure 4.10 and 4.11 and could account for the broad temperature peaks predicted by Megaera. In addition, the thermal conductivity is likely high resulting in low temperature gradients in the calculated data.

Changing the position of the surface used by Megaera to calculate the current integral produces variations in calculated temperatures of up to 0.1°C. Hence, a ±0.1°C uncertainty was assumed for all temperatures calculated by Megaera. The ±0.1°C uncertainty takes into account a

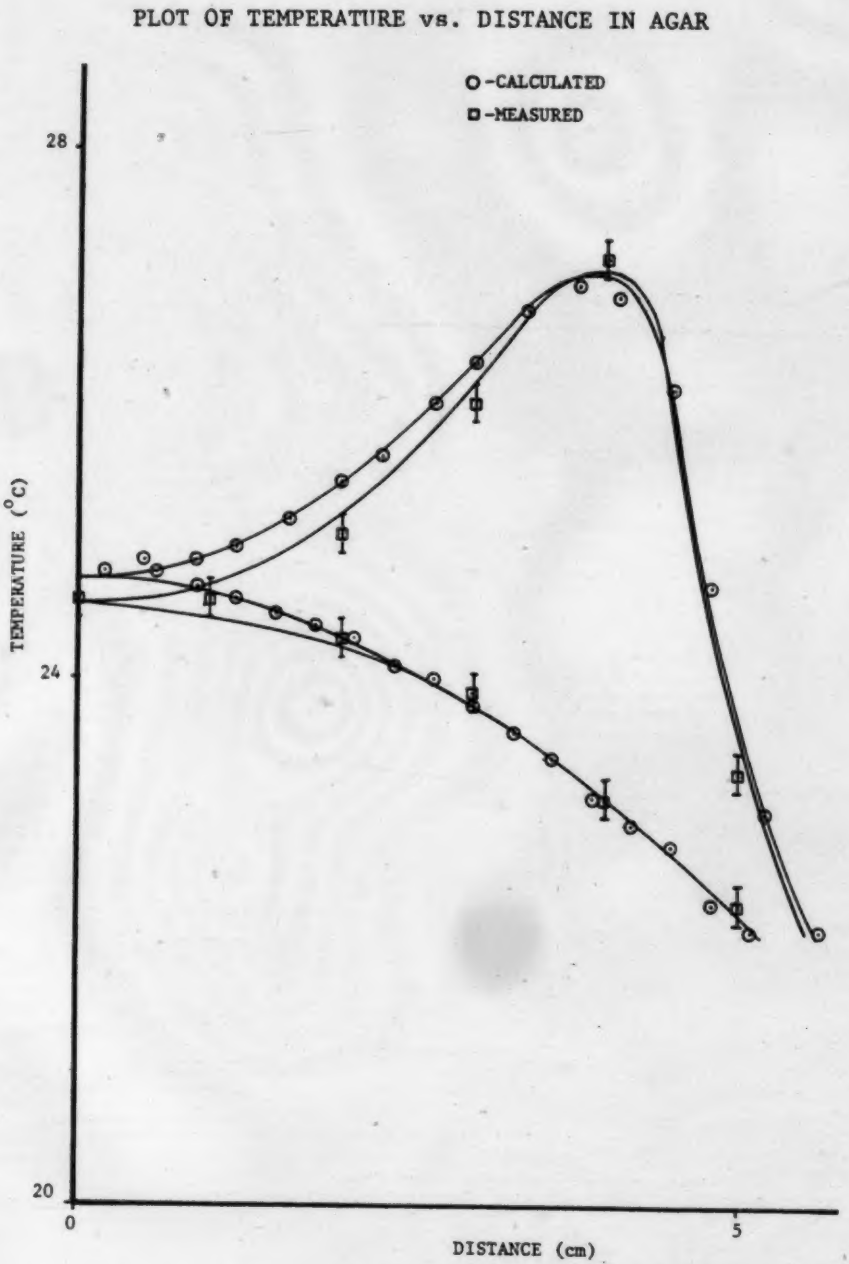

FIGURE 4.11 Temperature profile measured in agar and calculated by Megaera.

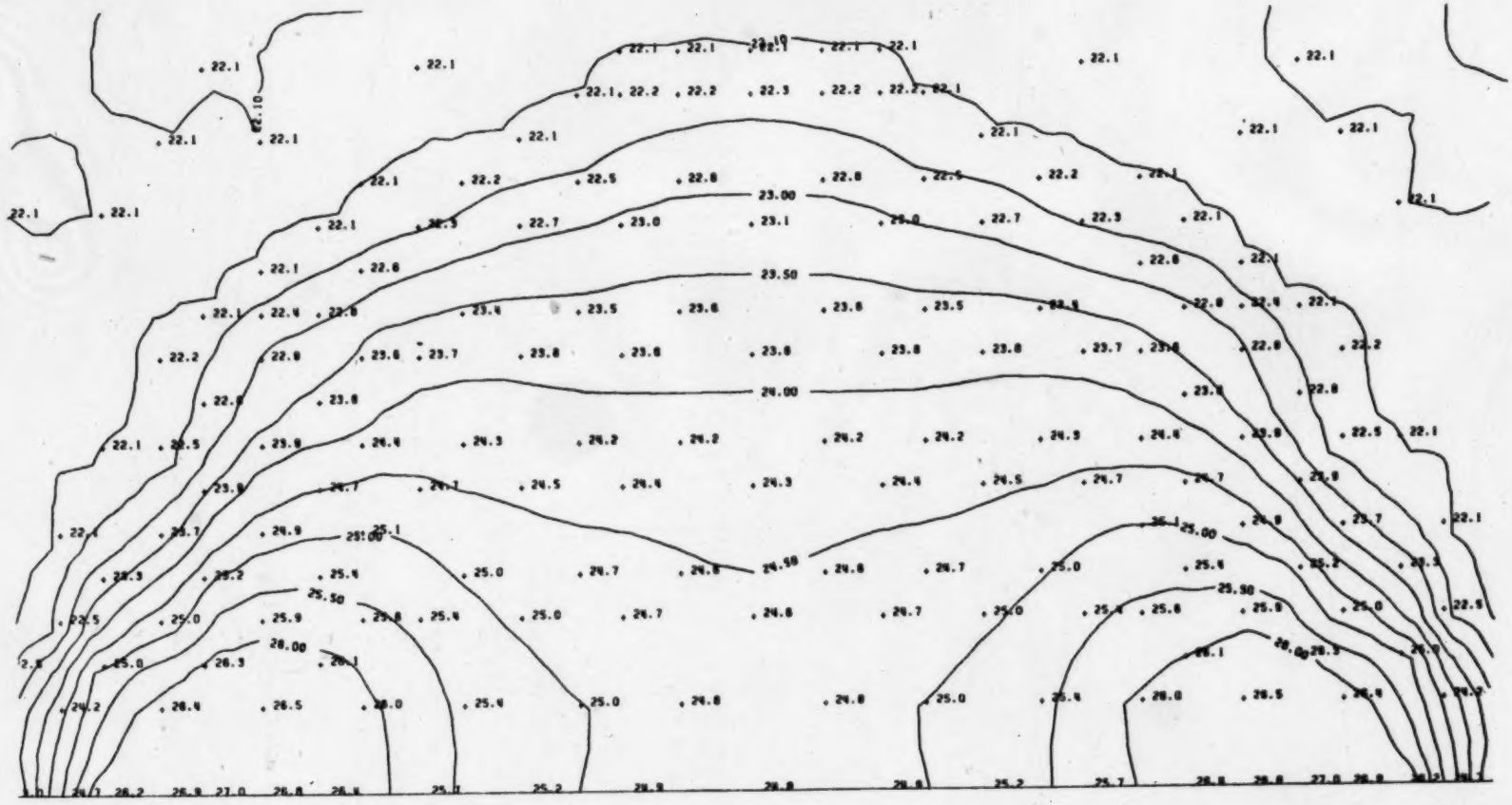

FIGURE 4.12 Calculated temperature distribution produced inside agar by symmetric electrodes.

possible programming error not the error associated with using an approximate means of calculation.

Within certain limits, as outlined above, Megaera is capable of accurately simulating heating in an agar cylinder exposed to r.f. (3.75 MHz or lower) energy from symmetric electrodes.

Asymmetric electrode simulations were also made using Megaera. The results showing the maximum and minimum temperature limits are shown in figure 4.13 and 4.14 (a) and (c). Figure 4.13 (b) shows the measured x-axis temperature profile and figure 4.14 (b) shows the measured y-axis profile. In figure 4.13 the measured values lie well within the simulated maximum and minimum limits. The simulation does not show the very slight temperature increase in the distant electrode side of the agar. This could be the result of using a high thermal conductivity which would tend to smooth out temperature peaks. Also, the temperature peak was so small, practically within the bounds of experimental error, that round-off and approximation error could have deleted it from the simulation results.

Along the y-axis (Figure 4.14) the measured temperature profile sits between the maximum and minimum calculated limits. The high measured readings at the 4.0

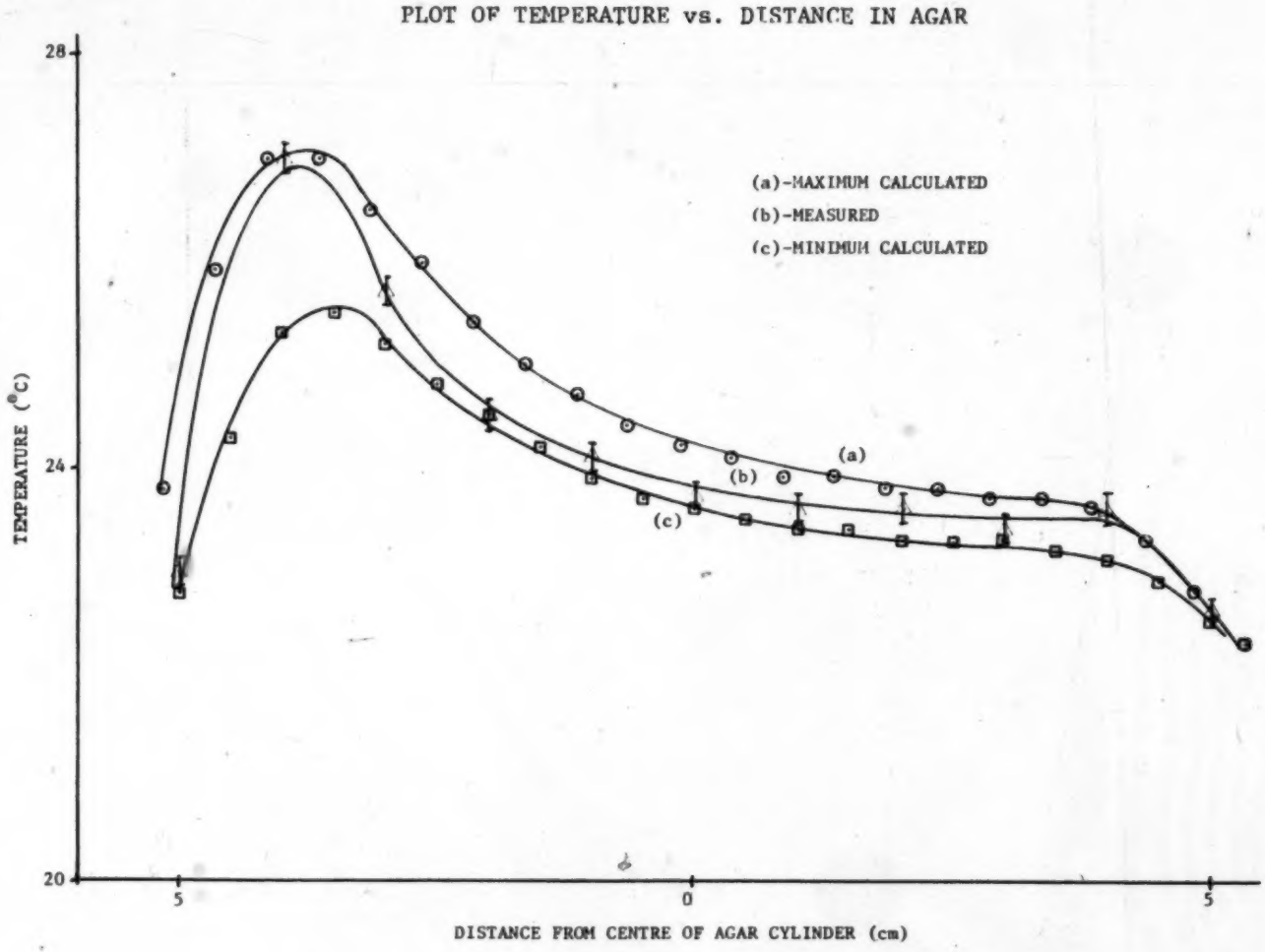

FIGURE 4.13 Temperature profile in agar irradiated with asymmetric electrodes.

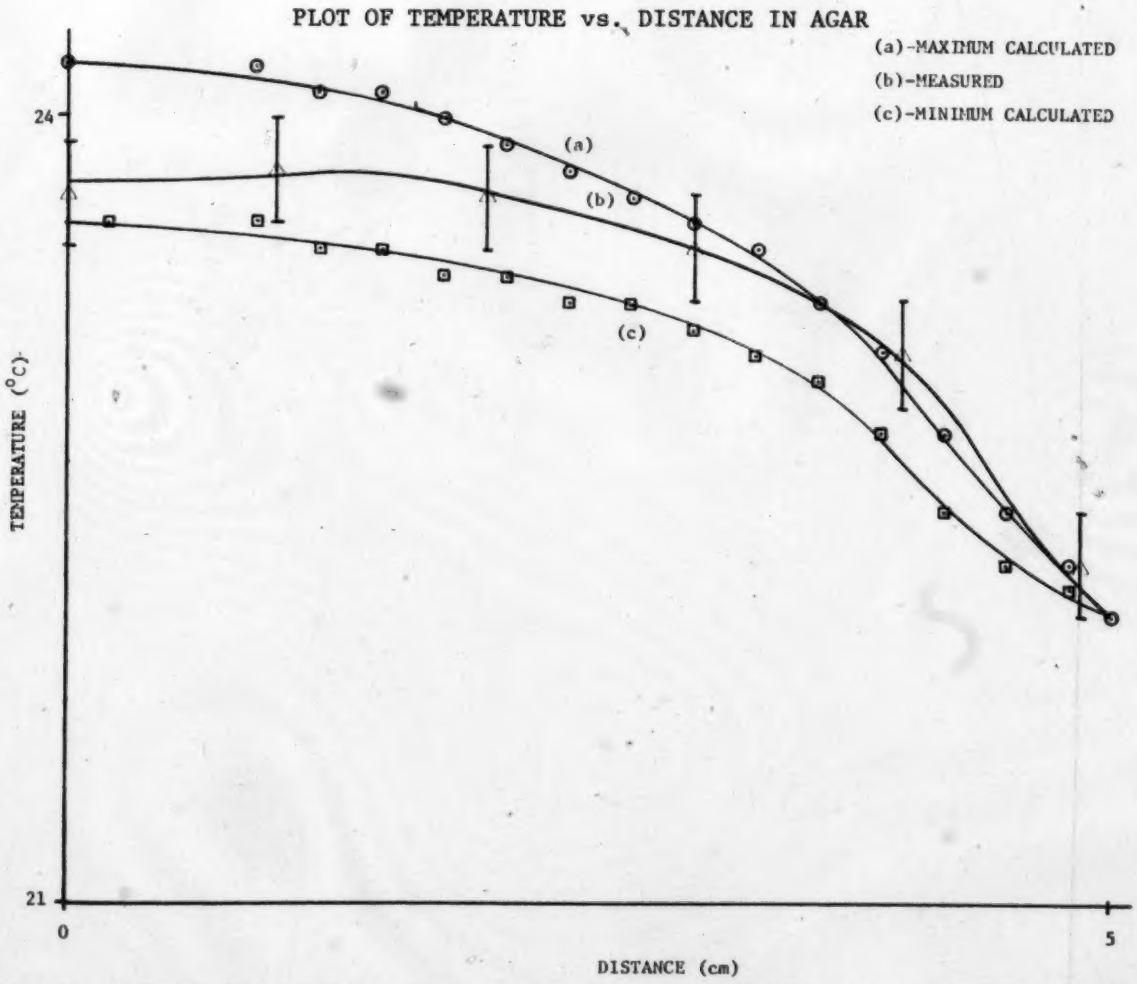

FIGURE 4.14 Temperature profile along y-axis in agar irradiated by asymmetric electrodes.

and 4.8 cm distances indicate that the thermal conductivity used in the simulation was too high.

Figure 4.15 (a) shows the measured asymmetric electrode temperature profile along the x-axis. Figure 4.15 (b) shows the analogous profile as predicted by Megaera with,

$\sigma_{\text{water bath}}$ -1.98 S/m

σ_{agar}-1.96 S/m

C_v-4.1x10⁶J/°C m³

k-0.47 W/m°C

Power-13.94 W

Near electrode distance-1.85 cm

Far electrode distance-6.8 cm

These two temperature profiles along the x-axis are very close to one another. Figure 4.16 also shows how close the measured and simulated temperature profiles are along the y-axis. The high centre temperatures in the simulation are likely due to the two dimensional approximation (Appendix #3). The steep temperature gradients in the measured plot and the lower peak temperature in the simulation indicate that the thermal conductivity measured for the agar is high. As with the symmetric electrode case, however, the plots are sufficiently close within experimental limits to show that Megaera can closely simulate this kind of heating (Figure 4.17).

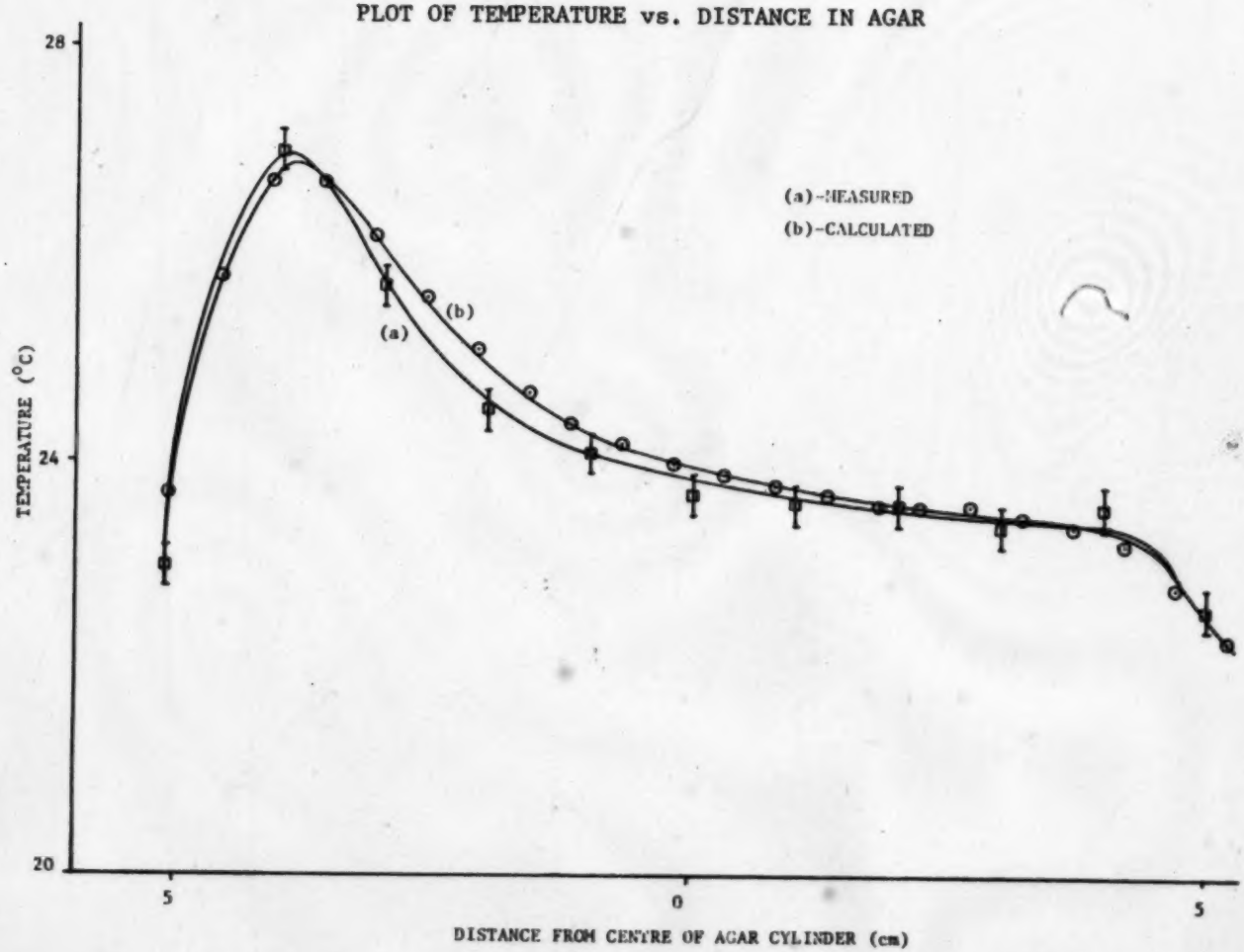

FIGURE 4.15 Temperature profile along x-axis in agar cylinder.

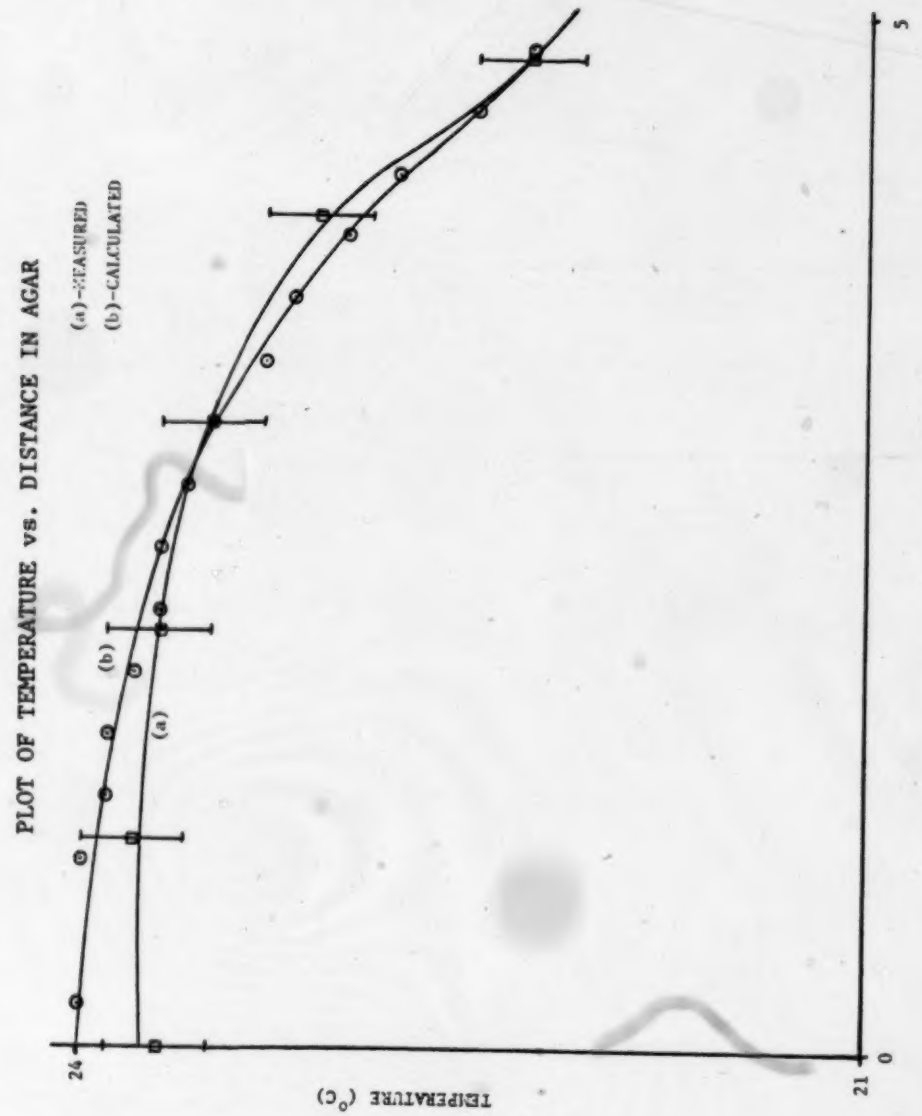

FIGURE 4.16 Temperature profile along y-axis in agar.

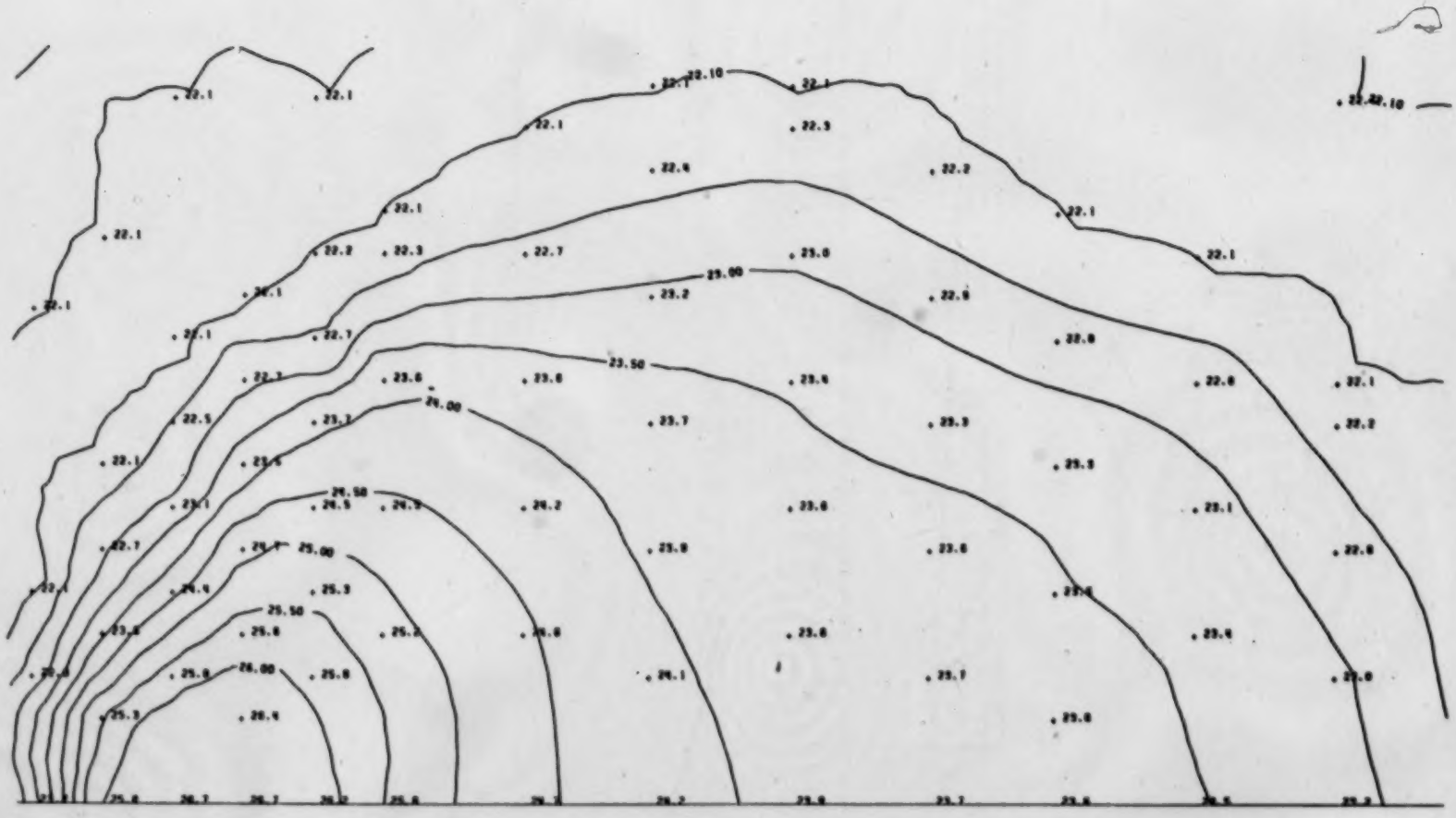

FIGURE 4.17 Calculated temperature distribution produced inside agar cylinder heated with asymmetric electrodes.

SIMULATION OF MOVING ELECTRODE HEATING

Applying the sinusoidal motion weighting function to the data obtained using static symmetric electrodes produced the temperature distribution in figure 4.18. The simulated temperatures were compared to measured temperatures along the 0°, 45°, and 90° radial lines (Figure 4.19). Temperatures along the 0° line were too low (Figure 4.20) while the temperatures along the 45° (Figure 4.21) and 90° (Figure 4.22) lines were too high. Water resistance impeded electrode motion enough so that the speed variation represented a flattened sinusoid, or semi-circle, rather than a perfect sinusoid.

A circular variation in electrode speed results in the temperature distribution in Figure 4.23. Along the 0° radial the temperatures are very close to those actually measured (Figure 4.20). The same holds true along the 45° (Figure 4.21) and 90° (Figure 4.22) radials. The assumption of a 'circular' variation in electrode speed is a good one producing results very close to the measured values.

A flattened sinusoid can be approximated by averaging the circular and sinusoidal weighting functions. The temperature distribution which results is shown in Figure

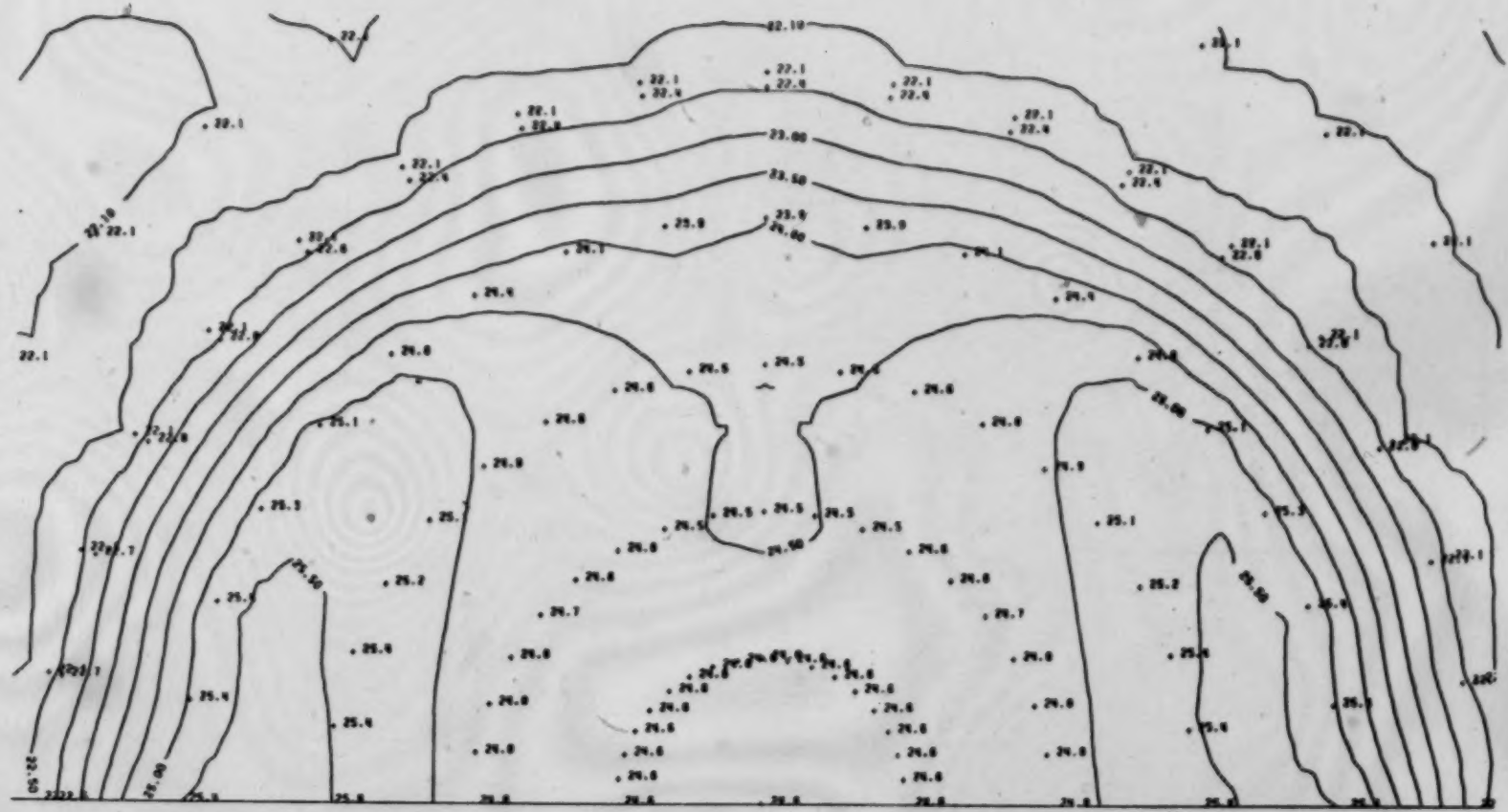

FIGURE 4.18 Calculated temperature distribution inside agar cylinder heated with orbiting symmetric electrodes under going sinusoidal speed variation through ±40° arc.

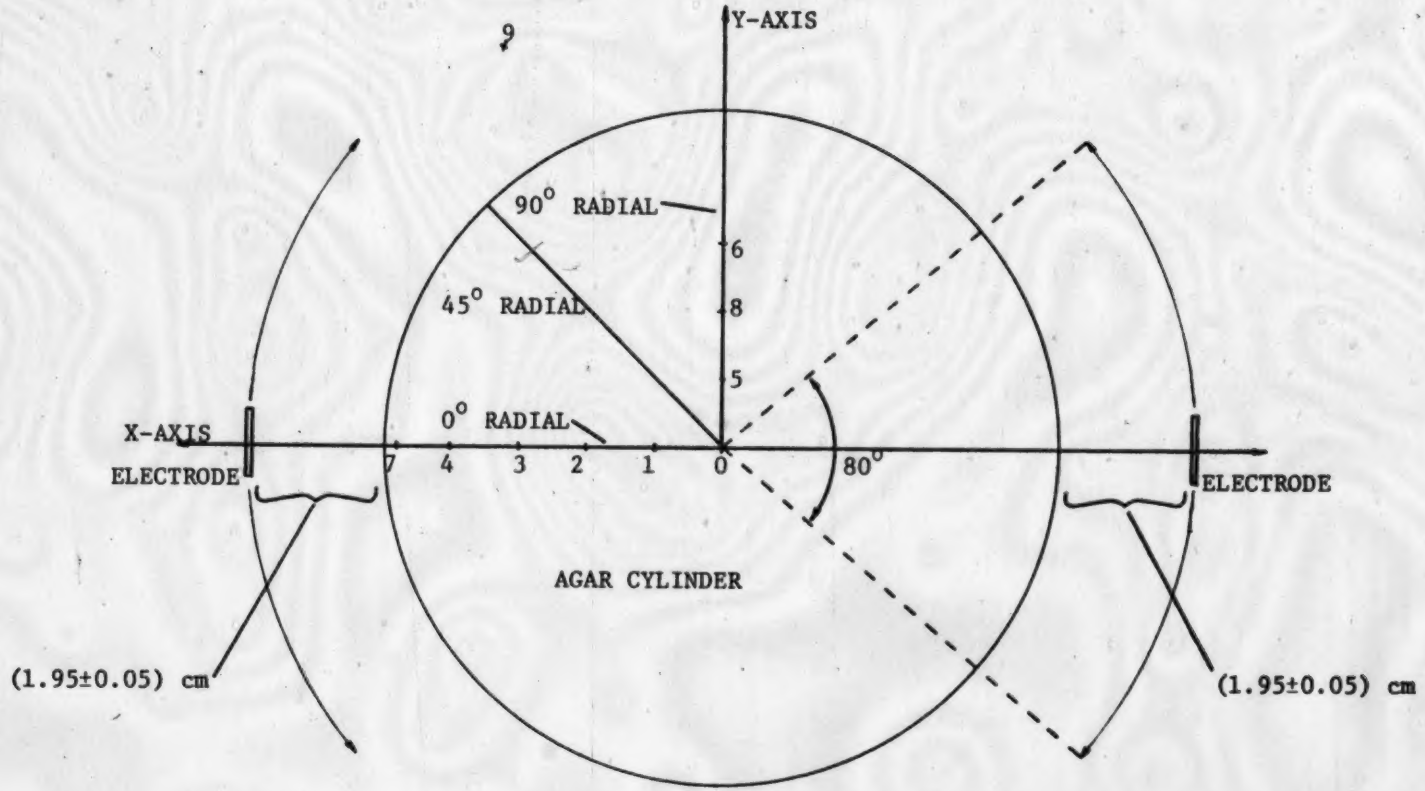

FIGURE 4.19 Placement of numbered thermocouples in agar cylinder (top view).

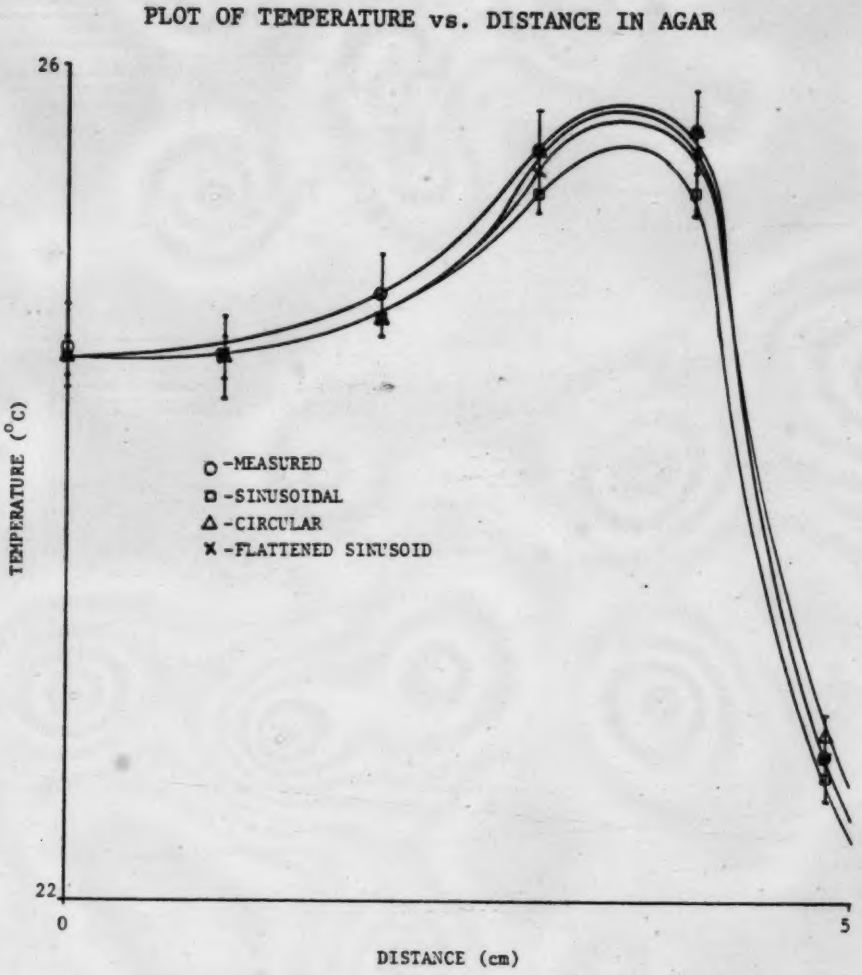

FIGURE 4.20 Temperature profile along 0^{o} radial.

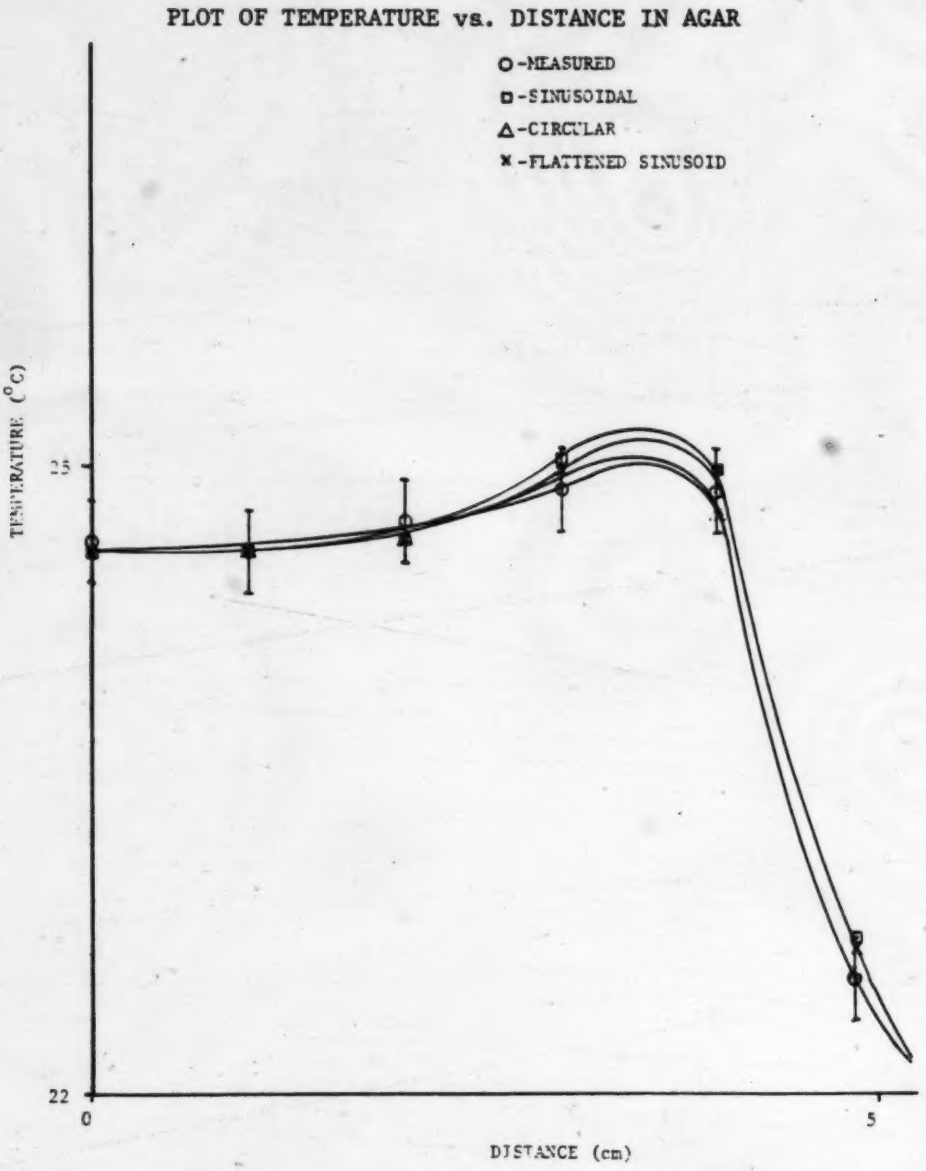

FIGURE 4.21 Temperature profile along 45° radial.

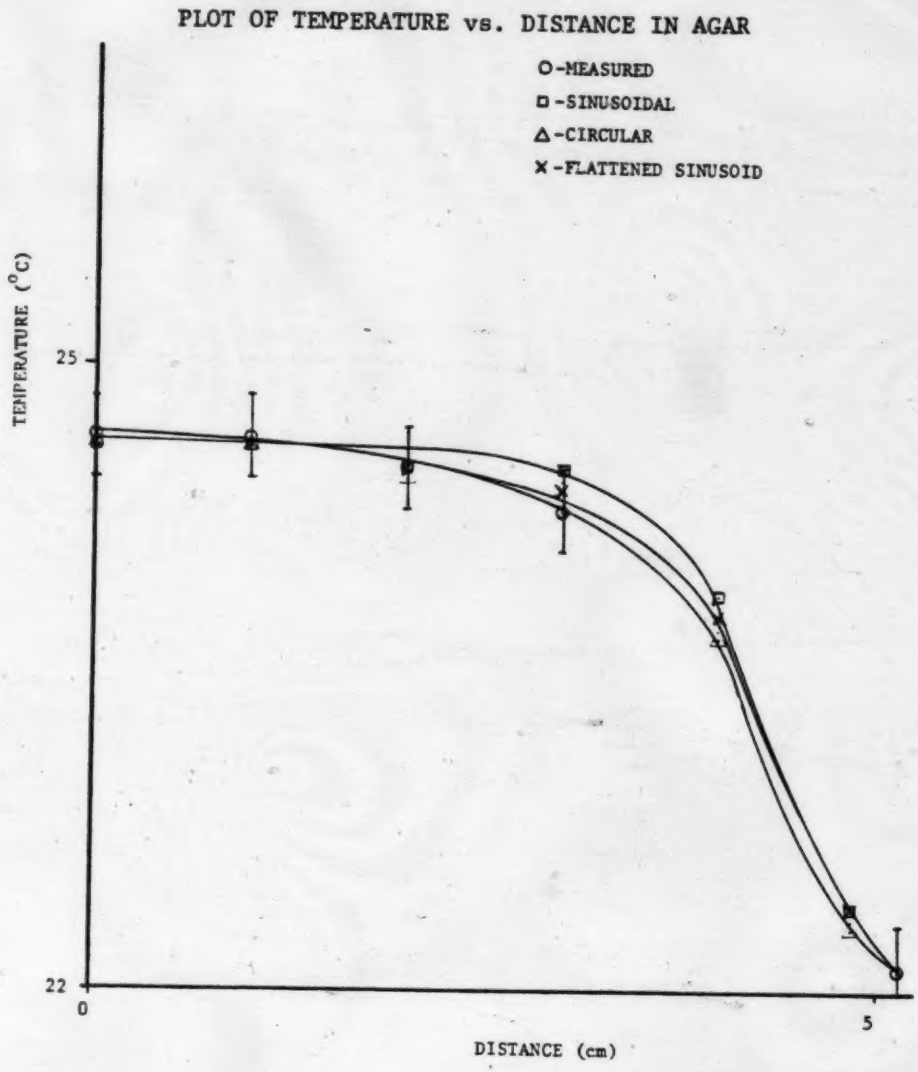

FIGURE 4.22 Temperature profile along 90° radial.

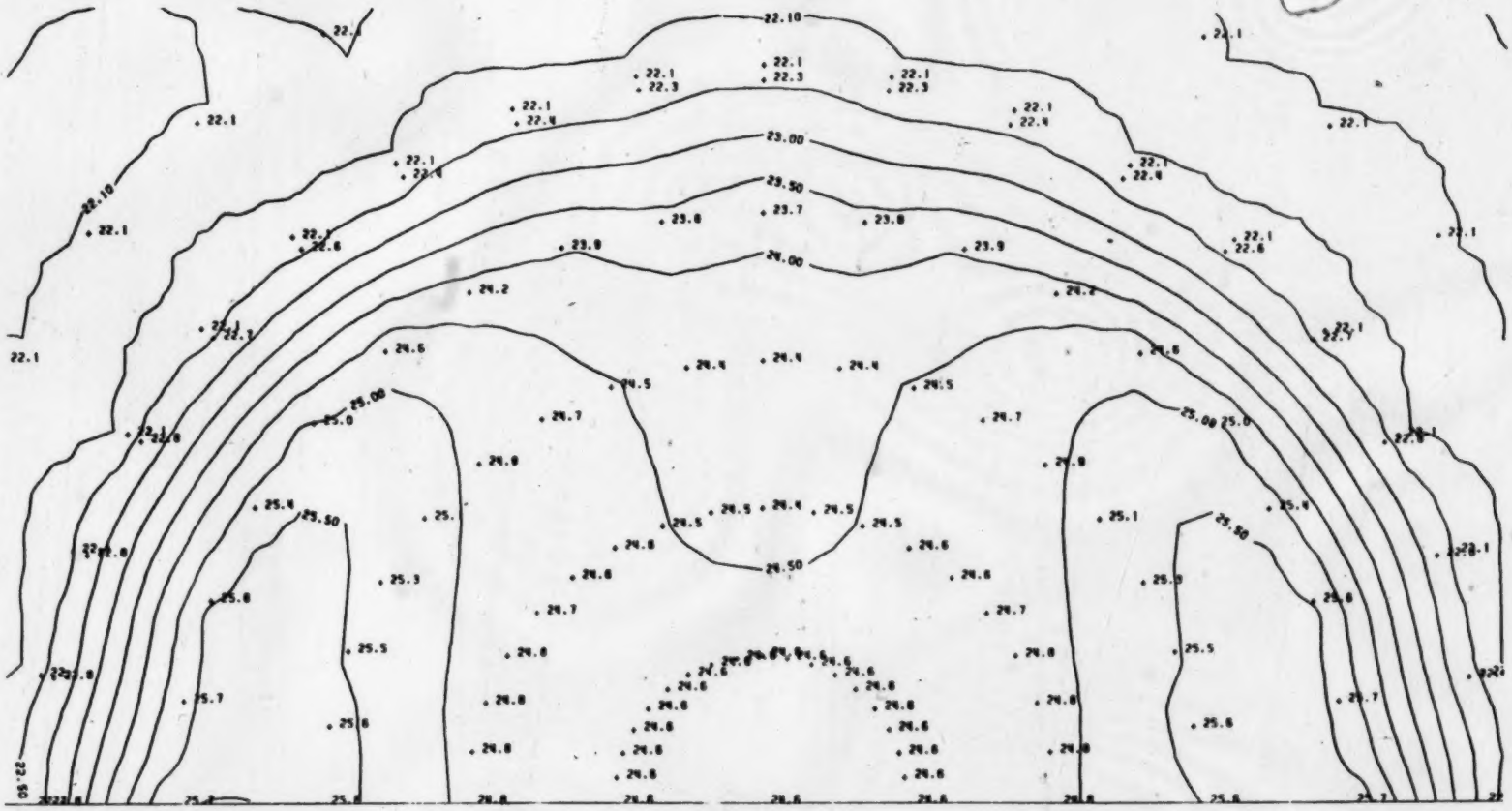

FIGURE 4.23 Calculated temperature distribution inside agar cylinder heated with orbiting symmetric electrodes undergoing circular speed variation through ±40° arc.

4.24. Along the 0° radial the temperatures are slightly low (Figure 4.20). Along the 45° (Figure 4.21) and 90° (Figure 4.22) radials the temperatures are slightly high.

The preceding evidence indicates that the circular electrode speed variation most closely resembles the actual electrode speed. Within experimental limits the flattened sinusoid weighting function also approximates the measured temperatures, though not as well as the circular function.

Temperature patterns for moving asymmetric electrodes have also been calculated using the three averaging functions. These profiles are compared, as with the symmetric electrodes, to temperatures measured along radial lines in the agar. These radial lines are at 0°, 45°, 90°, and 135° (Figure 4.25). Very little temperature variation occurs over arcs centered on the 180° radial line so this data is not included for comparison.

Figure 4.26 shows the temperature distribution which would occur if the asymmetric electrodes travelled with a sinusoidally varying speed. Along the 0° radial the predicted temperature profile is too low compared to the measured profile (Figure 4.27). As with the symmetric electrode case, this shows that the actual electrodes are travelling with a slower peak speed than the sinusoid assumption would indicate. Hence, the electrode speed

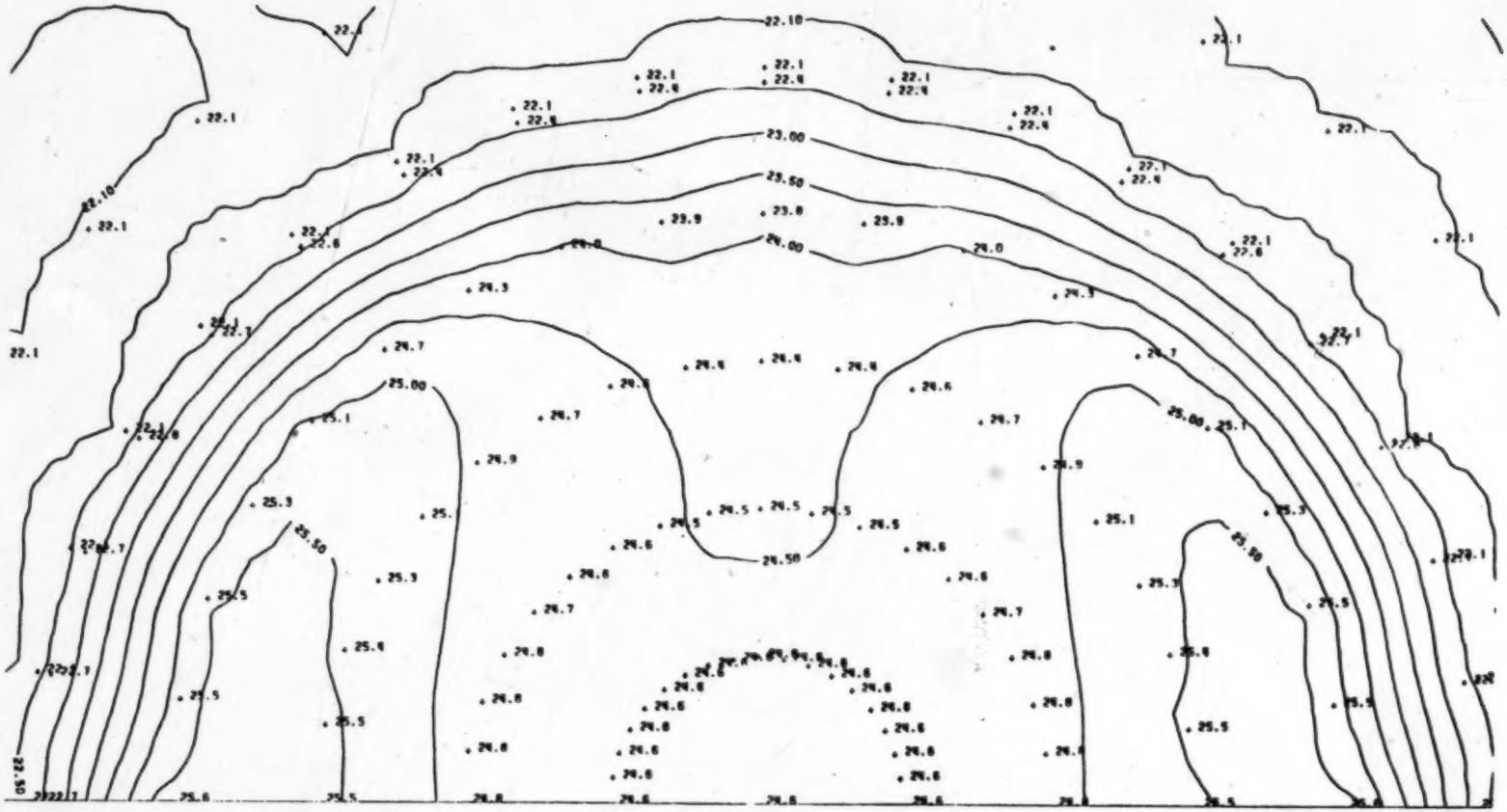

FIGURE 4.24 Calculated temperature distribution inside agar cylinder heated with orbiting symmetric electrodes undergoing flattened sinusoidal speed variation through ±40° arc.

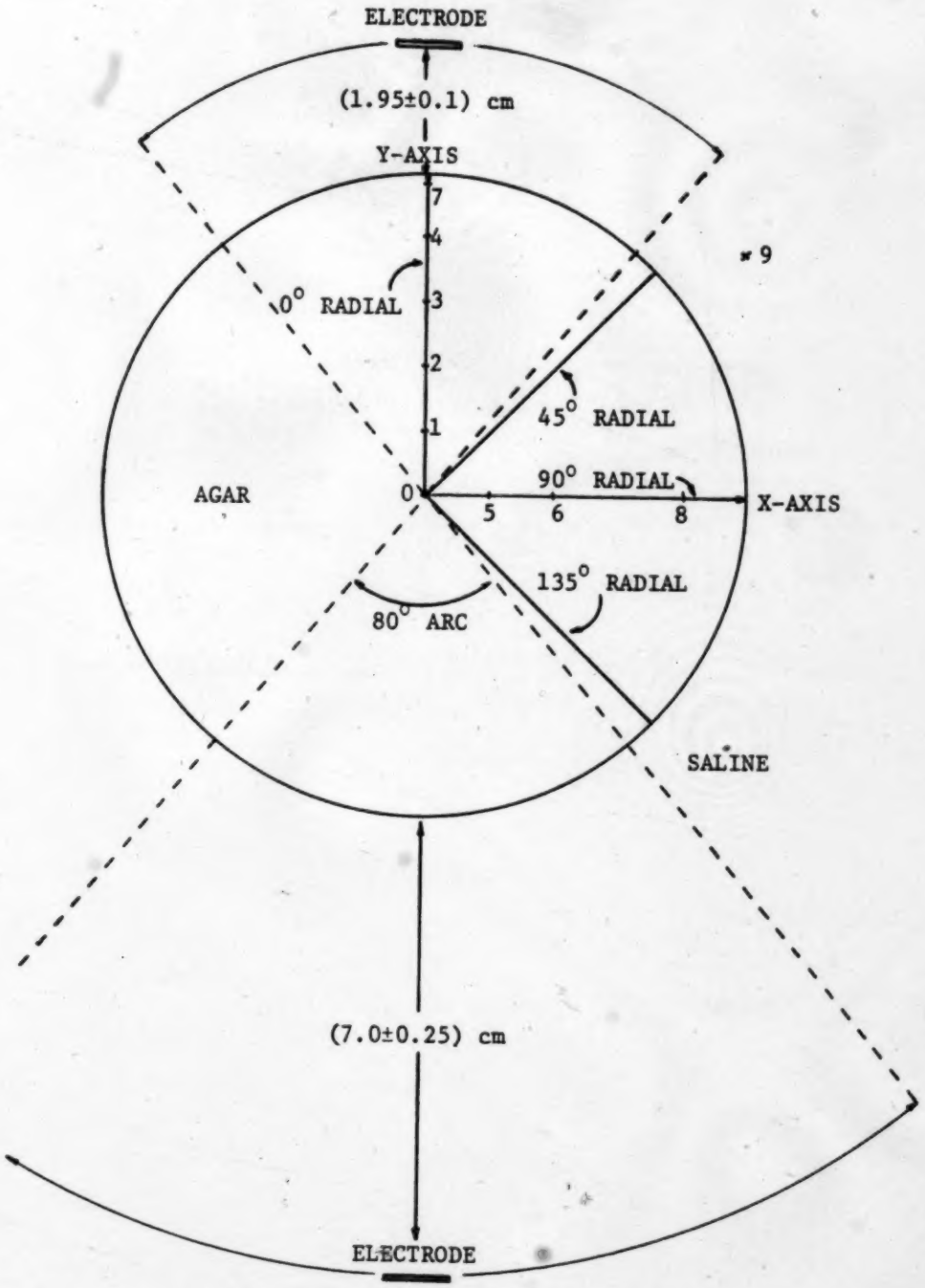

FIGURE 4.25 Placement of numbered thermocouples in agar cylinder (top view).

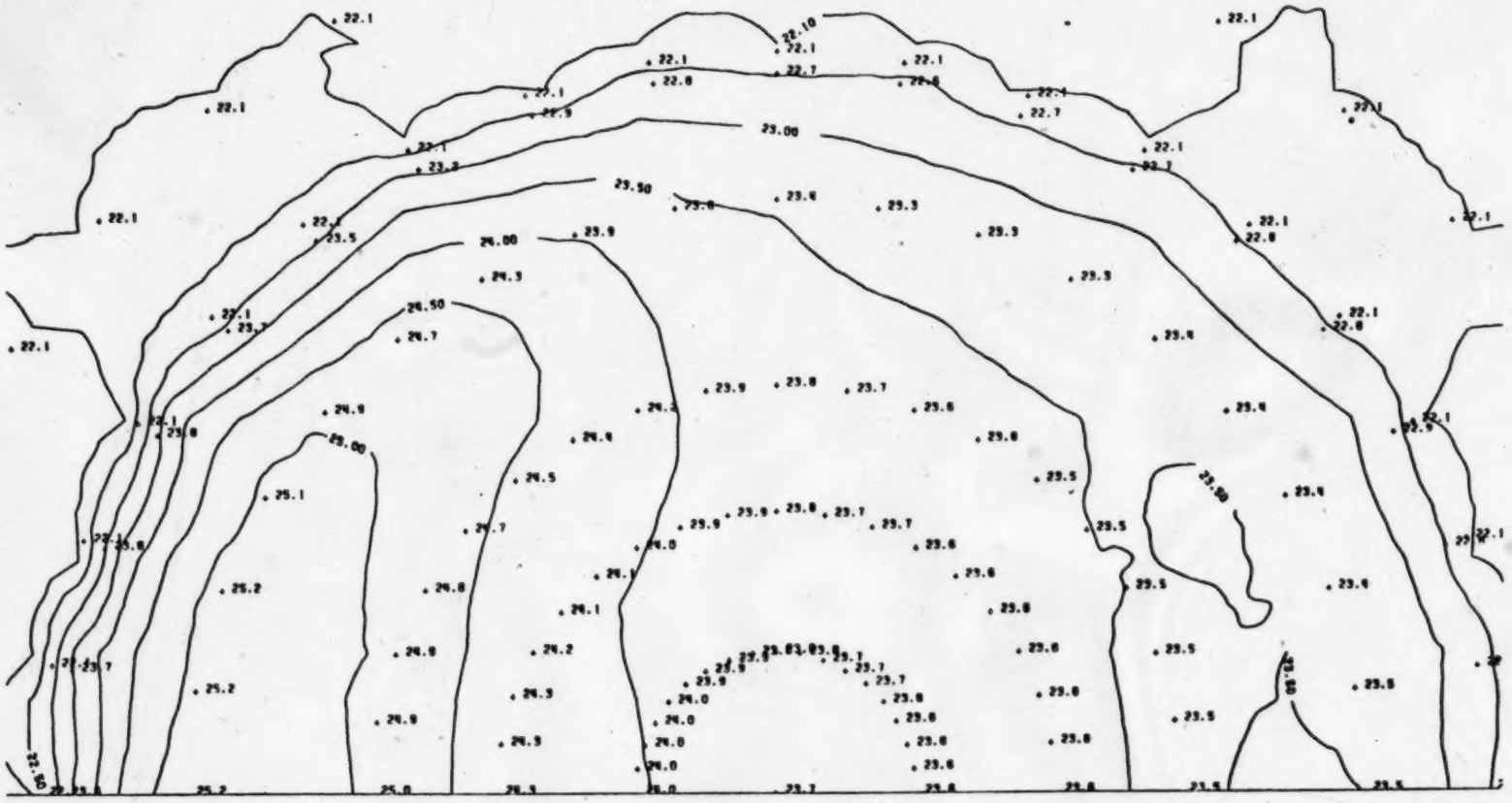

FIGURE 4.26 Calculated temperature distribution inside agar cylinder heated with asymmetric orbiting electrodes undergoing sinusoidal speed variation through $\pm 40^{\circ}$ arc.

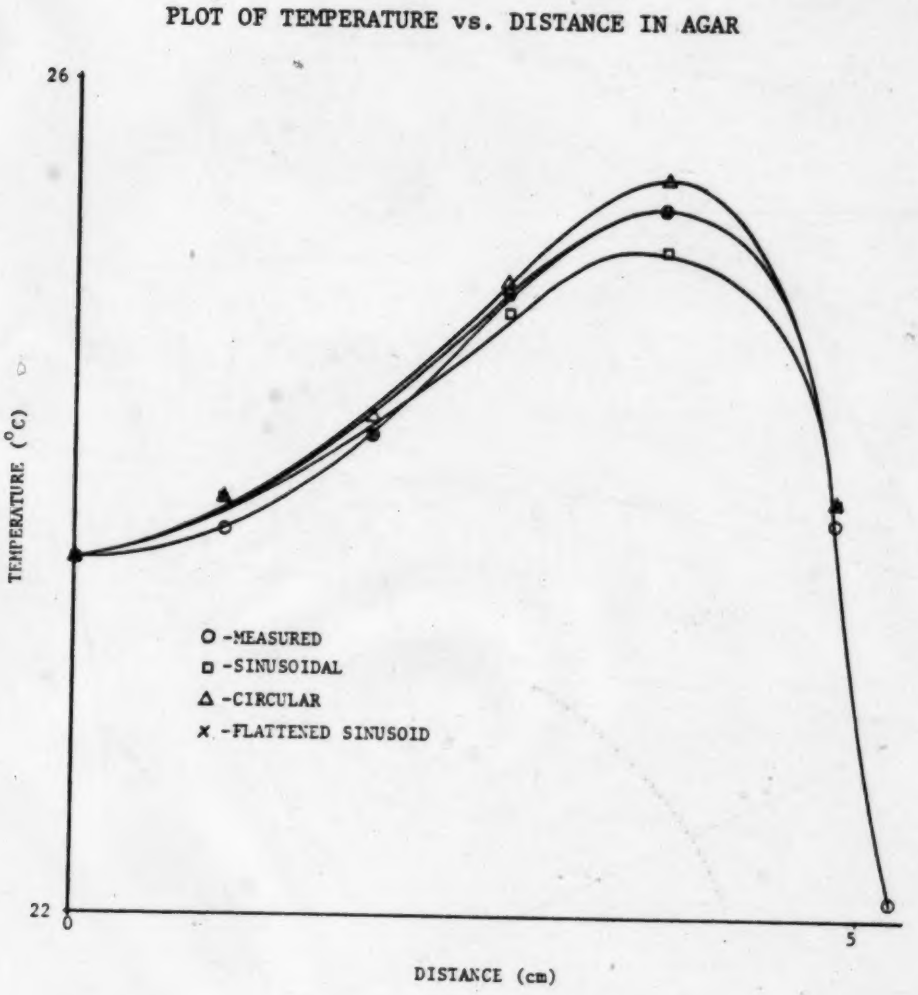

FIGURE 4.27 Temperature profiles along 0° radial.

variation is more closely approximated by a flattened sinusoid. Along the 45° (Figure 4.28) and 90° (Figure 4.29) radials the temperatures are slightly higher than those measured. Along the 135° radial (Figure 4.30) the measured and calculated temperature profiles are essentially the same regardless of weighting factor used.

The temperature distribution resulting from a circular variation in asymmetric electrode speed is shown in Figure 4.31. This motion produces a temperature profile along the 0° radial (Figure 4.27) which is slightly higher than the measured profile. Along the 45°, 90°, and 135° radials (Figures 4.28-4.30) the temperature profiles are close to the measured profiles.

The temperature distribution resulting from the flattened sinusoid weighting function is shown in Figure 4.32. Calculated profiles along the 0°, 45°, and 135° radial lines (Figures 4.27, 4.28, and 4.30) are very close to the measured ones for this type of motion. Along the 90° radial (Figure 4.29) the calculated profile is high but within experimental error compared to the measured profile.

The measured temperatures in Figures 4.27-4.30 are often found to be lower than the calculated temperatures. Round off errors in the computed and measured values could account for some of this. A comparison of the temperatures

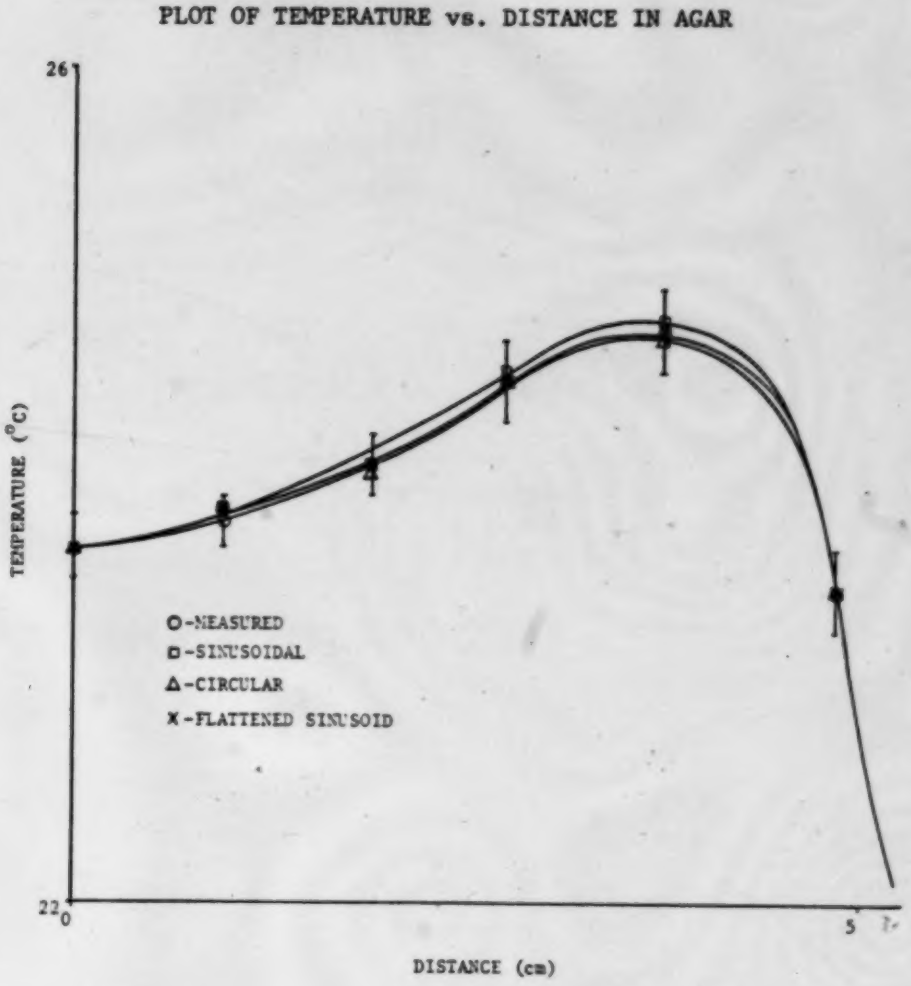

FIGURE 4.28 Temperature profiles along 45° radial.

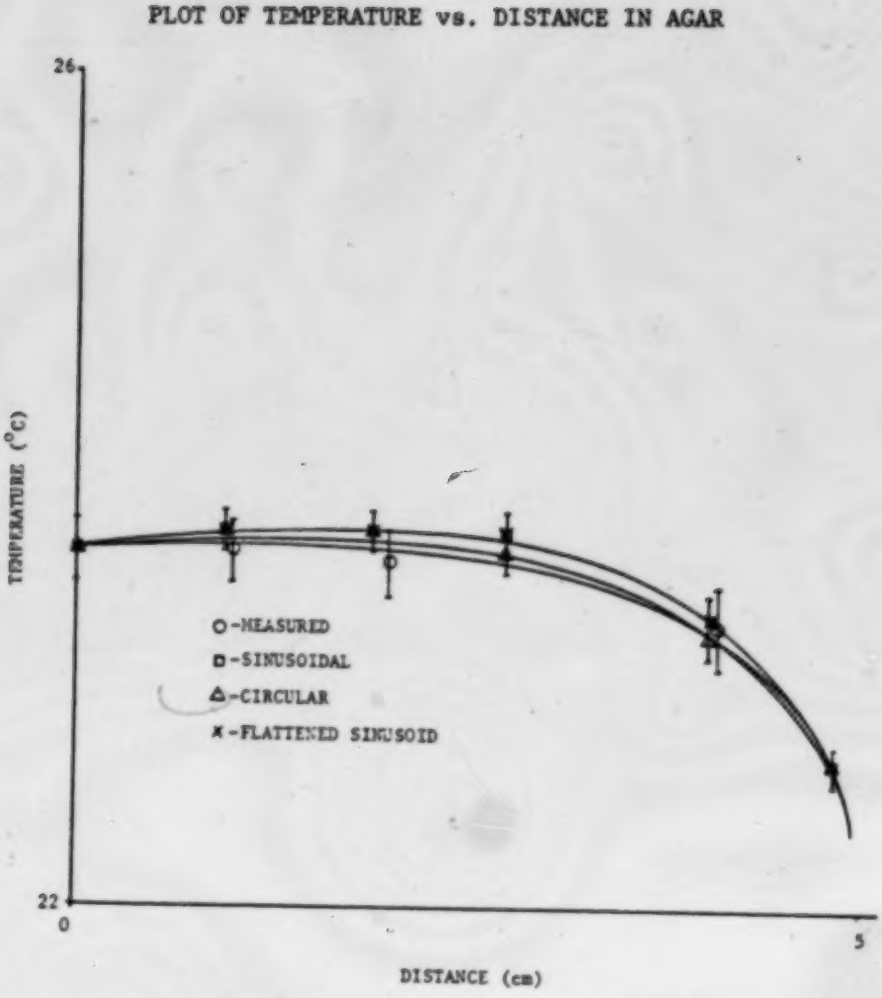

FIGURE 4.29 Temperature profiles along 90° radial.

PLOT OF TEMPERATURE vs. DISTANCE IN AGAR

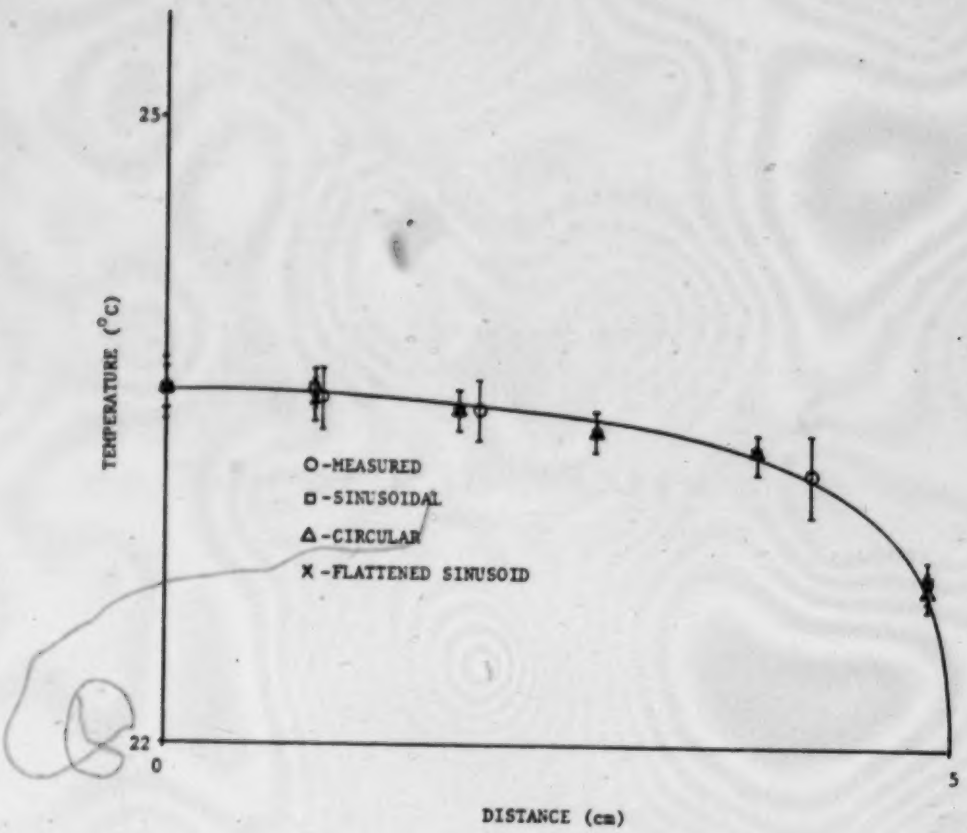

FIGURE 4.30 Temperature profiles along 135° radial.

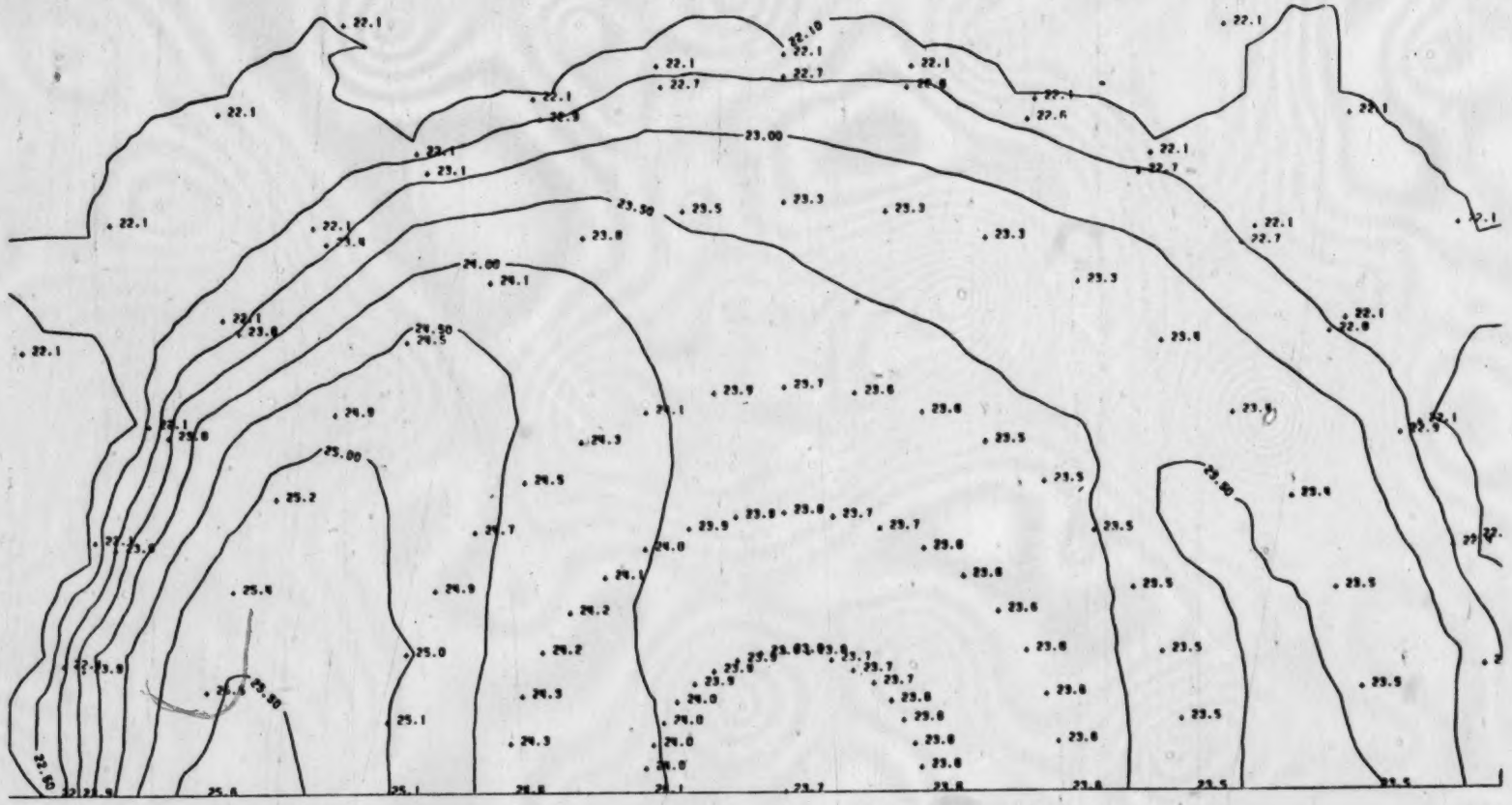

FIGURE 4.31 Calculated temperature distribution inside agar cylinder heated with asymmetric orbiting electrodes. Electrodes undergoing circular speed variation through ±40° arc.

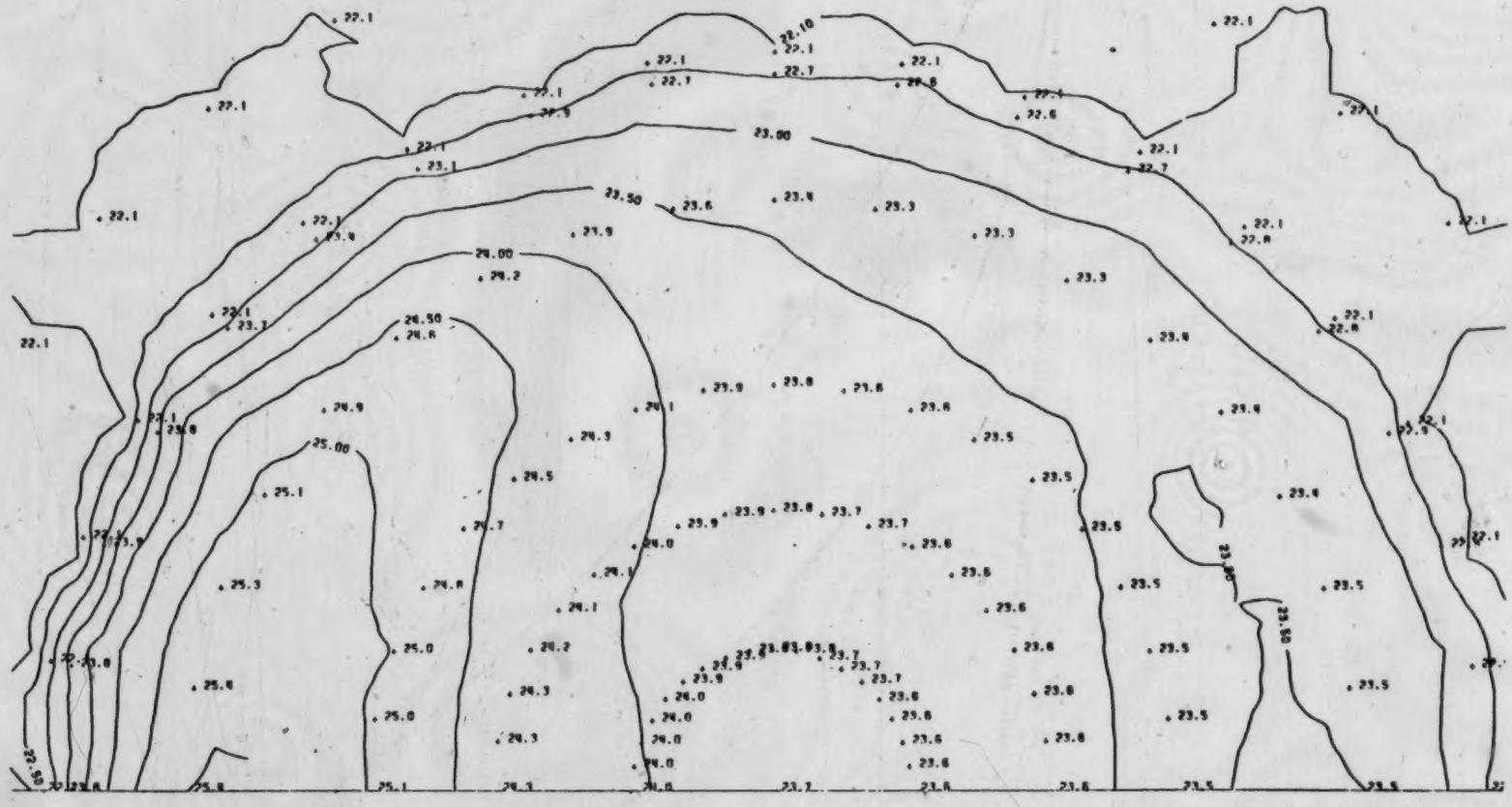

FIGURE 4.32 Calculated temperature distribution inside agar cylinder heated with asymmetric orbiting electrodes. Electrodes undergoing flattened sinusoid speed variation through $\pm 40^{\circ}$ arc.

measured at the centre of the agar phantom for the stationary and orbiting electrode cases revealed a difference in power absorption which could account for much of the discrepancy. During the moving asymmetric electrode measurements slightly less power was absorbed than during the stationary electrode measurements. This was the result of an inability to accurately maintain the power output to the phantom. The temperature difference was too small, probably about 0.05°C, to be picked up with the equipment used. Nontheless, a borderline measurement like 23.85°C (*i.e.* Figure 4.27) might have been 23.9°C with slightly more power. These variations are well within the experimental error already outlined.

Figures 4.27-4.30 show that the calculated temperature profiles are all equivalent to the measured profiles within experimental bounds of uncertainty. Consistent trends, however, show that the flattened sinusoid and circular weight functions produce better results than the sinusoidal function.

The averaging programs HTAVE.3, HTAVE.4, and HTAVE.5 (see Appendix #1) use the sinusoidal, circular, and flattened sinusoid weighting functions to calculate the moving electrode temperature distributions. The results, when compared to measured values, show that these programs can accurately simulate moving electrode temperatures by

using static electrode data.

SIMULATED VARIATION OF APPLICATOR PARAMETERS

The preceding sections establish the validity of using MEGAERA and the HTAVE programs to simulate stationary and moving electrode heating. This provides a means of observing the effect, on the temperature distribution, of altering various parameters.

Figure 4.33 results from using twice the power as in Figure 4.12 with all other parameters the same. The change in centre temperature,

$$\Delta T_c = T_c - 22.1\ ^{o}C$$

where,

T_c-the temperature (°C) at the centre of the agar phantom.

ΔT_c-the change in the centre temperature (°C).

is about 100% higher than in Figure 4.12. Similarly the change in peak temperature,

$$\Delta T_p = T_p - 22.1\ ^{o}C$$

where,

T_p-the highest temperature (°C) occurring in the phantom.

ΔT_p-the change in peak temperature (°C)

is about 100% higher. These results are expected in view

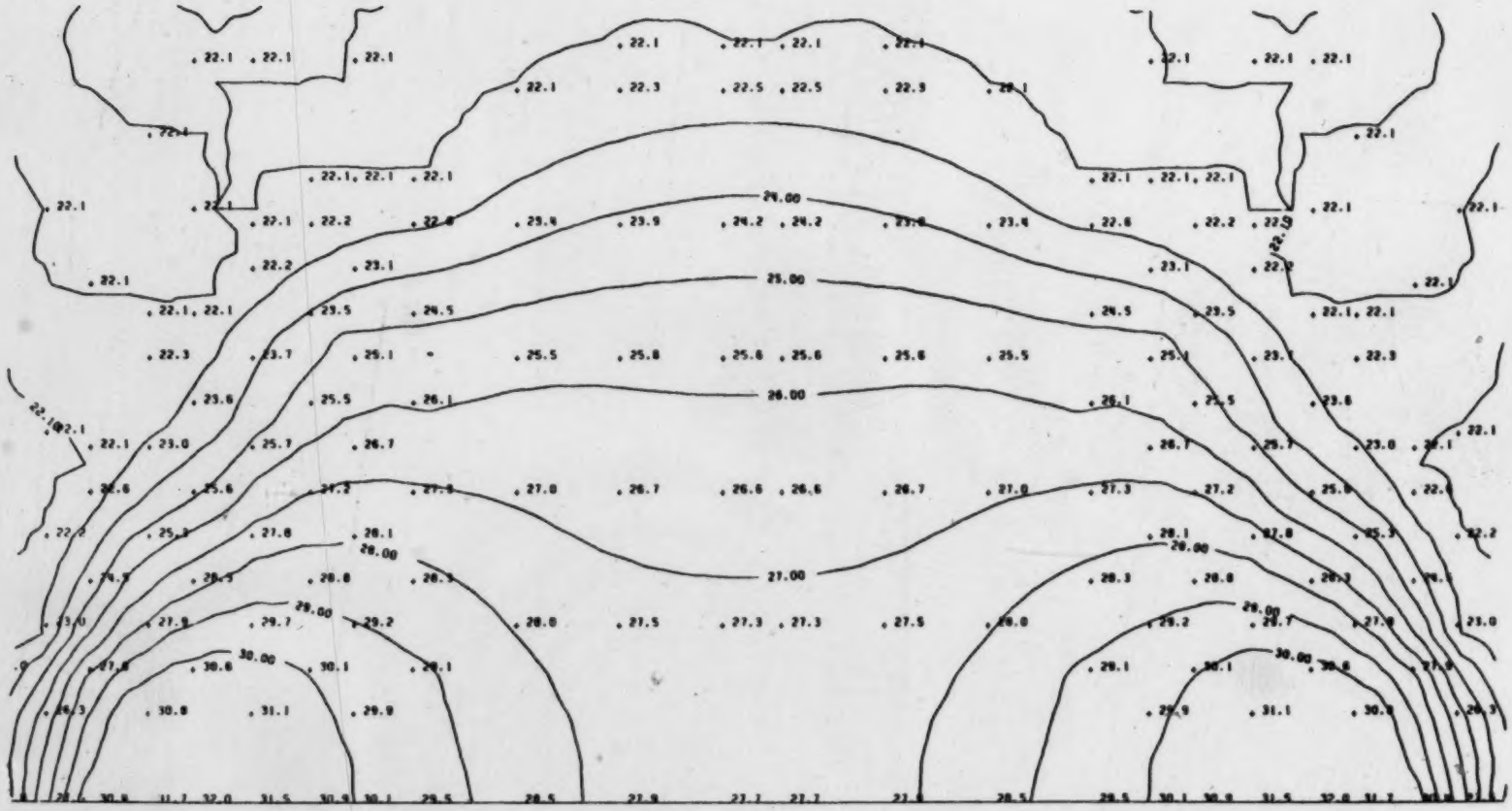

FIGURE 4.33 Calculated temperature distribution using same parameters as in Figure 4.12 except twice the power.

of the doubled input power. However, this linear relation is not obtained at higher power levels.

Figure 4.34 results from using the same parameters as in Figure 4.12 except that the power is set four times higher to 50.4 watts. The temperature peaks occur at about the same positions in each case. ΔT_p is 296% higher and ΔT_c is 311% higher than in Figure 4.12. Thermal conduction into the water bath prevents ΔT_p and ΔT_c from being linearly proportional to the power used.

The effect of varying the water bath temperature is shown in Figure 4.35. The parameters used are the same as in Figure 4.34 except that the saline bath temperature is assumed to be 10°C. The temperature peaks are in the same positions as with the 22.1°C bath but ΔT_p is [illegible]% lower while ΔT_c is only 1.8% lower. This demonstrates the importance of having a cooling water bath. A substantial decrease in superficial temperatures can be achieved without significantly affecting deep temperatures.

Figure 4.36 results from using the same parameters as in Figure 4.33 except that the saline bath electrical conductivity is set to be five times higher. The temperature changes ΔT_p and ΔT_c are both about 47% lower than in Figure 4.33. This demonstrates the importance of using a bath, or bolus, which provides an electrical match

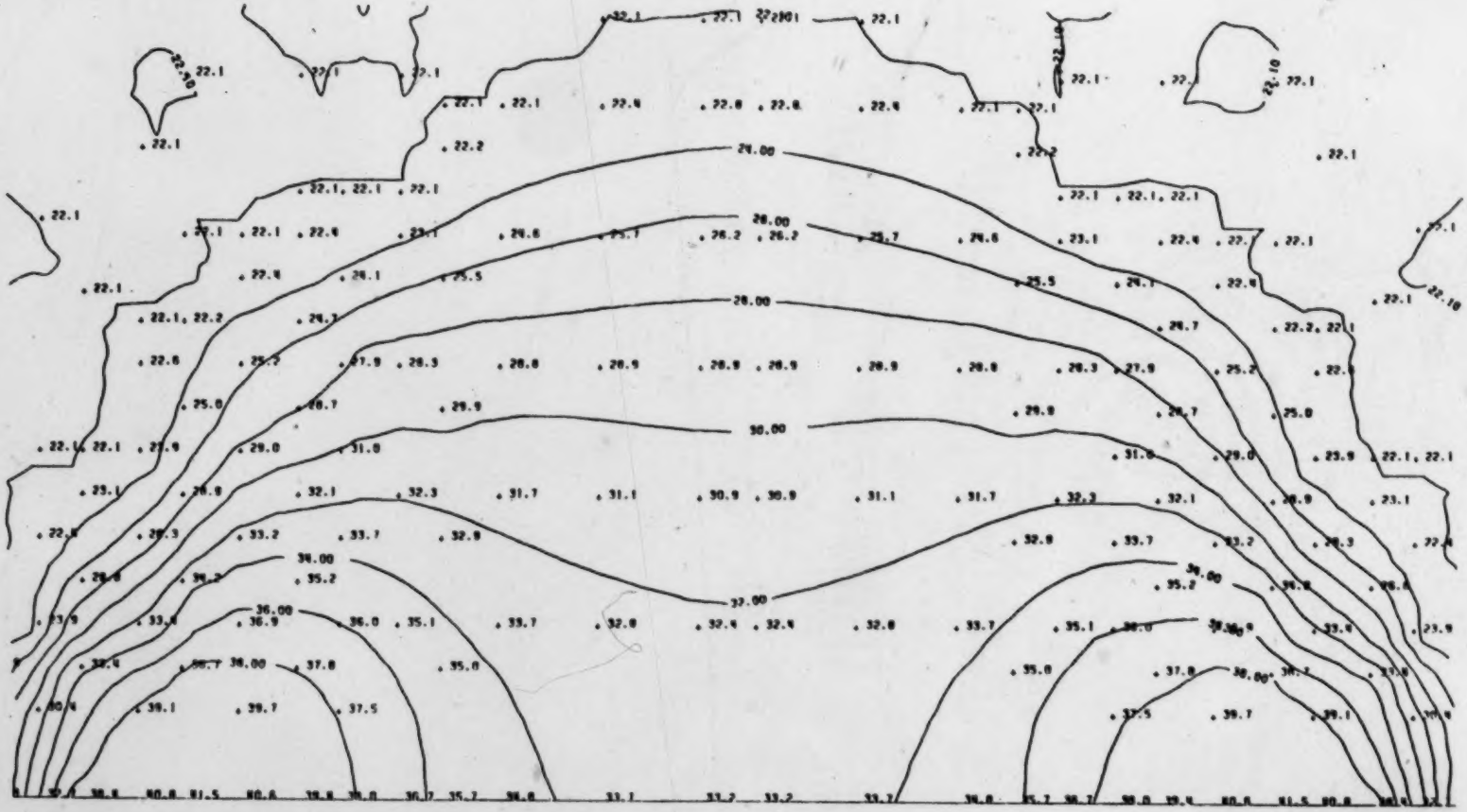

FIGURE 4.34 Calculated temperature distribution using same parameters as in Figure 4.12 except four times the power.

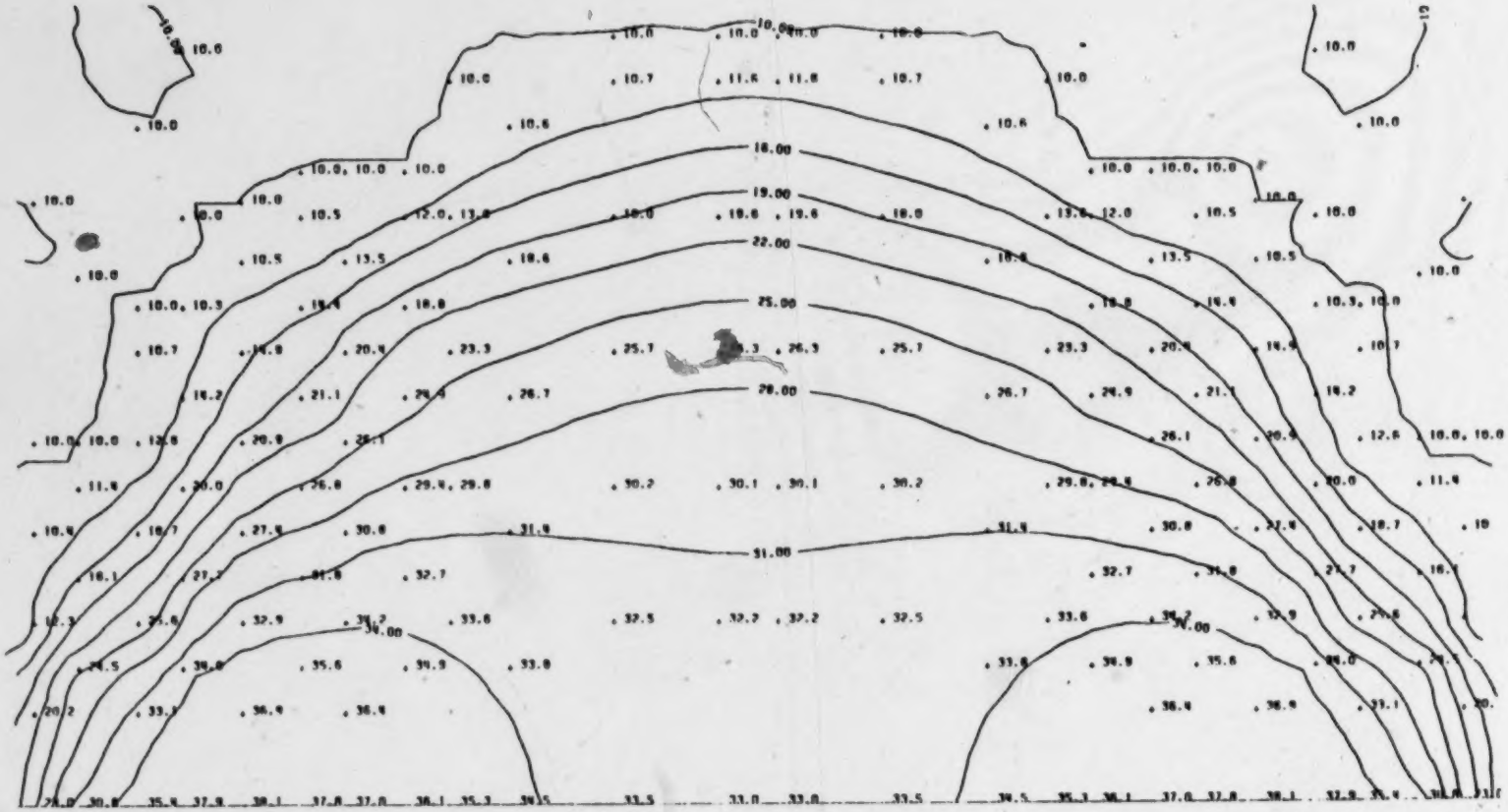

FIGURE 4.35 Calculated temperature distribution using the same parameters as in Figure 4.34 except a 10°C saline bath.

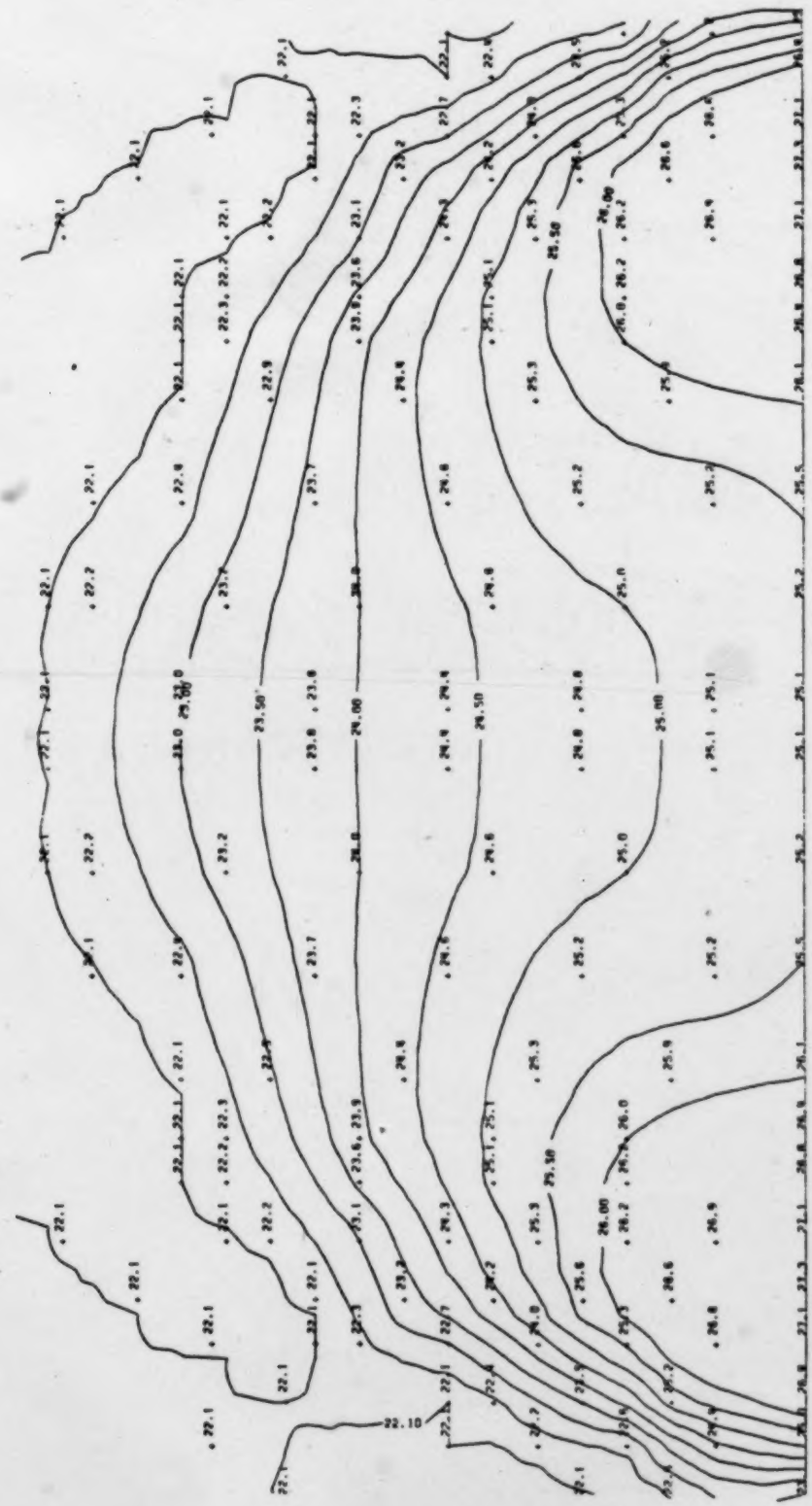

FIGURE 4.36 Calculated temperature distribution using the same parameters as in Figure 4.33 except five times the bath electrical conductivity.

to the irradiated dielectric. Matched impedances result in maximum power transfer.

Figure 4.37 shows again the effect of having a massive impedance mismatch. In this case the electrical conductivity of the bath is assumed to be about nineteen times lower than in Figure 4.33. The ΔT_p is 75% lower and the ΔT_c 80% lower than in the matched situation.

Figure 4.38 demonstrates the effect of positioning the electrodes 3.55 cm from the agar instead of 1.85 cm. The ΔT_p is reduced by 56% and the ΔT_c by 41%. The smaller drop in ΔT_c implies that slightly improved deep heating may result from this configuration over that in Figure 4.33.

The change in temperature distribution produced by using progressively wider electrodes is illustrated in Figures 4.39 to 4.44. To produce these figures the parameters are slighty different from those used for Figures 4.12 or 4.33. As a result, they cannot be directly compared to those figures. Taken between themselves, however, Figures 4.39-4.44 serve to demonstrate the trend produced by widening electrodes.

Figures 4.39 and 4.40 show the temperature pattern produced using 1 cm wide electrodes. Temperature peaks are high and close to the surface. The centre temperature is

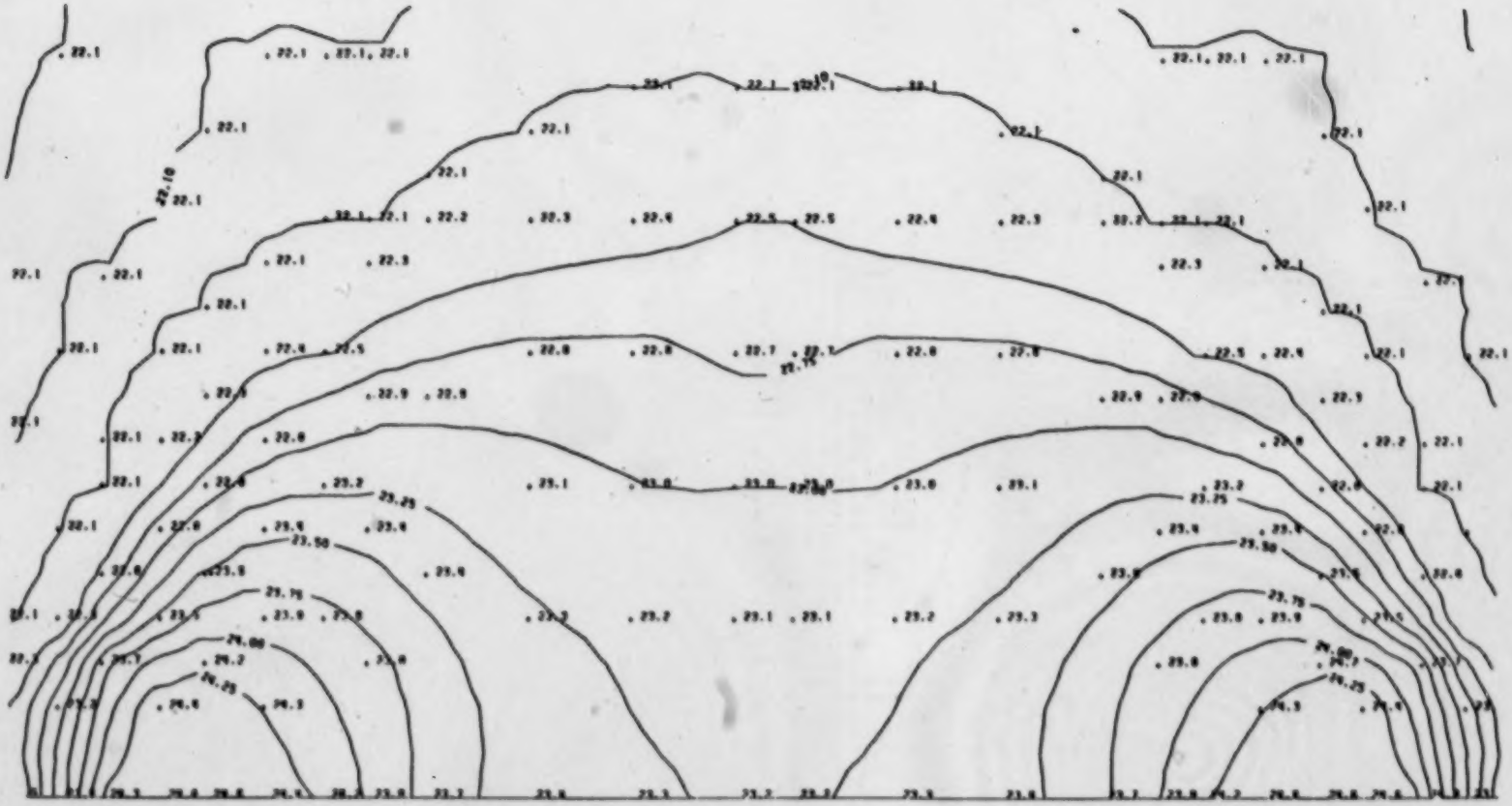

FIGURE 4.37 Calculated temperature distribution using the same parameters as in Figure 4.33 except one nineteenth the bath electrical conductivity.

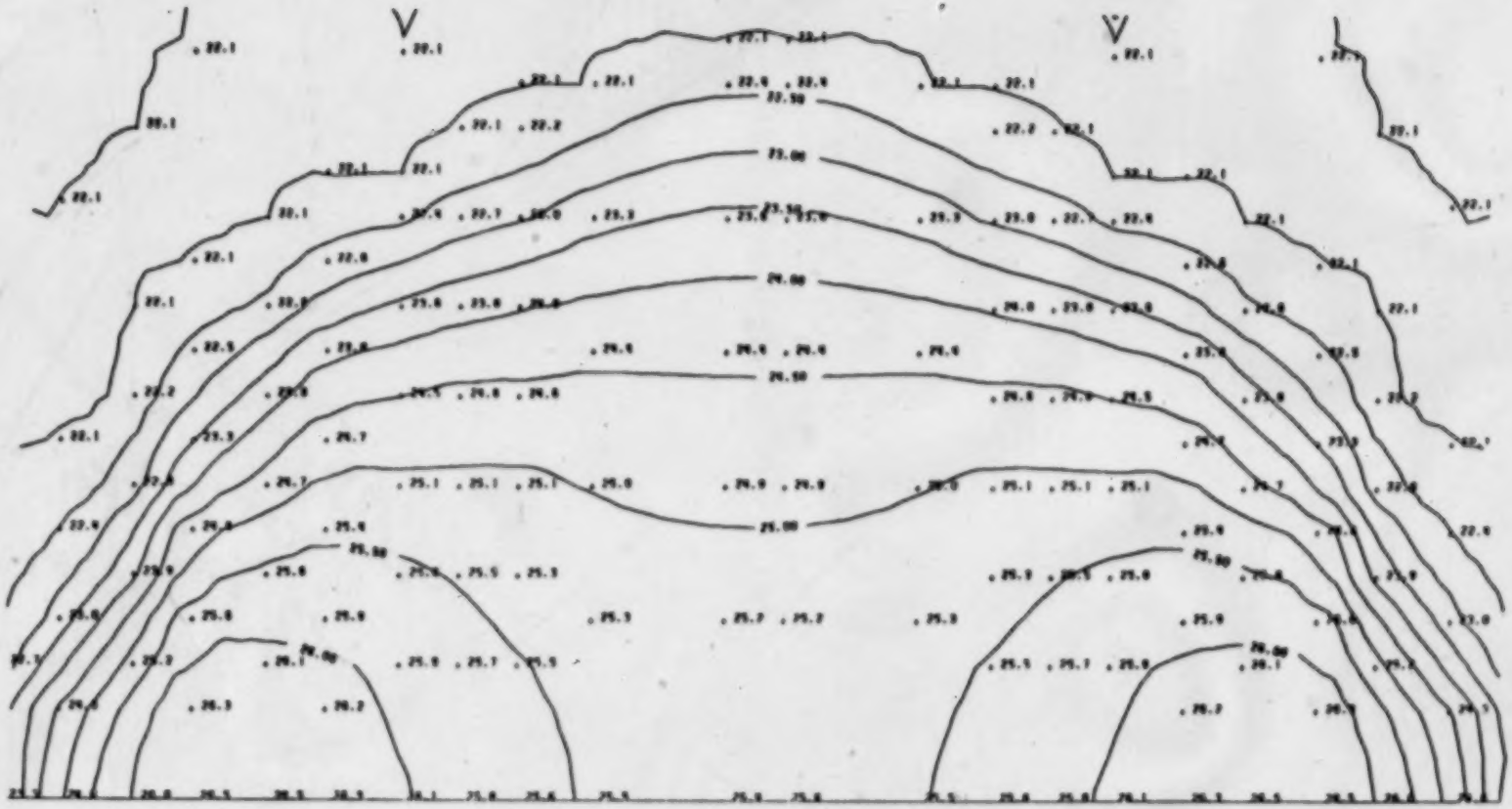

FIGURE 4.38 Calculated temperature distribution using the same parameters as in Figure 4.33 except the electrodes are farther (3.55 cm) apart.

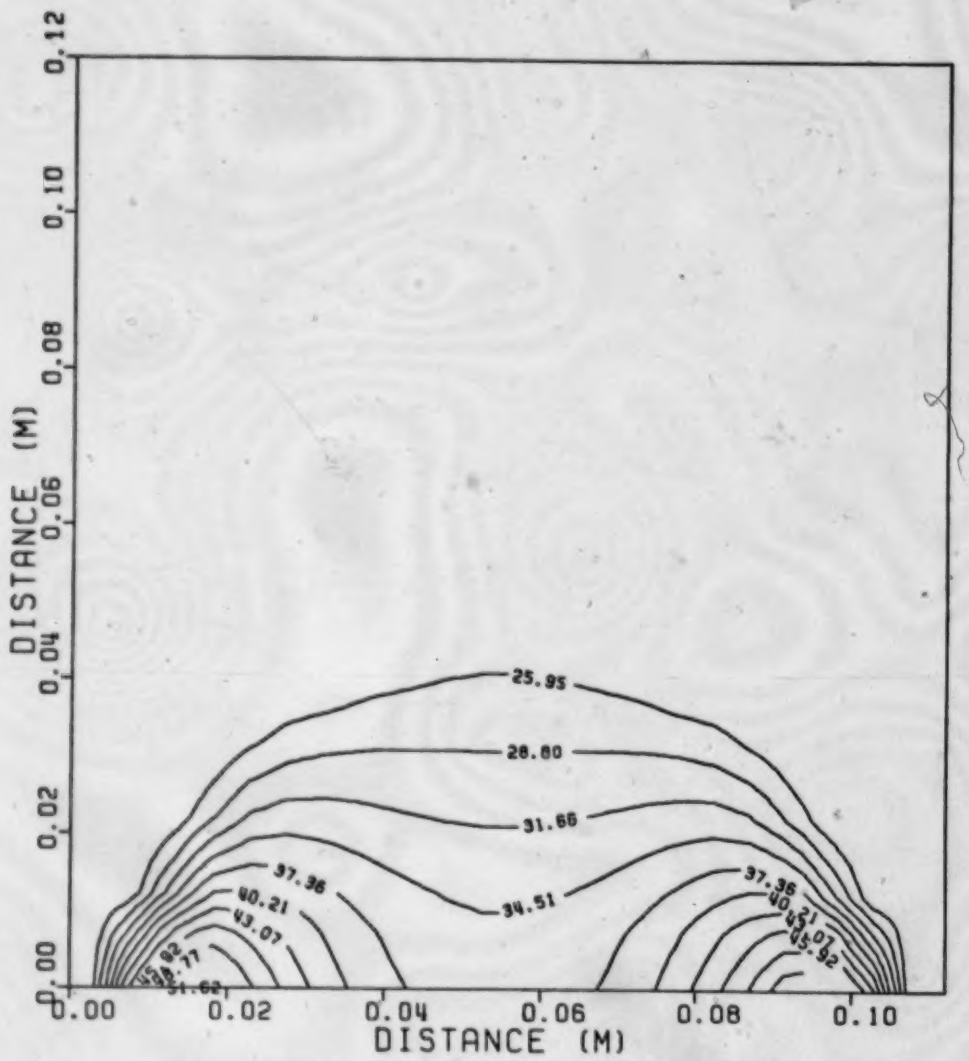

FIGURE 4.39 Calculated temperature distribution in medium using 1 cm wide stationary symmetric electrodes.

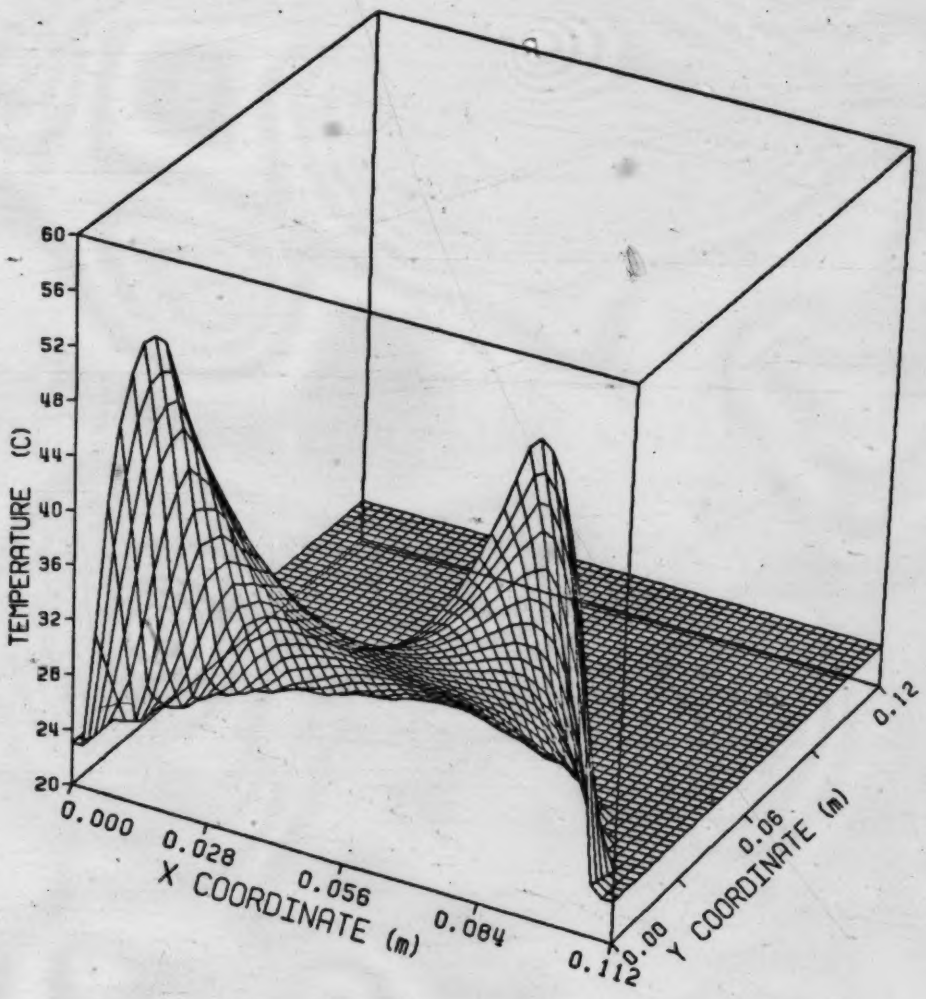

FIGURE 4.40 Three dimensional plot of Figure 4.39.

low resulting in large thermal gradients. Figures 4.41 and 4.42 show the pattern resulting from 2 cm wide electrodes. Temperature peaks occur slightly deeper than with the 1 cm electrodes. The ΔT_p is 8.5% lower with the 2 cm electrodes and the ΔT_c is 12% higher. A smoothing effect is seen to occur in the temperature distribution when wider electrodes are used. This effect is also demonstrated in Figures 4.43 and 4.44. These simulations assume 4 cm wide electrodes. Again, the temperature peaks are broader and occur about 0.5 cm deeper than in Figure 4.39. The ΔT_p is 26% lower than with 1 cm wide electrodes and the ΔT_c is 22% higher. For producing deep heating this levelling effect is most useful.

Higher centre temperatures are produced by wide electrodes because the field between them is more uniform. This situation is roughly analogous to comparing the E-field between two point charges with that between two infinite line charges. The electric field around a point charge varies with the inverse square of the distance from the charge. In the case of an infinite line charge the electric field is inversely proportional to the distance from it. Consequently the field between the lines does not vary as much as that between the two points. This is clearly seen in Figures 4.39 to 4.44 as the electrodes become more like lines of charge rather than points.

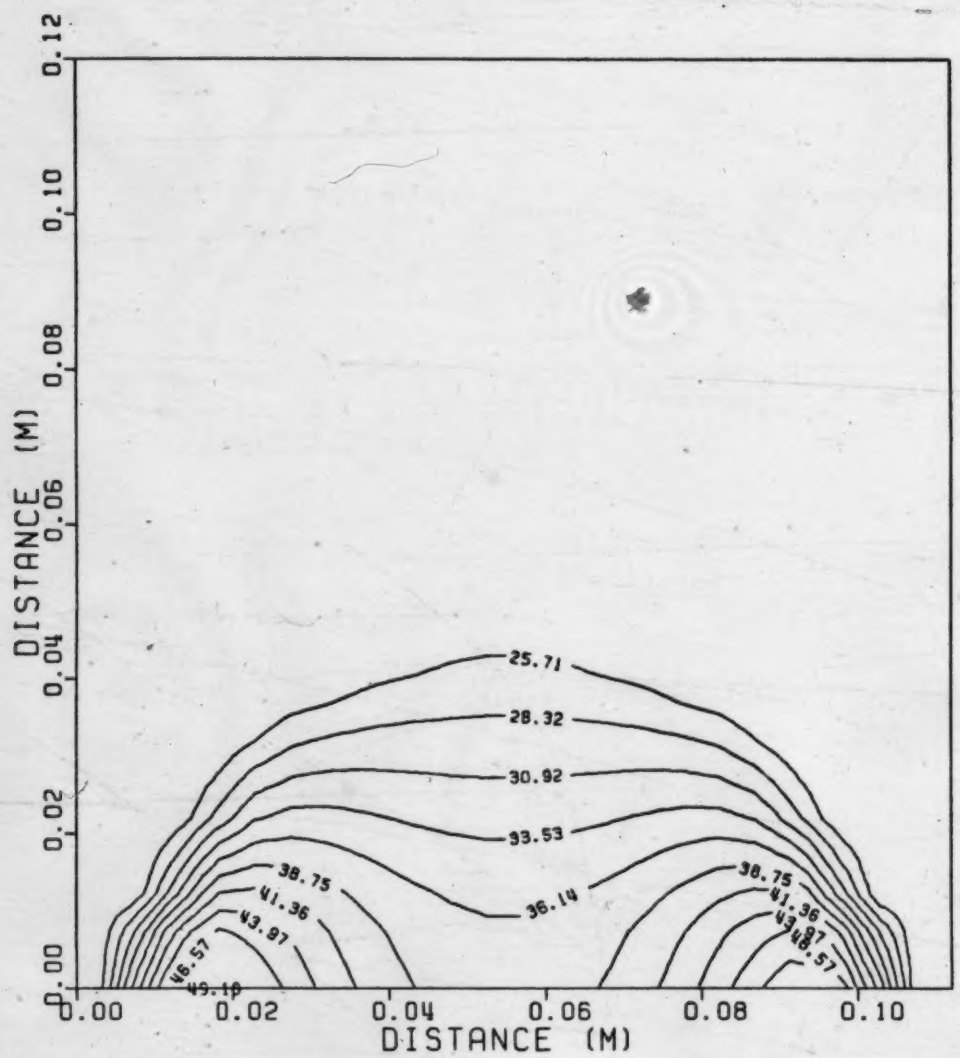

FIGURE 4.41 Calculated temperature distribution in medium using 2 cm wide stationary symmetric electrodes.

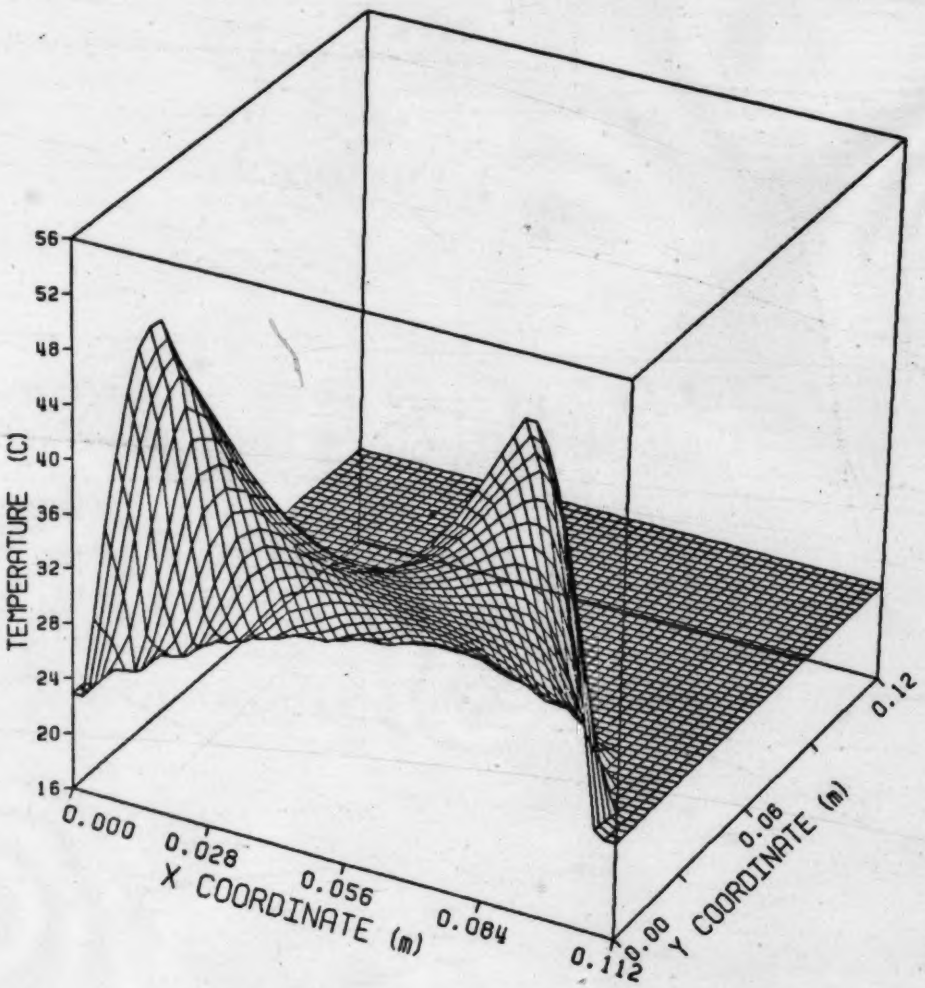

FIGURE 4.42 Three dimensional plot of Figure 4.41.

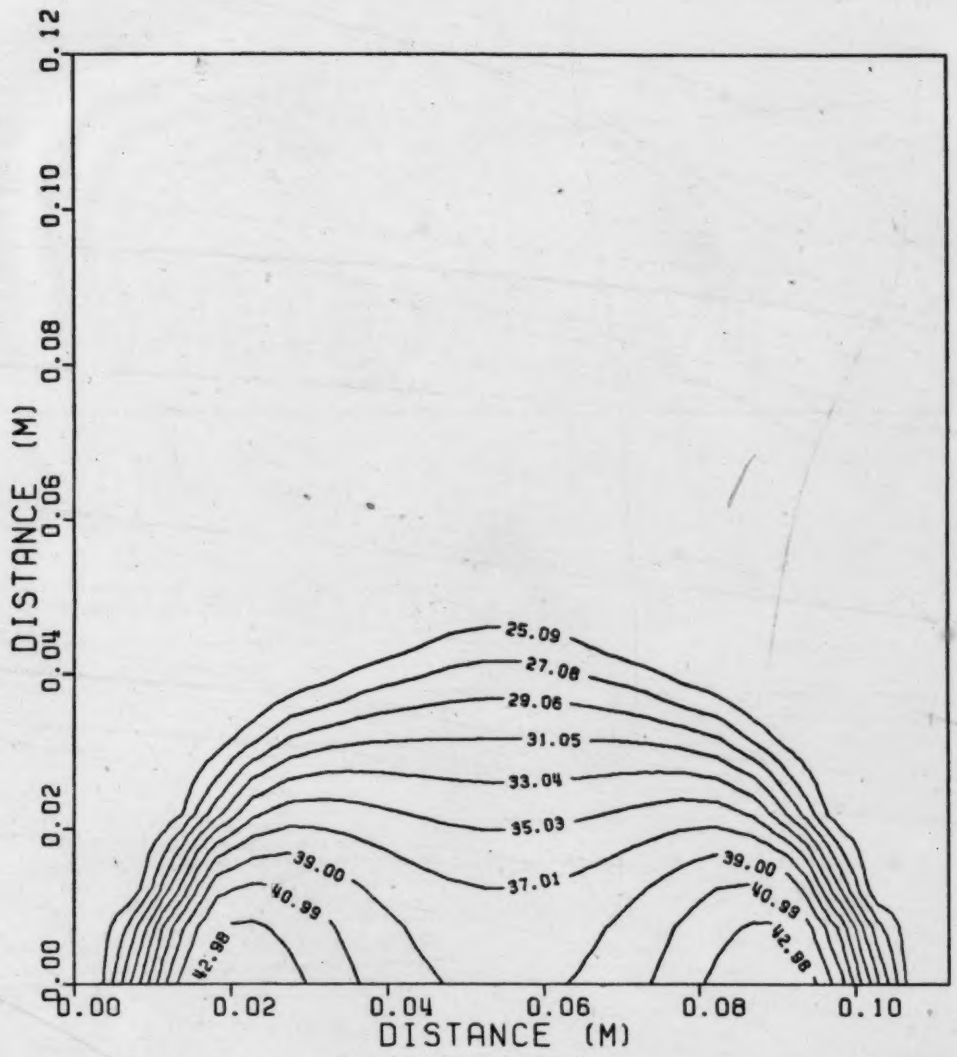

FIGURE 4.43 Calculated temperature distribution in medium using 4 cm wide stationary symmetric electrodes.

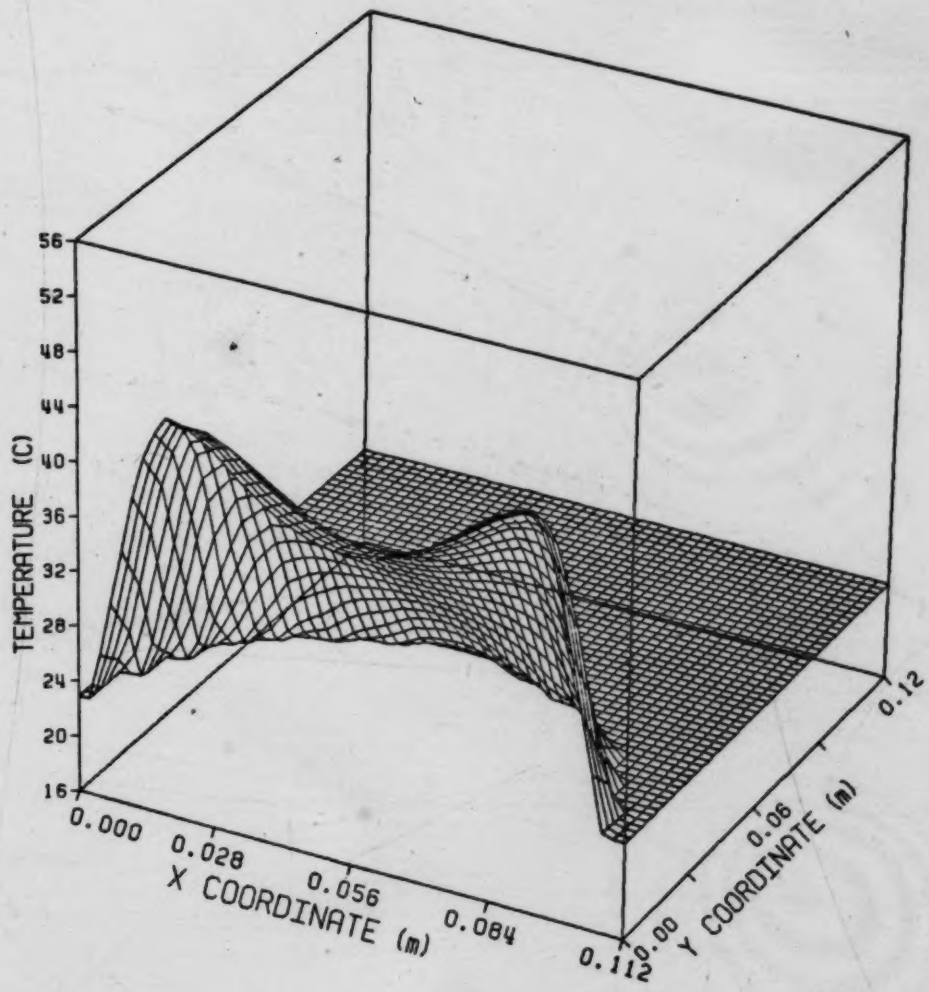

FIGURE 4.44 Three dimensional plot of Figure 4.43.

A trend exists which indicates that, for stationary electrodes, deep heating is most effectively produced by using large electrodes. When using submerged electrodes care must be taken to ensure that the r.f. power amplifier is not loaded down by the low impedance of large electrodes. A matching network can be used to protect the r.f. amplifier. However, there could be a problem with most of the power being dissipated in the matching network and not the load. This results in inefficiency but may not be important if sufficient power is available.

Having established that the temperature peaks get smaller and the centre temperature higher as the electrodes get wider, it is logical to see if the centre temperature can be maximized in this way.

Figure 4.45 was produced using the same parameters as Figure 4.33 except that the electrodes were set to be the same width as the agar phantom. Changes in the temperature distribution were similar to those encountered in Figures 4.39 to 4.44 with an important exception. Peak temperatures were slightly higher (1.3%) than those encountered with narrow electrodes. More power was dissipated between the wide electrodes, and less elsewhere in the saline bath, than in the narrow electrode case. Further, the agar phantom essentially filled the space between the electrodes. This led to relatively high

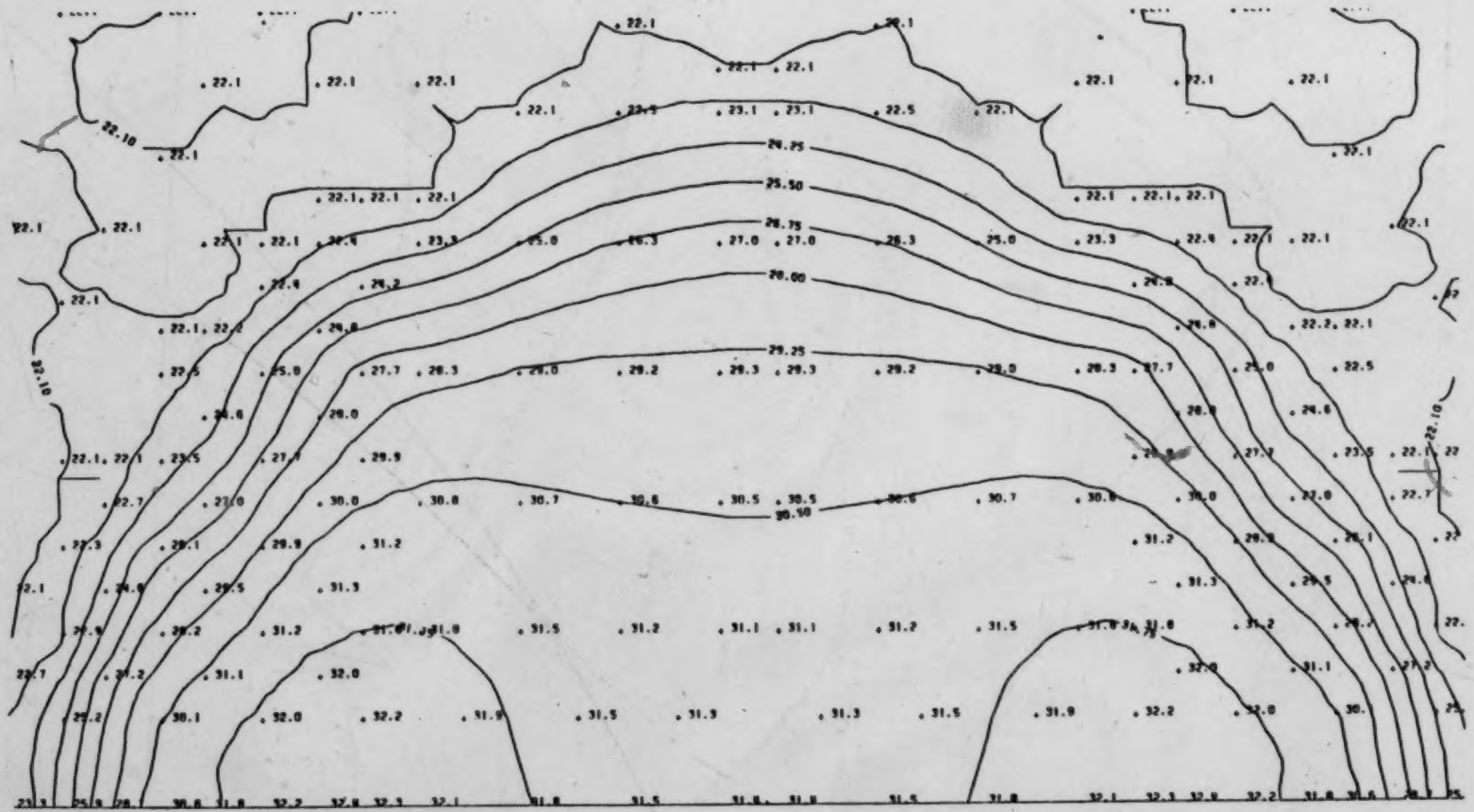

FIGURE 4.45 Calculated temperature distribution using the same parameters as in Figure 4.33 except the electrodes are 9.7 cm wide.

temperatures throughout the agar. The temperature peaks were high because they occurred over 1 cm deeper in the agar than in Figure 4.33. This mitigated the effect of the cooling bath on the peaks and allowed high temperatures to be obtained. ΔT_c was 13.4% higher than with the narrow electrodes. Stronger fields and smaller internal temperature gradients, as previously mentioned, were responsible for this result.

To make the fields inside the agar even more uniform heating from 23.7 cm wide electrodes was simulated (Figure 4.46). This produced one broad temperature peak in the centre of the phantom. The peak was quite low compared to the centre temperature in Figure 4.45 but higher than the centre temperature in Figure 4.33. The low temperature was the result of much of the power being dissipated in the saline between the wide electrodes.

For deep heating purposes the magnitude of the centrally produced 'hot spot' is unimportant. Higher temperatures can be obtained simply by using more power. What is important is the fact that the greatest temperature is produced deep within the agar and not near the surface. For stationary electrodes the oversized applicator produced the most desirable temperature pattern for deep heating.

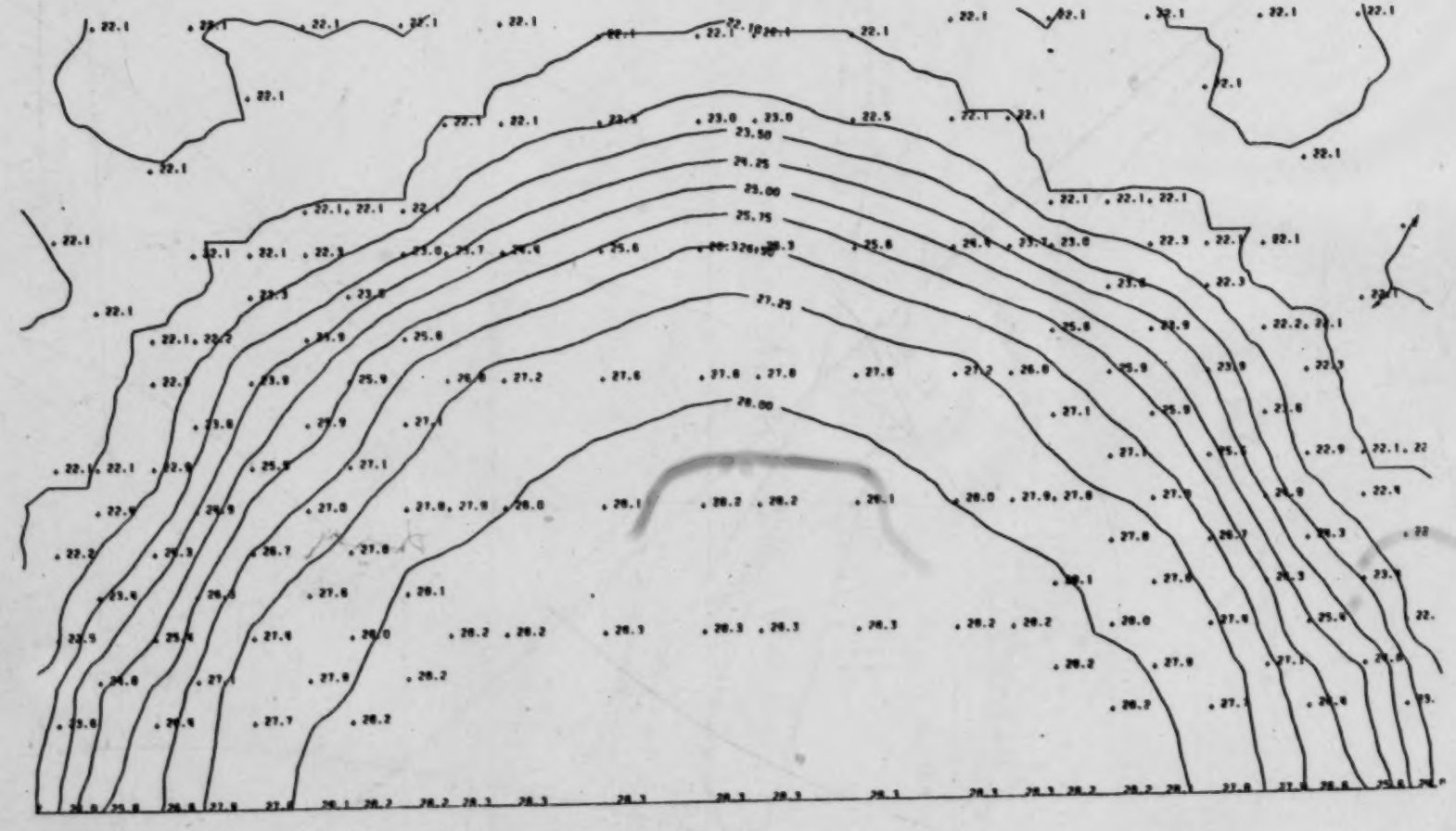

FIGURE 4.46 Calculated temperature distribution using the same parameters as in Figure 4.33 except that the electrodes are 23.7 cm wide.

ROTATING ELECTRODES

To improve deep heating orbiting electrodes can be used. This effect is clearly shown in Figure 4.4. The solid lines correspond to the temperature profiles measured along the x-axis (a) and the y-axis (b) for the stationary electrode case (Figures 4.5 and 4.6). The dashed lines (a) and (b) are the profiles measured along the x and y axes, respectively, for the orbiting electrode case (Figures 4.8 and 4.9). In each case the electrodes are (1.95±0.1) cm from the agar surface. The orbiting electrodes travel through an angle of ±40°, or an 80° arc, for these figures. This movement produces a ΔT_ρ which is 30% lower than the stationary electrode case with no change in the ΔT_c. Spreading the r.f. field exposure over the surface of the phantom produces lower, broader, slightly deeper peak temperatures than found with stationary electrodes.

The effect produced by orbiting electrodes can be maximized by making the electrodes revolve completely and continuously around the phantom. Figure 4.47 is the simulated result of using such revolving electrodes. Data from Figure 4.5 is used along with an averaging program to produce Figure 4.47. Temperature peaks are annular regions which have a ΔT_ρ 41% lower than the stationary electrode case (Figure 4.5). The ΔT_c is the same as with stationary

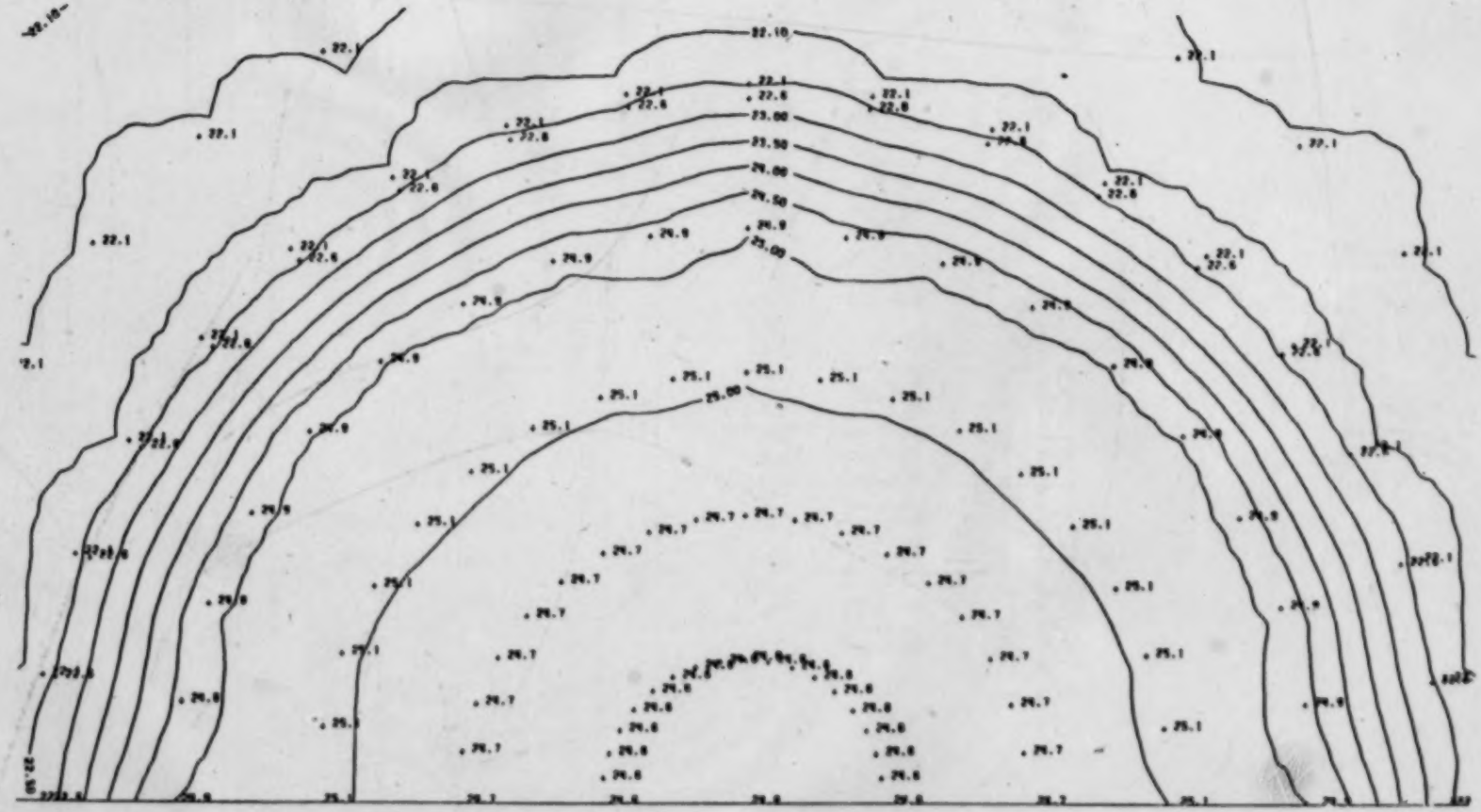

FIGURE 4.47 Calculated temperature distribution using the same parameters as in Figure 4.5 except that the electrodes revolve completely around the phantom.

electrodes. Further, the annular peak is 2.2 cm deep inside the agar where as the stationary electrode peaks are only 0.9 cm deep.

Figure 4.48, based on data from Figure 4.9, shows the expected temperature distribution from revolving asymmetric electrodes. The temperature peak is an annular region with a ΔT_p 59% lower than in the stationary electrode case. This large drop occurs because the temperatures are averaged over one temperature peak instead of two as in Figure 4.47. There is no change in the centre temperature. The temperature peak occurs 1.5 cm deep within the agar instead of 1.1 cm with stationary electrodes (Figure 4.9).

Applying the revolving electrode program to the data in Figure 4.45 results in Figure 4.49. The temperature peak is no longer an annular region but a broad peak in the centre of the agar phantom. Unlike Figure 4.46 this central temperature peak is quite substantial having relatively steep temperature gradients using the same amount of power. The revolving 9.7 cm electrode configuration appears to be the best choice for producing deep heating in a 10 cm diameter agar cylinder.

The model indicates that the best electrode configuration for producing deep hyperthermia uses electrodes which are the same width as the heated subject.

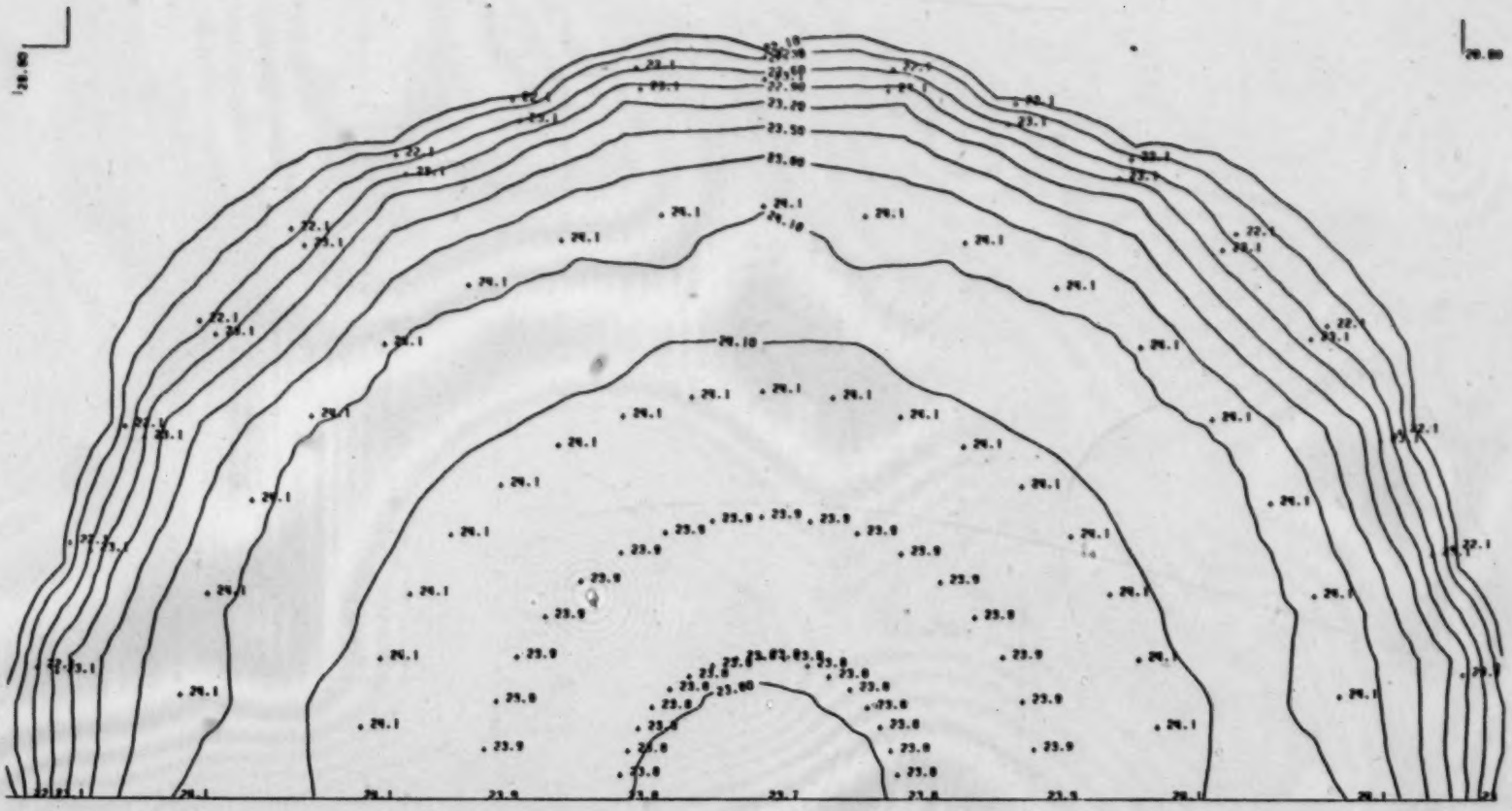

FIGURE 4.48 Calculated temperature distribution using the same parameters as in Figure 4.9 (asymmetric electrodes) except that the electrodes revolve completely around the phantom.

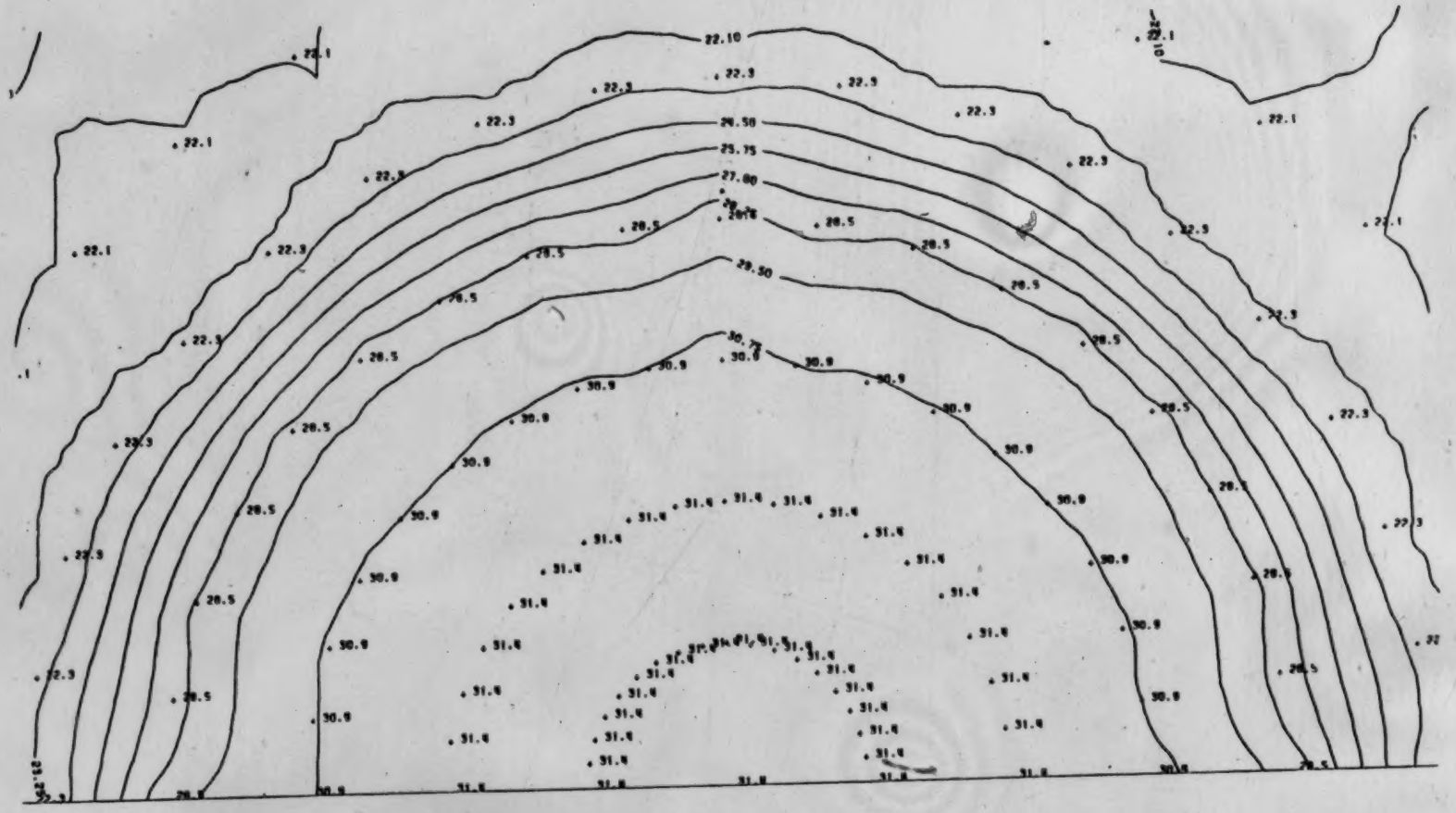

FIGURE 4.49 Calculated temperature distribution using the same parameters as in Figure 4.45 (9.7 cm wide stationary symmetric electrodes) except that the electrodes rotate completely around the phantom.

Also, the electrodes should be symmetrically placed relative to, and revolve continuously around, the subject.

HYPERTHERMIA IN A LIVE ANIMAL

A temperature profile obtained inside a live cat irradiated with orbiting symmetric electrodes is shown in Figure 4.50. Due to a lack of r.f. power the temperatures were quite low. The saline bath and matching network absorbed a significant amount of the energy from the electrodes. Blood flow may have reduced much of the temperature increase which would have occurred. Heating for longer than 20 minutes would probably have increased the core temperature but the cat could have awakened.

The initial temperature in the cat was not actually uniform. The skin temperature was about 38.3°C due to the use of a heating pad during surgery and gradually fell to about 37.4°C deep inside the animal. This variation in temperature likely influenced the final temperature distribution. Time could not be taken to allow the animal's body temperature to reach a uniform steady state because of the danger of the anaesthetic wearing off. A cooler water bath was not used even though it would have controlled the subcutaneous fat temperature because the danger of producing hypothermia in the anaesthetized animal. The small temperature increase exhibited by the tied off kidney was probably due to surrounding blood vessels acting as heat sinks and a low initial

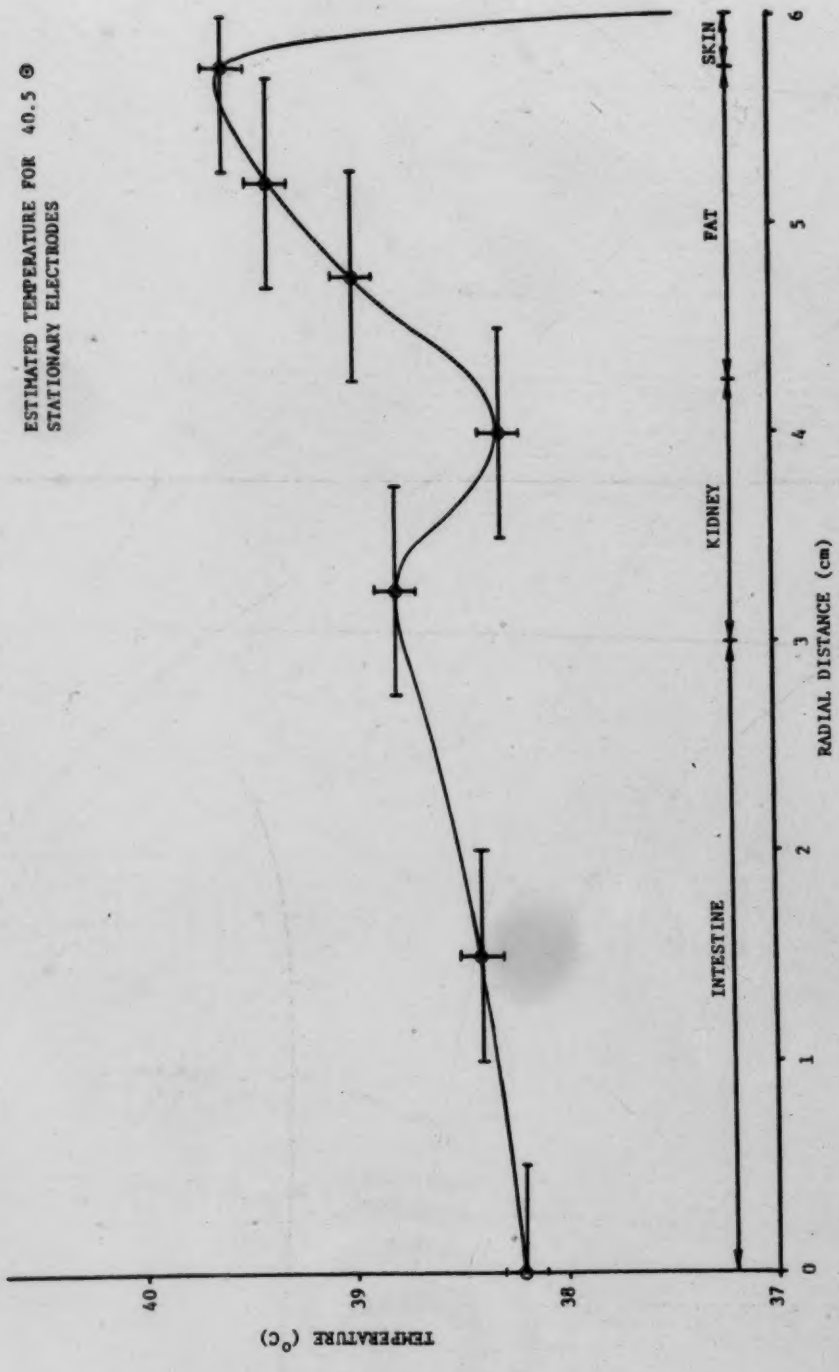

FIGURE 4.50 Temperature profile obtained in a live cat irradiated with symmetric electrodes orbiting between ±40°.

temperature. The temperature peak which occurred at the part of the kidney furthest from the electrode was found in two cats which were treated. A probable explanation was the lack of cooling bloodflow in this region.

The peak temperature in the fat (40.5°C) for stationary electrodes was estimated using the difference between moving and stationary electrode data in the agar (Figures 4.5 and 4.23). This was likely a conservative amount.

DISCUSSION

EVALUATION OF ELECTRODE CONFIGURATIONS

A figure of merit which could describe any hyperthermia applicator is the 'target heating specificity',

$$\eta = \frac{\Delta T_{target}}{\Delta T_{non\text{-}target\ maximum}}$$

where,

ΔT_{target} -the temperature change produced at the target site.

$\Delta T_{non\text{-}target\ maximum}$ -the greatest temperature change produced in the dielectric at a site other than the target site.

Ideally the target heating specificity η should be greater than one. This would imply that the target, or tumor, is hotter than any other part of the irradiated body. Hence, therapeutically significant temperatures could be obtained at the tumor site without risk of damaging any other tissues.

A value for η of one, or slightly less, for an applicator heating agar could still indicate a useful device. Vigorous blood flow in healthy tissue could

produce lower temperatures than implied by the agar or simulations while sluggish circulation in a tumor could produce higher temperatures. As a result, an applicator with an $\eta \leq 1$ in agar or simulations could conceivably produce an $\eta > 1$ in a live subject.

Plainly the symmetric electrode applicator which produced the temperature distribution in Figure 4.5 would give an $\eta < 1$ unless a tumor happened to exist at the site of each temperature peak. While the second temperature peak in healthy tissue would likely be smaller than that in the tumor, there would always by the risk of overheating healthy tissue.

A more practical configuration would use asymmetric electrodes (Figure 4.9). The asymmetry could take the form of differently spaced electrodes, as used in this case, or different sized electrodes. Either case would produce one temperature peak as in Figure 4.9. As long as the tumor was positioned properly this type of applicator could be very useful. Deep heating would be beyond the ability of this type of applicator though. Some steering of the hot spot could be accomplished by varying the bath temperature, electrode size, electrode distance, and by moving the electrodes. However, the results would be difficult to predict, especially in an inhomogeneous human, and the hot spot would grow large and diffuse as depth increased. This

large hot spot would negate the need for steering.

Very few applicators are capable of heating deep seated lung tumors. For these tumors an applicator with an $\eta_{CENTRE} \geq 1$ is required. Table 5.1 lists η_{CENTRE} values for most of the electrode configurations considered in this work. It should be noted that the η_{CENTRE} figures based on Megaera simulations are likely to be slightly high due to the two dimensional nature of the program.

The electrode configurations which produced an $\eta_{CENTRE} \geq 1$ were the 23.7 cm stationary symmetric electrodes and the 9.7 cm revolving symmetric electrodes. In each case the temperature peak occurred in the centre of the agar phantom. Field spreading could reduce these temperature peaks in a three dimension situation but the η_{CENTRE} value would probably change very little. The temperature peaks were broad and relatively flat. This would reduce the need for accurately aiming the hot spot. A tumor with poor blood flow situated anywhere in the temperature peak region would tend to heat up substantially more than its surroundings. From this point of view a small, sharply peaked, hot spot would be undesirable because of difficulty in accurately positioning it inside an inhomogeneous human.

TABLE 5.1

SUMMARY OF TARGET SPECIFICITIES (η) FOR VARIOUS APPLICATORS

η_{CENTRE}	Figure #	Description
0.49	4.5	1 cm wide stationary symmetric electrodes, measured data
0.33	4.9	1 cm wide stationary asymmetric electrodes, measured data
0.55	4.12	1 cm wide stationary symmetric electrodes, simulated
0.38	4.17	1 cm wide stationary asymmetric electrodes, simulated
0.71	4.18	1 cm wide symmetric electrodes, sinusoidal speed variation orbiting $\pm 40^{\circ}$, simulated
0.68	4.23	1 cm wide symmetric electrodes, circular speed variation orbiting $\pm 40^{\circ}$, simulated
0.69	4.24	1 cm wide symmetric electrodes, flattened sinusoidal speed variation orbiting $\pm 40^{\circ}$, simulated
0.5	4.26	1 cm wide asymmetric electrodes, sinusoidal speed variation orbiting $\pm 40^{\circ}$, simulated
0.47	4.31	1 cm wide asymmetric electrodes, circular speed variation orbiting $\pm 40^{\circ}$, simulated
0.48	4.32	1 cm wide asymmetric electrodes, flattened sinusoidal speed variation orbiting $\pm 40^{\circ}$, simulated
0.57	4.33	1 cm wide stationary symmetric electrodes, 25.2 watts, simulated
0.57	4.34	1 cm wide stationary symmetric electrodes, 50.4 watts, simulated
0.68	4.35	1 cm wide stationary symmetric electrodes, 50.4 watts, simulated, 10°C bath
0.58	4.36	1 cm wide stationary symmetric electrodes, 25.2 watts, simulated, $5 \times \sigma_{bath}$

TABLE 5.1 (continued)

η_{CENTRE}	Figure #	Description
0.44	4.37	1 cm wide stationary symmetric electrodes, 25.2 watts, simulated, σ_{bath} / 19
0.75	4.38	1 cm wide stationary symmetric electrodes, 25.2 watts, simulated, electrodes 3.55 cm from agar
0.90	4.45	9.7 cm wide stationary symmetric electrodes, 25.2 watts, simulated
$\geq$1.0	4.46	23.7 cm wide stationary symmetric electrodes, 25.2 watts, simulated
0.83	4.47	1 cm wide rotating symmetric electrodes, 25.2 watts, measured data, rotation through 360^{0}
0.80	4.48	1 cm wide rotating asymmetric electrodes, 25.2 watts, measured data, rotation through 360^{0}
$\geq$1.0	4.49	9.7 cm wide rotating symmetric electrodes, 25.2 watts, simulated data, rotation through 360^{0}

Figure 4.49 shows a temperature distribution which is more desirable than that in Figure 4.46. The temperatures are much higher for the same amount of power which shows that the thinner electrodes are more efficient. More power is dissipated in the agar with 9.7 cm electrodes than with 23.7 cm electrodes. Using the revolving electrodes the temperature peak is not as flat as with the wider stationary electrodes. This means a higher proportion of power is being deposited in the centre of the agar phantom than near the surface. The temperature peak could be made steeper by using a cooler saline bath. This is borne out by comparison of η_{CENTRE} values for Figures 4.34 and 4.35. Use of a 10°C bath increased η_{CENTRE} from 0.57 to 0.68. The need for having a bath or bolus for matching purposes is well demonstrated in Figures 4.33, 4.36, and 4.37. Changing the electrical conductivity of the bath either substantially lowers η_{CENTRE} (Figure 4.37) or has little effect on it (Figure 4.36). In each of Figures 4.36 and 4.37 less power is deposited in the agar than when there is an electrical match between the bath and agar (Figure 4.33). Increasing the spacing between the electrodes also increases η_{CENTRE} as in Figure 4.38 (*i.e.* η_{CENTRE} =0.75 instead of 0.57 for Figure 4.34). The price paid here is less efficient use of power. Simply using electrodes the same width as the subject being heated (Figure 4.45) gives a much higher η_{CENTRE} (η_{CENTRE} =0.9) and temperatures than changing electrode spacing. The improvement that results

from orbiting or revolving the electrodes around the phantom is clearly shown in Table 5.1. For the symmetric electrodes η_{CENTRE} is 0.49 for stationary electrodes (Figure 4.5) and 0.83 for the revolving electrodes (Figure 4.47). Similarly for asymmetric electrodes η_{CENTRE} is 0.33 for the stationary case (Figure 4.9) and 0.8 for the revolving case (Figure 4.48). The increase in η_{CENTRE} because of orbiting electrodes is dependent on the variation in temperature around the agar phantom. In fact, because the temperature contours are very close to being circular in Figure 4.46 moving electrodes would have virtually no effect on the temperature distribution. This result plus that with the widely spaced electrodes (Figure 4.38) argues against the utility of LeVeen's moving electrode hyperthermia applicator [38]. The results indicate that little benefit would be derived by moving the widely spaced electrodes about.

CLINICAL CONSIDERATIONS

The advantages of using orbiting electrodes with surface cooling and dielectric matching are apparent for heating deep tumors. In addition, if parallel electrodes are used they should be as wide as the object being heated. Unlike agar the human body has a layer of poorly conducting fat just below the skin which tends to overheat in high power r.f. fields. Fortuitously orbiting electrodes reduce surface, or near surface, temperatures the most. Combining orbiting electrodes with adequate surface cooling, sufficiently wide electrodes, and enough power, high core temperatures could be obtained with tolerable fat temperatures.

In a clinical setting more power could be made available to overcome the intrinsic inefficiency of this system. Large amounts of power can be absorbed by the coupling medium (saline) because it is lossy and acts as a heat sink. Clinically this power loss is not significant as temperature distribution not efficiency is the primary consideration.

CONCLUSIONS

The temperature distribution data clearly shows the advantages of using moving applicators to produce deep hyperthermia. Further, a cooling bolus which is electrically matched to the subject and electrodes as wide as the subject are important. This should allow high temperatures to be obtained deeply without overheating surface material. Clinically this means that deep tumors have a much better chance of being heated with the applicators described above than with the usual stationary applicators.

Live animal experiments have not yet demonstrated deep internal heating. More r.f. power, or a smaller animal, coupled with a cooled saline bath should produce better temperature distributions.

In summary, r.f. heating of agar has been simulated for both moving and stationary electrode cases. From this model an applicator using rotating electrodes the same width as the subject and a cooled, electrically matched bolus has been found to produce deep heating without high superficial temperatures.

BIBLIOGRAPHY AND REFERENCES

[1]Alpin, E., "Hyperthermia-Introduction-Cellular and Molecular". unpublished.

[2]Anderson, A.P., M. Melek, B.H. Brown, "Feasibility of Focused Microwave Array System for Tumour Irradiation", *Electronics Letters*, vol.15, no. 18, Aug. 30, 1979, pp.564-565.

[3]Antich, P.P., N. Tokita, J.H. Kim, E.W. Hahn, "Selective Heating of Cutaneous Human Tumours at 27.12 MHz", *IEEE Trans. Microwave Theory Tech.*, vol. MTT-26, no. 8, Aug. 1978. pp. 569-572.

[4]Arcangeli, G., E. Barnia, A. Cividalli, F. Mauro, Morelli, C. Nervi, M. Spano, A. Tabocchini, "Effectiveness of Microwve Hyperthermia Combined with Ionizing Radiation: Clinical Results on Neck Node Metastases", *Int. J. Radiation Oncology Bio. Phys.*,vol.6, 1980, pp. 143-148.

[5]von Ardenne, M., W. Kruger, "The Use of Hyperthermia Within the Frame of Cancer Multistep Therapy", *Ann. N.Y. Acad. Sci.*,vol.335, pp. 356-361, 1980.

[6]d'Arsonaval, "Therapeutic Applications of High Frequency Currents", *Arch. Phys. Therapy, X-ray, Radium*, vol.13, 1932, pp.715-717.

[7]Bottomley, P.A., "A Technique for the Measurement of Tissue Impedance From 1 to 100 MHz Using a Vector Impedance Meter", *J. Phys. E.: Sci. Instrum.*, vol.11, 1978, pp.413-414.

[8]Bowman, H.F., "Heat Transfer and Thermal Dosimetry", *JMP*, vol.16, no.2,1981, pp. 121-133.

[9]Bragg, G.M., *Principles of Experimentation and Measurement*, Prentice-Hall Inc., Englewood Cliffs, New Jersey, 1974. p.79.

[10]Breasted, J.H., "The Edwin Smith Surgical Papyrus", Chicago, 1930 (cited in S. Licht, "History of Therapeutic Heat," in *Therapeutic Heat and Cold* , ch.VI) New Jersey: E. Licht, 1965.

[11]Carpenter, C.M. and A.B. Page, "The Production of Fever in Man by Short Radio Waves", *Science*, vol.LXXI, no. 1844, May 2, 1930, pp.450-452.

[12]Cavaliere, R., E.C. Ciocatto, B.C. Giovanella, C. Heidelberger, R.O. Johnson, M. Margottini, B.

Mondovi, G. Moricca, A. Rossi-Fanelli, "Selective Heat Sensitivity of Cancer Cells", *Cancer*, vol.20, pp.1351-1381, 1967.

[13]Cavaliere, R., G. Moricca, F. DiFilippo, A. Caputo, G. Monticelli, and F. Santori, "Heat Transfer Problems during Local Perfusion in Cancer Treatment", *Ann. N.Y. Acad. Sci.*, vol. 335,1980, pp.311-326.

[14]Cheung, A.Y., W.M. Golding, G.M. Samaras, "Direct Contact Applicators for Microwave Hyperthermia", *JMP*, vol.16, no. 2, 1981, pp.151-159.

[15]de Cholnoky, T., "Short Wave Therapy in Pyrogenic Skin Infections", *Arch. Phys. Med.*, vol. 16, Oct. 1935, pp. 537-594.

[16]Christensen, D.A., C.H. Durney, "Hyperthermia Production for Cancer Therapy: A review of Fundamentals and Methods", *JMP*, vol.16, no.2, 1981, pp.89-105.

[17]Coley, W.B., "The Treatment of Malignant Tumors by Repeated Innoculations of Erysipelas: With a Report of Ten Original Cases", *Am. J. Med. Sci.*, vol. 105, 1893, pp. 487-511.

[18]Crile, G., "The Effects of Heat and Radiation on Cancers Implanted on the Feet of Mice",*Cancer Research*, vol. 23, March 1963, pp. 372-380.

[19]Dickson, J.A., D.S. Muckle, "Total-body Hyperthermia vs. Primary Tumour Hyperthermia in the Treatment of the Rabbit VX-2 Carcinoma",*Cancer Research*, vol. 32, Sept. 1972, pp.1916-1923.

[20]Dickson, J.A., "Conference Summary: Hyperthermia",*Ann. N.Y. Acad. Sci.*, vol. 335, 1980, pp.524-527.

[21]Doss, J.D. and C.W. McCabe, "A Technique for Localized Heating in Tissue: An Adjunct to Tumour Therapy",*Medical Instrumentation*, vol. 10, 1976, pp. 16-21.

[22]Durney, C.H., C.C. Johnson, P.W. Barber, H. Massoudi, M.F. Iskander, J.L. Lords, D.K. Ryser, S.J. Allen, J.C. Mitchell, *Radio Frequency Radiation Dosimetry Handbook (Second Edition)*, USAF School of Aerospace Medicine, Brooks Air Force Base, Report SAM-TR-78-22, May 1978.

[23]Gentleman, J.F., R.M. Dunn, *Polyreg-ST: Package*, University of Waterloo, Waterloo, Ontario. converted to MTS by J.P. Chenier, University of Alberta,

Edmonton, Alberta, Canada, Feb. 1980.

[24]Gibbs Jr., F.A., "Clinical Evaluation of a Microwave/Radiofrequency System (BSD Corporation) for Induction of Local and Regional Hyperthermia",*JMP*, vol.16, no.2, 1981, pp.183-192.

[25]Graham, G.D., "Dessication of Hemorrhoids",*Arch. Phys. Therapy, X-ray, Radium*, vol.16, Dec. 1935, pp.741-742.

[26]Guy, A.W., J.F. Lehmann, J.B. Stonebridge, C.C. Sorensen, "Development of a 915-MHz Direct-Contact Applicator for Therapeutic Heating of Tissues",*IEEE Trans. on Microwave Theory Tech.*, vol. MTT-26, no. 8, Aug. 1978. pp. 550-556.

[27]Hahn, G.M., P. Kernahan, A. Martinez, D. Pounds, S. Prionas, T. Anderson, G. Justice, "Some Heat Transfer Problems associated with Heating by Ultrasound, Microwaves or Radio Frequency",*Ann. N.Y. Acad. Sci.*, vol. 335, 1980, pp.327-346.

[28]Hall, R.R., R.O.K. Schade, J. Swinney, "Effects of Hyperthermia on Bladder Cancer", *British Medical Journal*, vol. 2, 1974, pp.593-594.

[29]Hand, J.W., S.P. Hume, J.E. Robinson, J.C.L.

Marigold, S.B. Field, "A Microwave Heating System for Improving Temperature Uniformity in Heated Tissue", *JMP*, vol. 14, no. 2, 1979, pp.145-149.

[30]Hiebert, A.D., *Computer Simulation of In situ , Low Frequency, Electrical Heating of Oil Sand Formations*, Master of Science Thesis, University of Alberta, 1981.

[31]von Hippel, A.R. (ed.), *Dielectric Materials and Applications*, M.I.T. Press, Cambridge, Mass., 1954.

[32]Iizuka, K., "An Agar-Agar Chamber for Study of Electromagnetic Waves in an Inhomogeneous Medium", *IEEE Trans. Ant. Prop.*, vol. AP-19, no.3, May 1971, pp.365-377.

[33]Jackson, J.D., *Classical Electrodynamics*, John Wiley and Sons, Inc. United States of America, 1975.

[34]Law, H.T., R.T. Pettigrew, "Heat Transfer in Whole-Body Hyperthermia". *Ann. N.Y. Acad. Sci.*, vol. 335, 1980, pp.298-310.

[35]Lehmann, J.F., A.W. Guy, J.B. Stonebridge, B.J. deLateur, "Evaluation of a Therapeutic Direct-Contact 915 MHz Microwave Applicator for Effective Deep-Tissue Heating in Humans", *IEEE Trans. Microwave Theory*

Tech., vol. MTT-26,no. 8, Aug. 1978, pp.556-563.

[36]Lele, P.P., "Induction of Deep, Local Hyperthermia by Ultrasound and Electromagnetic Fields-Problems and Choices", *Radiat. Environ. Biophys.*, vol.17, pp.205-217, 1980.

[37]LeVeen, H.H., S. Wapnick, V. Piccone, G. Falk, N. Ahmed, "Tumour Eradication by Radiofrequency Therapy. Response in 21 Patients", *JAMA*, vol. 235, no. 20, pp.2198-2200, May 17, 1976.

[38]LeVeen, H.H., N. Ahmed, V.A. Piccone, S. Shugaar, G.Falk, "Radio-Frequency Therapy: Clinical Experience", *Ann. N.Y. Acad. Sci.*, vol. 335, pp.362-371, 1980.

[39]LeVeen, H.H., "Radio Frequency, Electromagnetic Radiation Device Having Orbital Mount", United States Patent No. 4,230,129, Oct. 28, 1980.

[40]Licht, S., H.L. Kamenetz (ed.), *Therapeutic Heat and Cold (2nd ed.)*, E. Licht, publ.,1965, Waverly Press Inc., Maryland.

[41]Ludgate, C.M., N. McLean, W.S. Tulloch, "Hyperthermic Irrigation of Bladder in Treatment of Transitional

Cell Carcinoma: Its Effectiveness in Controlling Persistent Haematuria", *J.Royal Soc. Med.*, vol. 72, May 1979, pp.336-340.

[42]Magin, R.L., G. Kantor, "Comparison of the Heating Patterns of Small Microwave (2450 MHz) Applicators", *J. Bioengineering*, vol. 1,1977, Pergamon Press, Inc. pp.493-509.

[43]Maurer, A., "Cold Clamp". *Omni*, March 1982,Omni Publications International Ltd.,B. Guccione (ed.), p.39.

[44]Mendecki, J., E. Freidenthal, C. Botstein, F. Sterzer, R. Paglione, "Therapeutic Potential of Conformal Applicators for Induction of Hyperthermia", *JMP*, vol. 14, no. 2, 1979, pp.139-144.

[45]Muckle, D.S. J.A. Dickson, "Hyperthermia (42 °C.)as an Adjunct to Radiotherapy and Chemotherapy in the Treatment of the Allogeneic VX2 Carcinoma in the Rabbit". *Br. J. of Cancer*, vol. 27, 1973, pp.307-315.

[46]Overgaard, K., J. Overgaard, "Investigations on the Possibility of Thermic Tumour Therapy-II...Action of Combined Heat-Roentgen Treatment on a Transplanted

Mouse Mammary Carcinoma", *Eur. J. Cancer*, vol. 8,1972, pp.573-575.

[47]Overgaard, J., "Effect of Hyperthermia on Malignant Cells in vivo", *Cancer*, vol. 39, 1977, pp.2637-2646.

[48]Overgaard, J., "Biological Effect of 27.12 MHz Short-Wave Diathermic Heating in Experimental Tumours", *IEEE Trans. Microwave Theory Tech.*, vol. MTT-26, no. 8, Aug 1978, pp.523-529.

[49]Paglione, R., F. Sterzer, J. Mendecki, E. Freidenthal, C. Botstein, "27 MHZ Ridged Waveguide Applicators for Localized Hyperthermia Treatment of Deep-Seated Malignant Tumours", *Microwave J.*, Feb.1981.

[50]Pettigrew, R.T., J.M. Galt, C.M. Ludgate, A.N. Smith, "Clinical Effects of Whole-Body Hyperthermia in Advanced Malignancy", *Br. Med. Jr.*, vol. 4, pp.679-682, Dec. 1974.

[51]Ramo, S., J.R. Whinnery, T. Van Duzer, *Fields and Waves in Communication Electronics*, John Wiley and Sons, Inc., New York, 1965.

[52]Robinson, J.E., "Hyperthermia as an Adjunct to Cancer

Therapy", *J. Bioeng.*, vol .1, pp.467-469, 1977, Pergamon Press Inc.

[53]Rosen, D., R. Bignall, J.D.M. Wisse, A.C.M. van der Drift, "Radio Frequency Measurement of the Dielectric Constant of Conducting Liquids With tan up to 500", *J. Sci. Instr. (J.Phys. E.)*, 1969, ser. 2, vol.2, pp.22-28.

[54]Short, J.G., P.F. Turner, "Physical Hyperthermia and Cancer Therapy", *IEEE Proc.*, vol.68, no.1, Jan. 1980, pp.133-142.

[55]Sokal, S.S., F.J. Rohlf, *Biometry: The Principles and Practice of Statistics in Biological Research*, W.H. Freeman and Co., San Francisco, 1969.

[56]Stauffer, P.R., T.C. Cetas, R.C. Jones, "A System for Producing Localized Hyperthermia in Tumours Through Magnetic Induction Heating of Ferromagnetic Implants", Paper Te35, *The Third International Symposium: Cancer Therapy by Hyperthermia, Drugs and Radiation*, Colorado State University , Fort Collins, Colorado, June 22-26, 1980. (cited in [16]).

[57]Stehlin Jr.,J.S., "Hyperthermic Perfusion for Melanoma of the Extremities: Experience with 165 Patients, 1967

to 1979", *Ann. N.Y. Acad. Sci.*, vol. 335,, pp.352-355. 1980.

[58]Sterzer, F., R. Paglione, M. Nowogrodzki, E.Beck, J. Mendecki, E. Freidenthal, C. Botstein, "Microwave Apparatus for the Treatment of Cancer", *Microwave Journal*, Int. Edition, vol.23, no.1, Jan. 1980. pp.39-44.

[59]Sterzer, F., R.W. Paglione, J. Mendecki, E. Freidenthal, C.Botstein, "RF Therapy for Malignancy", *IEEE Spectrum* , Dec. 1980, pp.32-37.

[60]Storm, F.K., W.H. Harrison, R.S. Elliot, D.L. Morton, "Hyperthermic Therapy for Human Neoplasms: Thermal Death Time", *Cancer*, vol.46, Oct. 15,1980, pp.1849-1854.

[61]Storm, F.K., W. Harrison, R.S. Elliot, L.R. Kaiser, A.W. Silberman, D.L. Morton, "Clinical Radiofrequency Hyperthermia by Magnetic-Loop Induction", *JMP*, vol.16, no.2, 1981, pp.179-184.

[62]Strohbein, J.W., E.D. Bowers, J.E. Walsh, E.B. Douple, "An Invasive Microwave Antenna for Locally-Induced Hyperthermia for Cancer Therapy", *JMP*, vol.14, no.4, 1979, pp.339-350.

[63]Stuchly, M. (ed.), "Health aspects of Radio Frequency and Microwave Radiation Exposure Part I", Environmental Health Criteria Document. Environmental Health Directorate. Health Protection Branch. Publ. by authority of the Minister of Nat'l Health and Welfare. 77-EHD-13, Nov. 1977.

[64]Stuchly, M.A., S.S. Stuchly, G. Kantor, "Diathermy Applicators with Circular Aperture and Corrugated Flange", *IEEE Trans. Microwave Theory Tech.*, vol. MTT-28, no.3, March 1980, pp.267-271.

[65]Sugaar, S., H.H. LeVeen, "A Histopathologic Study on the Effects of Radiofrequency Thermotherapy on Malignant Tumours of the Lung", *Cancer*, vol. 43, no. 2, pp.767-783, 1979.

[66]Susskind, C., "The Story of Nonionizing Radation Research", *Bull. N.Y. Acad. Med.*, vol.55, no.11, Dec. 1979. pp.1152-1163.

[67]Szmigielski, S., M. Bielec, M. Janiak, M. Kobus, M. Luczak, E. De Clercq, "Inhibition of Tumour Growth in Mice by Microwave Hyperthermia, Polriboinosinic-Polyribocytidylic and Mouse Interferon", *IEEE Trans. Microwave Theory Tech.*, vol. MTT-26, no. 8, pp.520-522, Aug. 1978.

[68]Taylor, L.S., "Brain Cancer Therapy Using an Implanted Microwave Radiator", *Microwave J.*, Jan. 1981, pp.66-68 and 71.

[69]Toler, J., J. Seals, "R.F. Dielectric Properties Measurement System: Human and Animal Data", *DHEW (NIOSH) Report 77-176*, Contract No. 210-76-0136, Georgia Institute of Technology, Atlanta, Ga. July 1977.

[70]Turner, P.F., "Deep Heating of Cylindrical or Elliptical Tissue Masses", Paper Te42, *The Third International Symposium: Cancer Therapyby Hyperthermia, Drugs and Radiation*, Colorado State University, Fort Collins, Colorado, June 22-26, 1980. (cited in [16])

[71]Vermeulen, F.E., F.S. Chute, M.R. Cervenan, "Physical Modelling of the Electromagnetic Heating of Oil Sand and other Earth-type and Biological Materials", *Can. Elec. Eng. J.*, vol.4, No.4, 1979, pp.19-28.

[72]Westra, A., W.C. Dewey, "Variation in Sensitivity to Heat Shock During the Cell-cycle of Chinese Hamster Cells *in vitro*", *Int. J. Rad. Biol.*, vol. 19, No. 5, 1971, pp. 467-477.

APPENDIX 1.

COMPUTER PROGRAMS TO SIMULATE R.F. HEATING WITH ROTATING ELECTRODES

The following are printouts of the computer programs used to calculate orbiting electrode temperature distributions using stationary electrode data. These programs assume that the electrodes travel back and forth through an arc of plus-minus 40°. Throughout this arc of travel the electrodes vary in speed from a minimum at the ends of the arc to a maximum at the centre. Ideally the variation in electrode speed would follow simple harmonic motion. This would mean a sinusoidal variation in speed with time. For reasons discussed in the text this is not the case. A graph of electrode speed vs. time yields not a perfect sinusoid but a sinusoid with flattened peaks and troughs. In the extreme the variation in electrode speed was assumed to follow curve which, over a range of 180°, was a half-circle instead of a sine wave. An average of the 'circular' variation and the sinusoidal variation was used to give a 'flattened sinusoidal' variation.

The program in Figure A.1.1 produced the temperature distribution for sinusoidally varying

electrode speed. Figures A.1.2 and A.1.3 are for circular and flattened sinusoid speed variations respectively.

SINUSOIDAL ELECTRODE SPEED VARIATION

```
REAL R(216),TH(216),T(216),TA(160)
N=216
READ(5,10) (R(I),TH(I),T(I),I=1,N)
10 FORMAT(2F5.2,F6.2)
M=5
DO 20 I=1,160
TA(I)=0.04704*T(M)+0.05007*(T(M-1)+T(M+1))
*+0.06141*(T(M-2)+T(M+2))+0.09409*(T(M-3)
*+T(M+3))+0.2709*(T(M-4)+T(M+4))
PRINT50,R(M),TH(M),TA(I)
50 FORMAT(3F7.2)
IF(M.EQ.23) GOTO 30
IF(M.EQ.50) GOTO 30
IF(M.EQ.77) GOTO 30
IF(M.EQ.104) GOTO 30
IF(M.EQ.131) GOTO 30
IF(M.EQ.158) GOTO 30
IF(M.EQ.185) GOTO 30
IF(M.EQ.212) GOTO 40
M=M+1
GO TO 20
30 M=M+9
20 CONTINUE
40 CONTINUE
STOP
```

```
END
$ENDFILE
```

FIGURE A.1.1

CIRCULAR ELECTRODE SPEED VARIATION

```
REAL R(216),TH(216),T(216),TA(160)
N=216
READ(5,10) (R(I),TH(I),T(I),I=1,N)
10 FORMAT(2F5.2,F6.2)
M=5
DO 20 I=1,160
TA(I)=0.0811*T(M)+0.0832*(T(M-1)+T(M+1))
*+0.0905*(T(M-2)+T(M+2))+0.1088*(T(M-3)
*+T(M+3))+0.177*(T(M-4)+T(M+4))
PRINT50,R(M),TH(M),TA(I)
50 FORMAT(3F7.2)
IF(M.EQ.23) GOTO 30
IF(M.EQ.50) GOTO 30
IF(M.EQ.77) GOTO 30
IF(M.EQ.104) GOTO 30
IF(M.EQ.131) GOTO 30
IF(M.EQ.158) GOTO 30
IF(M.EQ.185) GOTO 30
IF(M.EQ.212) GOTO 40
M=M+1
GO TO 20
30 M=M+9
20 CONTINUE
40 CONTINUE
STOP
```

```
END
$ENDFILE
```

FIGURE A.1.2

FLATTENED-SINUSOIDAL ELECTRODE SPEED VARIATION

```
      REAL R(216),TH(216),T(216),TA(160)
      N=216
      READ(5,10) (R(I),TH(I),T(I),I=1,N)
   10 FORMAT(2F5.2,F6.2)
      M=5
      DO 20 I=1,160
      TA(I)=0.06407*T(M)+0.066635*(T(M-1)+T(M+1))
     *+0.075955*(T(M-2)+T(M+2))+0.101445*(T(M-3)
     *+T(M+3))+0.22396*(T(M-4)+T(M+4))
      PRINT50,R(M),TH(M),TA(I)
   50 FORMAT(3F7.2)
      IF(M.EQ.23) GOTO 30
      IF(M.EQ.50) GOTO 30
      IF(M.EQ.77) GOTO 30
      IF(M.EQ.104) GOTO 30
      IF(M.EQ.131) GOTO 30
      IF(M.EQ.158) GOTO 30
      IF(M.EQ.185) GOTO 30
      IF(M.EQ.212) GOTO 40
      M=M+1
      GO TO 20
   30 M=M+9
   20 CONTINUE
   40 CONTINUE
      STOP
```

```
END
$ENDFILE
```

FIGURE A.1.3

APPENDIX 2.

CALCULATION OF POWER ABSORBED BY LOAD

Knowing the impedance across the matching network in series with the load and the impedance of the load alone the power deposited in the agar can be calculated. A circuit representation for the r.f. heating apparatus used in this project is shown in Figure A.2.1.

From Figure A.2.1

$$Z_1+Z_2=50\angle 0^\circ\ \Omega$$

and by measurement

$$Z_2=89\angle 70^\circ\Omega=(30.44+j83.63)\ \Omega$$

therefore,

$$Z_1=(19.56-j83.63)\ \Omega$$

The power dissipated across Z_1+Z_2 was approximately 200 Watts. Therefore

$$I=P/V=200\ W/100\ V\angle 0^\circ=2\ Amps\angle 0^\circ$$

where I is the current in the circuit, V is the voltage across the two loads Z_1 and Z_2, and P is the power deposited in the two loads. So the power dissipated in Z_2 (the agar cylinder and saline solution) was

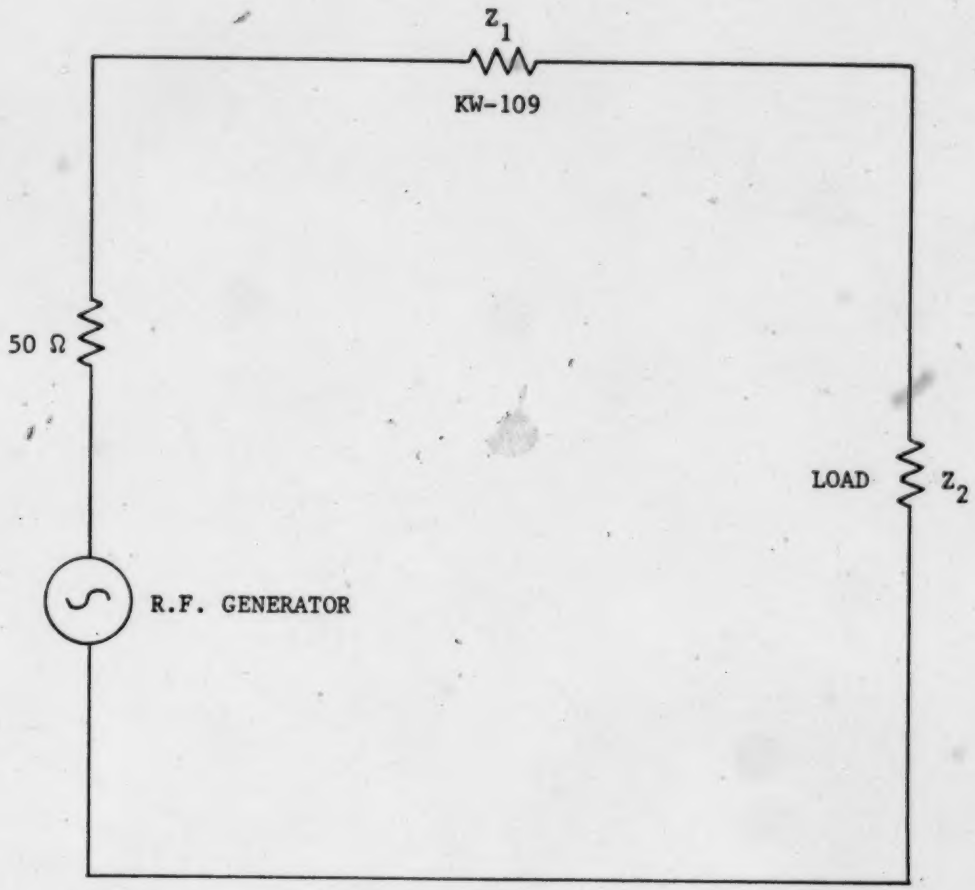

FIGURE A.2.1 Equivalent circuit for hyperthermia applicator

$$P_2 = I^2 R_2 = 121.76 \text{ Watts}$$

One tenth of the agar, saline bath, and electrodes were considered for all simulations so an applied power of 12.18 Watts was used.

APPENDIX 3.

MAXIMUM TEMPERATURE ERROR RESULTING FROM 2-D SIMULATION

Megaera was used to help determine the inaccuracy produced by applying a two dimensional program to a three dimensional world. To do this two heating simulations were made. In one case the electrodes and dielectric were closely confined by an insulating material (Figure A.3.1). The insulator kept current density uniform between the electrodes. In the second case the insulating boundary was far from the electrodes allowing the field to spread (Figure A.3.2). In each case power, electrode size, and dielectric properties were kept the same. The irradiated medium was given an extremely low thermal conductivity to minimize heat flow. Temperatures between the electrodes were found to vary by up to 7% between the two configurations in Figures A.3.1 and A.3.2.

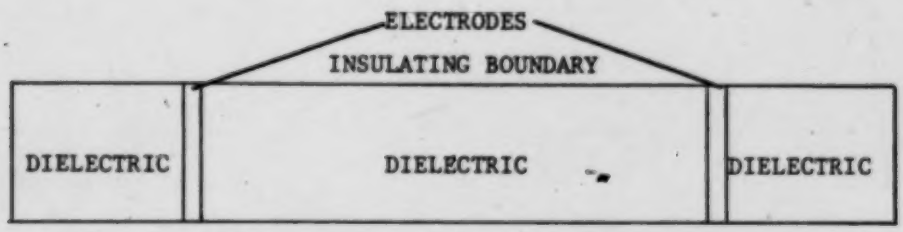

FIGURE A.3.1 Electrode - insulating boundary configuration for uniform current density

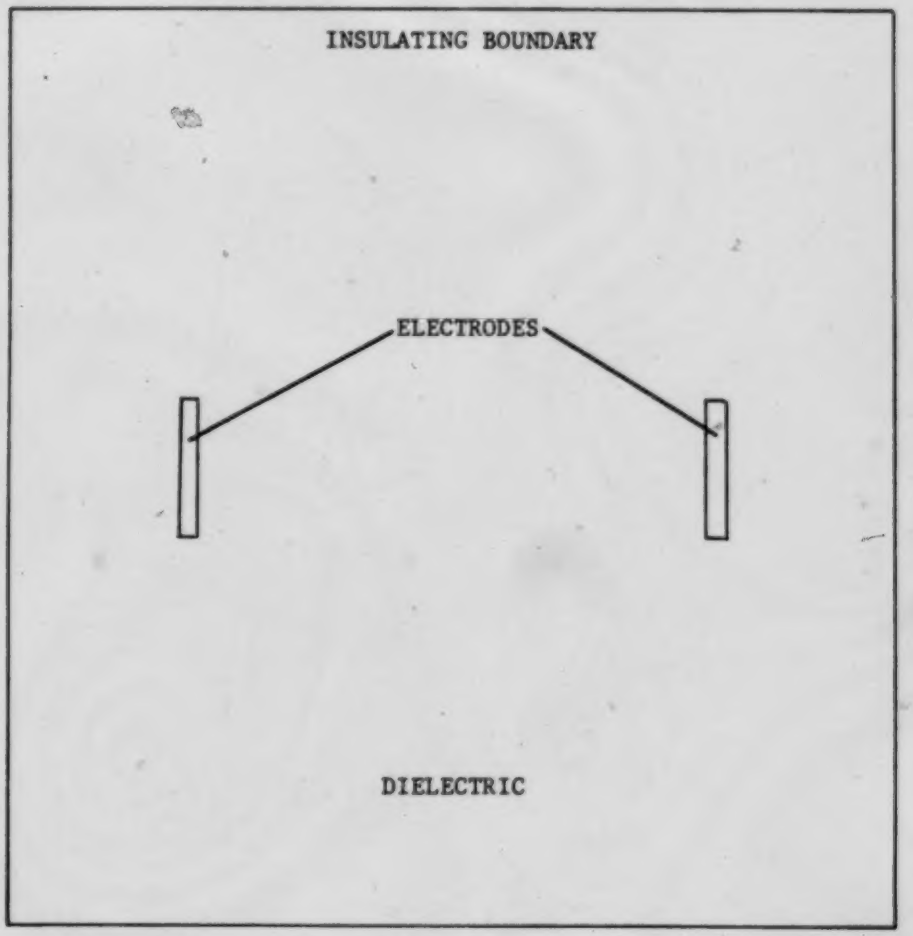

FIGURE A.3.2 Electrode - insulating boundary configuration for non-uniform current density

APPENDIX 4.

PERMITTIVITY AND CONDUCTIVITY DERIVATIONS FOR DIELECTRIC MEASURING CELL[7]

The equivalent circuit seen by the HP4815A vector impedance meter is shown in Figure A.4.1. R_p is the probe resistance, L_p is the probe inductance, C_p is the probe capacitance, C_o is the empty cell capacitance, C is the capacitance with the specimen inserted, and R is the measured resistance with the specimen inserted. Define

$$C_t = C_p + C_o + C$$

to simplify the following calculations. R_p is typically 0.5Ω so it can be ignored. Therefore the impedance of the circuit is

$$\vec{Z} = \frac{R}{1+R^2\omega^2C_t^2} + j\omega\left(L_p - \frac{R^2C_t}{1+R^2\omega^2C_t^2}\right)$$

where is the angular frequency of the applied signal. From Figure A.4.2 the imaginary and real components of $\vec{Z}$ can be specified by

$$z\sin\phi = \omega L_p - \frac{\omega R^2 C_t}{1+R^2\omega^2C_t^2} \qquad 1$$

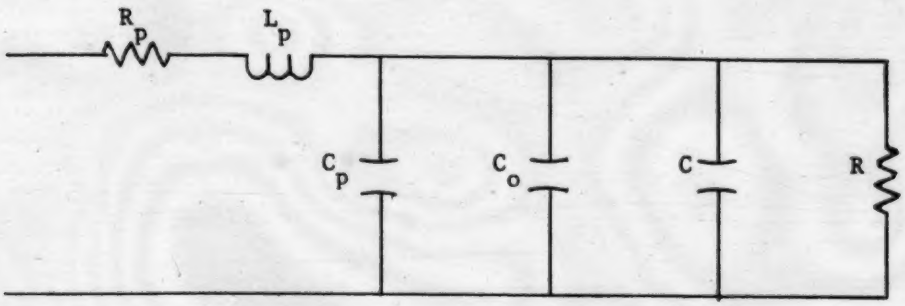

FIGURE A.4.1 Equivalent circuit for dielectric measuring apparatus

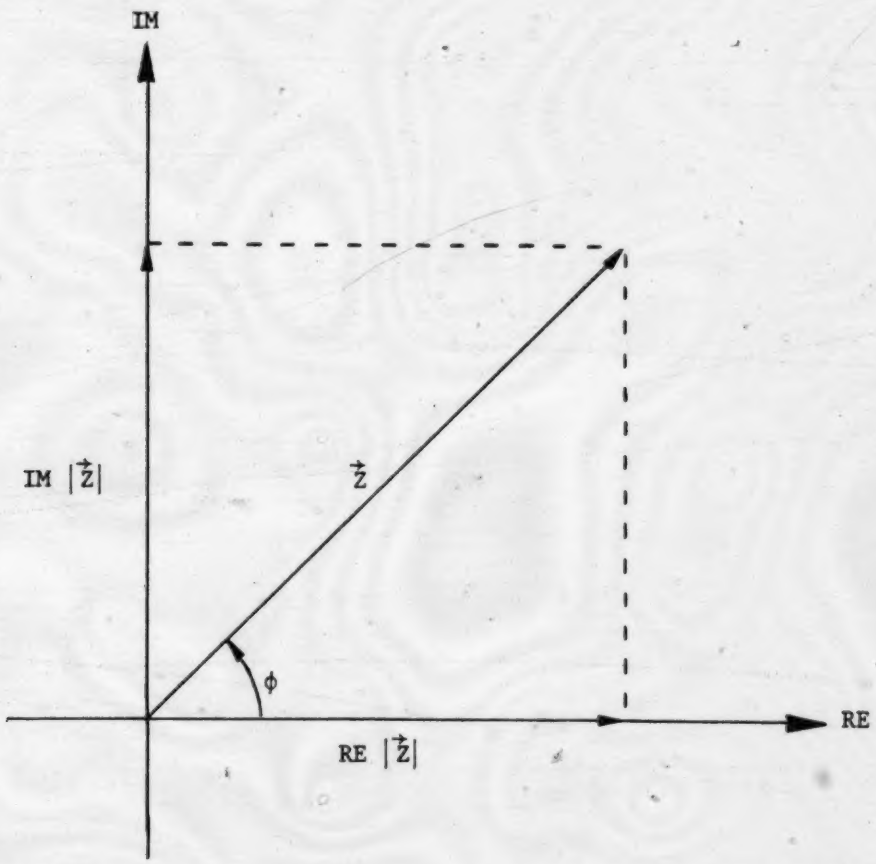

FIGURE A.4.2 Imaginary and real components of complex impedance

and

$$z\cos\phi = \frac{R}{1+R^2\omega^2C_t^2} \qquad 2$$

where $z=|\vec{Z}|$ and ϕ is the phase angle of $\vec{Z}$. From 2

$$1 + R^2\omega^2C_t^2 = \frac{R}{z\cos\phi}$$

or

$$C_t^2 = \frac{R-z\cos\phi}{R^2\omega^2 z\cos\phi} \qquad 3$$

Substituting 2 into 1 gives

$$z\sin\phi = \omega L_p - \omega RC_t z\cos\phi \qquad 4$$

Substituting 3 into 4 gives

$$z\sin\phi = \omega L_p - (Rz\cos\phi - z^2\cos^2\phi)^{\frac{1}{2}}$$

so

$$R = \frac{\omega^2L_p^2 - 2\omega L_p z\sin\phi + z^2}{z\cos\phi} \qquad 5$$

The cell constant for the measuring chamber is defined as [7]

$$\ell = \frac{C}{\epsilon_o\epsilon_r} = \frac{\rho}{R} \qquad 6$$

Substituting 6 into 5 gives

$$\rho = \frac{\ell(\omega^2 L_p^{\,2} - 2\omega L_p z\sin\phi + z^2)}{z\cos\phi}$$

or

$$\sigma = \frac{z\cos\phi}{\ell(\omega^2 L_p^{\,2} - 2\omega L_p z\sin\phi + z^2)} \qquad 7$$

Now from 1 and 2

$$\omega L_p - z\sin\phi = \frac{\omega R^2 C_t}{1+R^2\omega^2 C_t^{\,2}} = \omega R C_t z\cos\phi$$

or

$$\omega R C_t z\cos\phi = \omega L_p - z\sin\phi$$

so

$$C_t = \frac{\omega L_p - z\sin\phi}{\omega R z\cos\phi} \qquad 8$$

Substituting 5 into 8 gives

$$C_t = \frac{\omega L_p - z\sin\phi}{\omega(\omega^2 L_p^{\,2} - 2\omega L_p z\sin\phi + z^2)}$$

By definition

$$C_t = C_p + C_o + C$$

so

$$C = \frac{\omega L_p - z\sin\phi}{\omega(z^2 + \omega^2 L_p^2 - 2\omega L_p z\sin\phi)} - (C_p + C_o) \qquad 9$$

Substituting 6 into 9 gives

$$\varepsilon_r = \{\frac{\omega L_p - z\sin\phi}{\omega(z^2 + \omega^2 L_p^2 - 2\omega L_p z\sin\phi)} - (C_p + C_o)\}\frac{1}{\ell\varepsilon_o} \qquad 10$$

For frequencies below 5 MHz $L << 1$ so 7 and 10 can be approximated by

$$\sigma = \frac{\cos\phi}{z\ell} \qquad 11$$

and

$$\varepsilon_r = -\{\frac{\sin\phi}{\omega z} + (C_p + C_o)\}\frac{1}{\ell\varepsilon_o} \qquad 12$$